The Institute of Paper Chemistry

Appleton, Wisconsin

Doctor's Dissertation

An Investigation of Z-Direction Density Profile Development During Impulse Drying

Steven W. Burton

January, 1987
Reprint October, 1990

AN INVESTIGATION OF Z-DIRECTION DENSITY PROFILE DEVELOPMENT DURING IMPULSE DRYING

A thesis submitted by

Steven W. Burton

B.S. 1981, Miami University of Ohio

M.S. 1983, Lawrence University

in partial fulfillment of the requirements
of The Institute of Paper Chemistry
for the degree of Doctor of Philosophy
from Lawrence University
Appleton, Wisconsin

January, 1987

TABLE OF CONTENTS

ABSTRACT

Water removal from a moist paper web as it passes through a high temperature press nip is called impulse drying. This new process produces heat transfer and water removal rates substantially higher than those attained in conventional drying processes. Increased energy efficiency, decreased capital costs, enhanced sheet properties, and increased utilization of high yield and poorly bonding furnishes are all likely advantages of the impulse drying process.

Impulse drying results in the development of a unique density profile through the web thickness. This profile is characterized by a very high average value and a J or U shape, with the greatest density near the hot surface. Both the average density and the density distribution have an important influence on paper properties. The results of this investigation have clarified the mechanisms which lead to these unusual density profiles during impulse drying.

To simulate impulse drying, a dropping-weight press-nip simulator with one heated surface is used. The simulator is instrumented to measure the applied mechanical load, vapor pressure at the hot surface/paper interface, temperature history of the hot surface, and the apparent density profile through the web. The density profile measurement is unprecedented and requires handsheets with special open-mesh targets embedded at various levels during the forming process. In impulse drying, these targets move as the sheet is compressed. Displacement transducers, mounted in the unheated platen, track individual target motion. The instantaneous apparent densities of the regions within the web are calculated from target separations and known basis weights.

From measurements of the type described and others, it is apparent that density development in impulse drying depends on a number of driving forces not found in wet pressing or conventional drying. These include thermal softening,

large total vapor pressure gradients, thermally-induced liquid phase dewatering, and others. This thesis presents a mechanistic description of these densifying forces which is substantially supported by experimental measurements.

INTRODUCTION

Over the years, a great deal of effort has been put forth to improve the performance of the pressing and drying operations in paper manufacturing. With continual increases in paper machine speeds and higher energy costs, the necessity for increased dewatering capacity and improved energy efficiency is ever present. A number of developments have improved dewatering performance, but fundamental limitations of these processes suggest that further improvements are not likely to result in significant gains in performance. To achieve considerable improvements in dewatering capacity and energy efficiency is likely to require new or much more intensive water removal processes. With this spirit in mind, a number of scientists in the paper industry have pursued pressing/drying technology which, if implemented, would dramatically alter current papermaking practices. Impulse drying is such a technology.

Impulse drying is a descriptive term for water removal from a moist paper web as it passes through a high temperature press nip. This new process produces heat transfer and water removal rates substantially higher than those attained in conventional processes. Increased energy efficiency, decreased capital costs, enhanced sheet properties, and increased utilization of high yield and other poorly bonding furnishes are all likely advantages of impulse drying.

The enhanced sheet properties resulting from impulse drying are a strong function of the average sheet density that is developed.[1] Impulse drying is known to result in high average sheet densities and in nonuniform z-direction density profiles. The densifying forces have been shown to create J or U shaped density profiles. This thesis presents an experimental study in which

instantaneous density profiles are measured directly during impulse drying. The objective is to determine and understand the densification mechanisms responsible.

BACKGROUND

The moisture removed from the sheet during pressing and drying represents only about 1% of the total dewatering involved in the papermaking process. Despite this, these operations have a major impact on production costs as well as product quality. The American Paper Institute reported in 1975 that the total energy consumed per short ton of output, on an industry wide basis, averaged 33 million Btu.[2] It has been estimated that about 75% of the total energy consumed in a modern paper manufacturing operation is spent as steam fed to the dryer section of the paper machine.[3]

Given the high energy requirements of paper drying, it is easy to understand why increasing the solids level entering the dryer section is a major objective of most wet pressing research programs. In general, an increase of one percentage point in the solids content exiting the press section corresponds to a 4.5% decrease in dryer energy consumption per ton of final product. Consequently, optimization and maintenance of the press section is one of the most important factors in energy conservation in a paper mill.

In many cases, paper production is limited by the dewatering capacity of the pressing and drying operations. Past developments have significantly improved this capacity to the point where additional gains in capacity are likely to be small. This results from the fundamental limitations which restrict the performance of existing pressing and drying processes. Large increases in dewatering capacity are likely to require radical alterations of these processes in which new and/or much more intense dewatering and densifying forces are employed.[4]

One such process is impulse drying. Impulse drying denotes water removal from a moist paper web as it passes through a high temperature press nip.

Laboratory studies at The Institute of Paper Chemistry have demonstrated its effectiveness in water removal.[1,5-7] In a recent paper on impulse drying performance, Sprague[1] reported dewatering rates 100-1000 times those for cylinder dryers, specific energy use 1/3 to 1/2 that for conventional drying, and significant improvements in paper properties.

Physically, impulse drying encompasses both pressing and drying but involves new and more intense dewatering and densifying forces. By employing these forces, the fundamental limitations of conventional pressing and drying processes are, to some extent, overcome. Defining and understanding these forces are the objectives of much of the ongoing research in this area.

WET PRESSING

During the pressing operation on a paper machine, water removal is accomplished by mechanically squeezing water from the sheet. Thus, water removal is accomplished simply by reducing the sheet volume. It is the primary purpose of the press section to maximize water removal while simultaneously creating the density potential required for developing desirable paper properties. Over the years, press designs have been altered in efforts to improve the performance of the operation. These improvements include better felt designs, higher press loads, increased sheet temperatures, and extended nip residence times. Despite these improvements, the dryness level exiting modern press sections rarely extends beyond 50% dryness. Studies have shown,[8] however, that dryness levels of 70% or higher are potentially achievable by mechanical water removal.

Wahlstrom-Nilsson-Larsson Model of Wet Pressing

Little has changed in the fundamental description of the wet pressing process since the work of Wahlstrom[9,10] and of Nilsson and Larsson.[11] Since then, a number of investigations into the dynamic compression of fiber mats have been performed which tend to support much of their theoretical model. Most notably, Chang,[12] Ceckler, et al.,[13] and Carlsson[14] have made significant contributions to this field. Only Carlsson has investigated the full compression-expansion cycle of the pressing operation.

The behavior of a wet sheet in a dynamic press nip is defined by several important mechanisms.[13] These include the flow and compression characteristics of the fiber mat, and the dependence of this flow on the degree of compaction. In order to analyze this behavior in a quantitative manner, the flow resistance and capillarity of the fiber mat under different stages of compression and saturation together with a detailed knowledge of the compression-expansion behavior of paper must be known. Such an analysis is complicated by the development of hydraulic and structural pressure gradients across the sheet thickness that can produce a nonuniform compression profile.

Wahlstrom,[10] and Nilsson and Larsson[11] divided the pressing operation into four phases. This classical depiction is presented in Fig. 1. Three separate pressure distribution curves are given for the different phases: the total nip pressure, hydraulic pressure, and fiber structure pressure. The total sheet thickness curve is also given.

According to the Wahlstrom-Nilsson-Larsson theory, the unsaturated sheet/felt composite enters the nip in Phase One and air is driven out until the sheet reaches saturation. During this time, the applied force is taken up by the

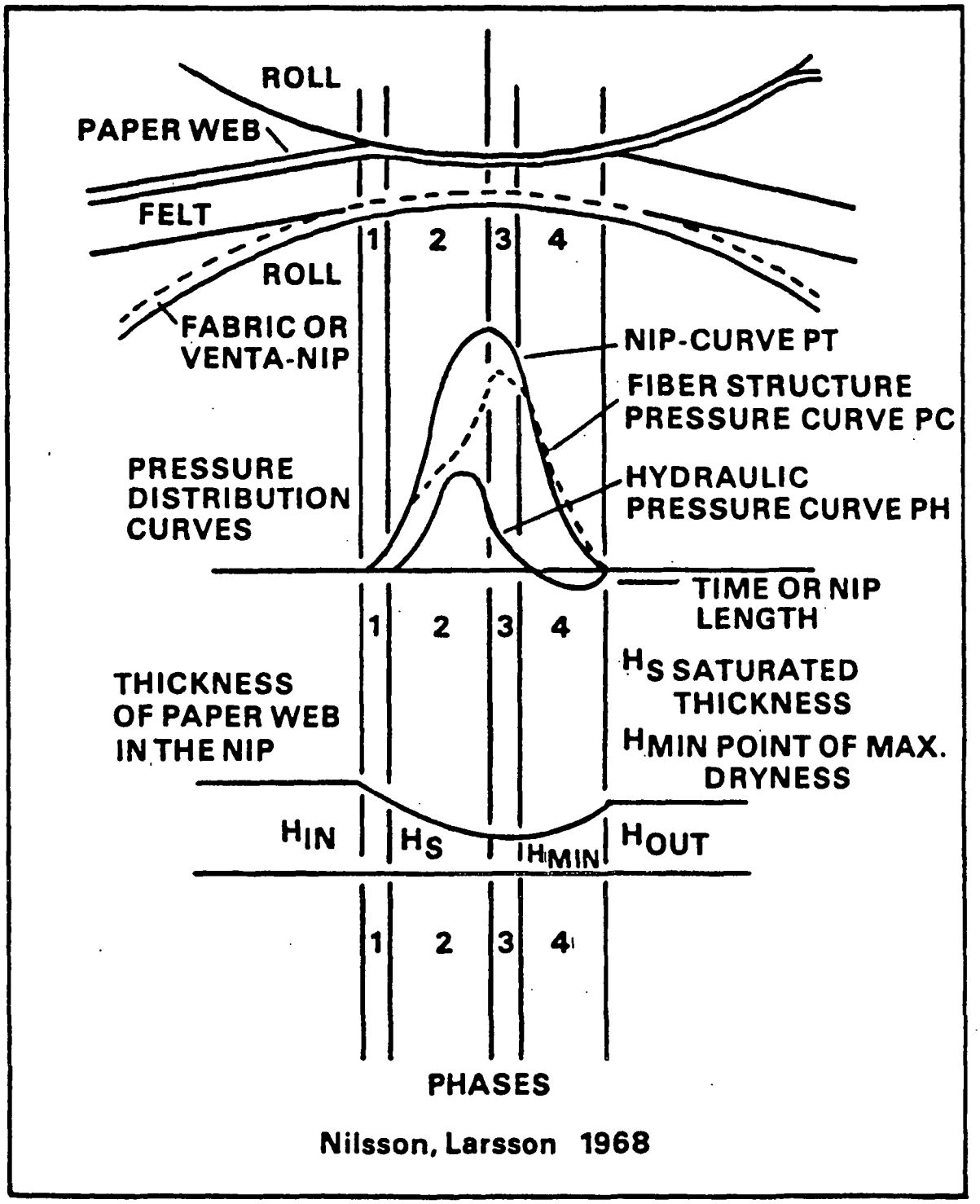

Figure 1. The pressure distribution and sheet thickness in a transversal flow press nip according to Wahlstrom[10] and Nilsson and Larsson.[11]

compression of the fiber network. Once saturation is reached (Phase Two), the water becomes pressurized and flows from the sheet to the felt. The magnitude of hydraulic pressure developed depends on the flow resistance of the fiber network, the moisture content, and the basis weight. Phase Two ends at the point of maximum total pressure. In Phase Three, it is postulated that the felt expands and the sheet compresses until the hydraulic pressure is reduced to zero. Thus, compressive forces continue to remove water as long as a hydraulic pressure gradient exists. In the final phase, both the sheet and felt are thought to expand, creating a negative pressure in both structures. According to theory, Phase Four is characterized by two phase flow of air and water back into the paper from the felt. This flow results primarily from a capillary suction mechanism.

Flow Controlled Versus Compression Controlled Pressing

An important concept of wet pressing theory is that the total applied load on a fiber mat is borne partly by the fiber network and partly by the water. This relationship is, in its most general form:

$$P_T = P_H + P_S$$

where

P_T = total applied pressure

P_H = hydraulic pressure

P_S = fiber structure pressure

The degree to which the fluid phase carries the total applied load depends, to a great extent, on the flow resistance of the fiber network. Ceckler, et al.,[13] and others,[10,15] have observed two main regions of press behavior arising from this dependence on sheet flow resistance. In the first region, typical of

high moisture, high basis weight, and high flow resistance sheets, a flow controlled situation exists. For flow controlled pressing, the primary impediment to water removal is the flow resistance of the fiber network. The amount of water removal in this region depends on the press impulse, with pressure and time being interchanged freely to achieve a given level of dewatering. In the second region, typical of low moisture, low basis weight, and low flow resistance sheets, a compression controlled situation exists. For compression controlled pressing, dewatering of the individual fibers becomes the dominant factor. Impulse is still important in this situation, but pressure now exhibits an important independent effect.

The Kelvin body is a simple model for linear viscoelastic behavior in which one elastic element (spring) and one viscous element (dashpot) are arranged in parallel.[16] This model, depicted in Fig. 2, is used to illustrate the dewatering behavior of a wet sheet.[14,17] During compression, the applied stress is divided between the spring and dashpot elements such that the strains on both elements are equal. In the compression of a wet sheet, the load carried by the fiber network corresponds to the spring while the load carried by the water corresponds to the dashpot. For flow controlled pressing, the dashpot dominates while for compression controlled pressing the spring dominates.

Density Development During Wet Pressing

Sheet density increases almost linearly with press exit dryness up to about 60% solids or more.[18] It is also a key factor in almost all sheet properties, especially strength. As indicated in Fig. 3, tensile and burst are linearly proportionate to density, whereas tear, after a maximum value is reached, is inversely proportional to density.[19] It should be noted that the density in

Fig. 3 was achieved by refining. Similar strength-density relationships may be developed by wet pressing but are somewhat poorer.

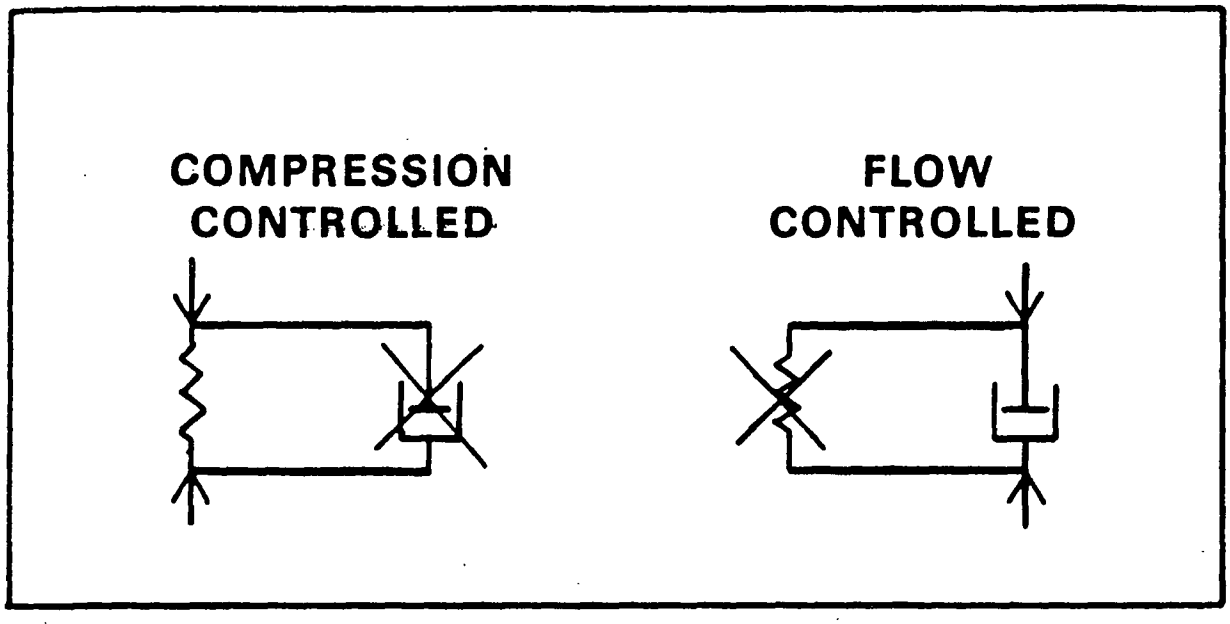

Figure 2. Kelvin body representation of a fiber mat including compression and flow controlled situations.[14]

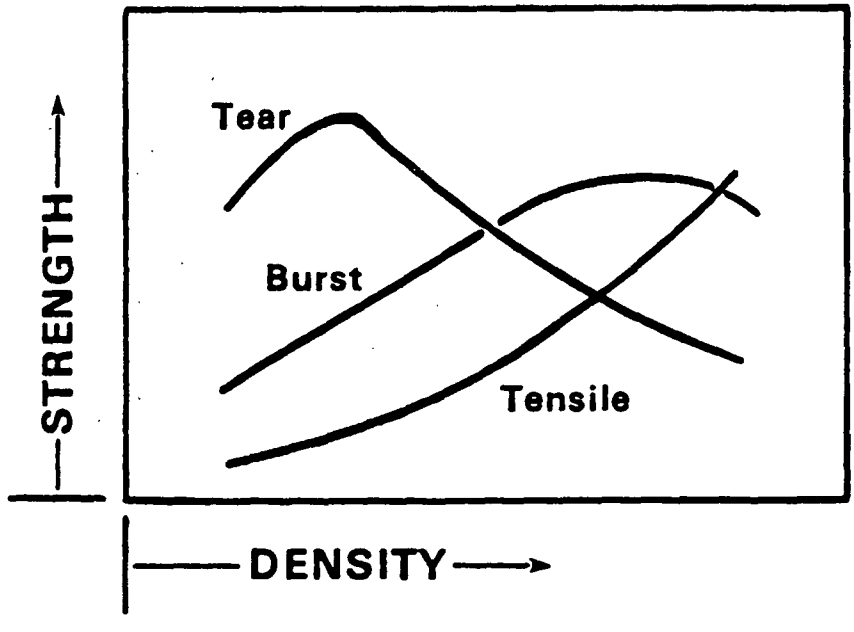

Figure 3. Typical strength versus density relationship,[19] as developed through refining.

In conventional paper manufacturing, most sheet densification is developed in the press section through the action of mechanical pressing and fluid shear forces. In some cases, an asymmetrical z-direction density profile is created in the sheet such that the flow exiting surface is most dense. This process, sometimes called stratification, and its practical effects have been discussed at length by MacGregor.[20,21]

Theoretically, the density profile developed during pressing is retained as the fiber network continues to be bonded during drying. However, since fiber network recovery and rewetting are known to occur during and after the nip opens and since bonding proceeds under the action of surface tension forces with little mechanical restraint, the final density profile may be quite different from that developed in the nip. In any case, wet pressing remains a primary means for achieving density.

Since flow must occur in the direction of a fluid pressure gradient and since the sheet is compressible, development of a z-direction density gradient is likely. Figure 4 is an illustration of what the z-direction hydraulic and structural pressure profiles may resemble. The hydraulic pressure is greatest on the surface of the sheet next to the press roll and lowest on the surface of the sheet next to the felt. Since the total pressure must be constant at any given point in the nip, the structural pressure must be highest on the felted side and lowest next to the plain roll. MacGregor,[20] in a review of sheet stratification caused by wet pressing, points out, ".... in the process of establishing water flow, the sheet must deform first at the flow exiting surface. This causes a greater flow velocity and fluid shear forces here, which in turn causes even more deformation. This creates a sheet which can be more densified at the flow exiting surface, depending on the extent of pressing."

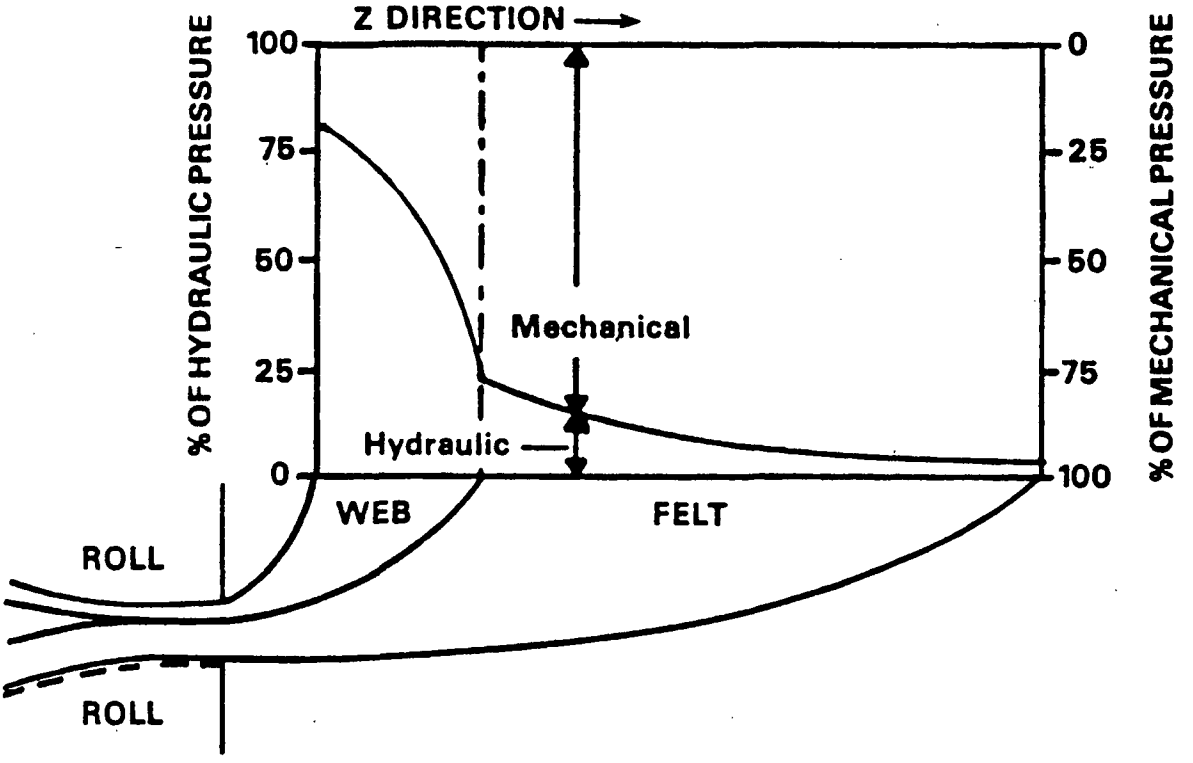

Figure 4. Z-direction hydraulic and structural pressure profiles in a single felted press arrangement.[22]

Evidence of nonuniform density profile development has been presented by several authors.[2,9] Ceckler, et al.,[9] indicated that in the early stages of compression the surface of the sheet through which dewatering takes place controls the rate of sheet compression. This surface layer may become so compacted that it may be the primary resistance to flow.

Many factors affect density profile development.[20] Its extent depends greatly on the rate of compression and the sheet flow resistance. The various factors which influence density profile development, together with their interrelationships are given in Fig. 5.

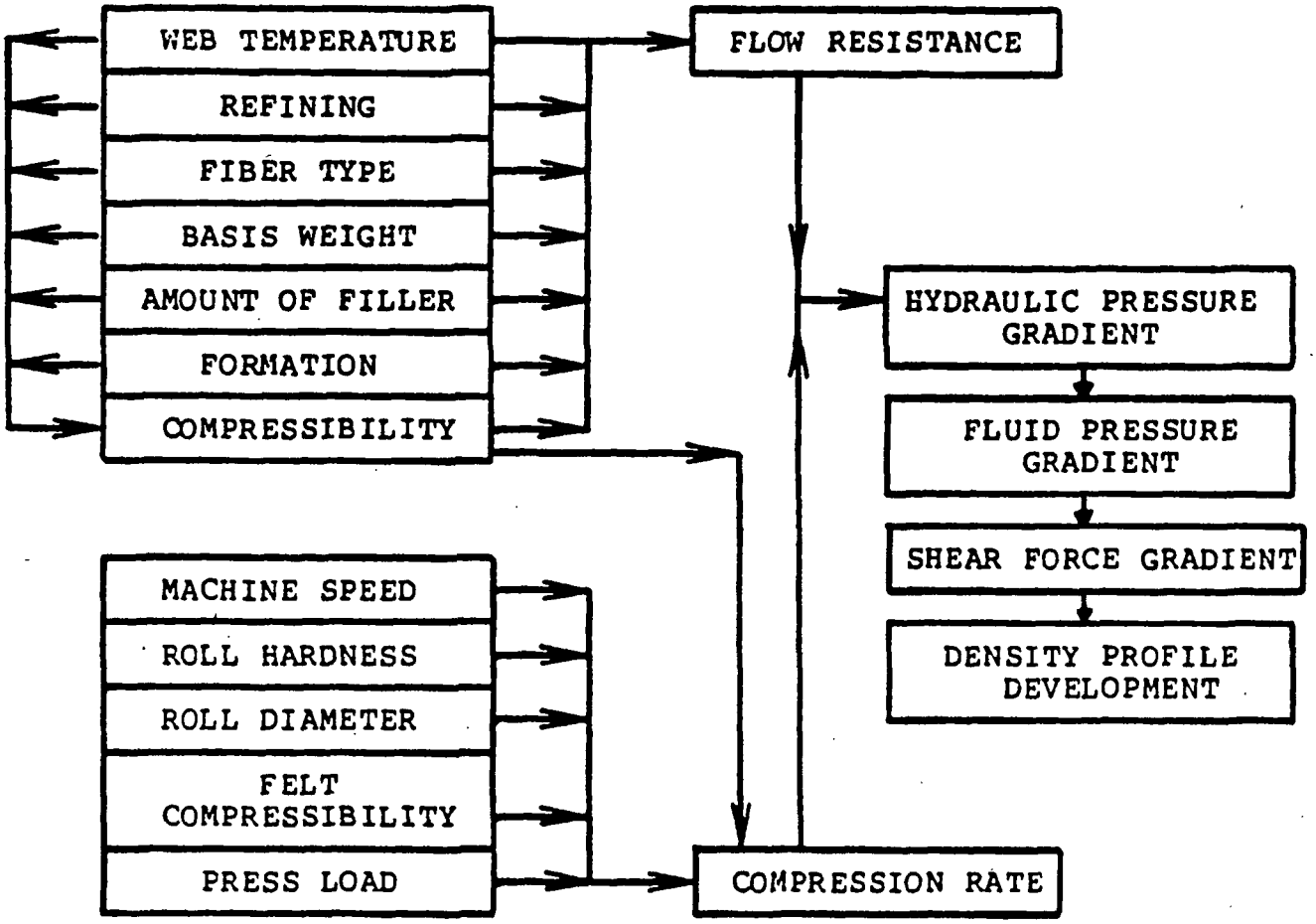

Figure 5. Factors affecting z-direction density profile development.[20]

Fiber Mat Compressibility

Han[23] describes three possible mechanisms of deformation in a fiber network. These include fiber bending at the free spans, fiber repositioning, and fiber conformation. Fiber bending at the free spans creates more fiber-to-fiber contact until a new and higher density is reached. Fiber density and stiffness are two important parameters. The investigation of the compression of glass fiber mats by Elias[24] demonstrates fiber bending and shows a direct proportionality between the number of contacts per fiber length and solid fraction. In fiber repositioning, fibers oriented out of plane reposition themselves into an in-plane position. Fiber conformation occurs when there is a change in the cross-

sectional shape of the fiber to a more flattened appearance. When this happens, there is an increase in the contact area between fibers.

Although compressibility studies may be either dynamic or static, most of the work presented in the literature deals with the static determination of sheet compressibility. In these experiments, a steady, uniform compacting load is applied to unbonded, water saturated sheets.

The power law description of wet fiber mat compressibility was first reported by Qviller[25] and later by Campbell.[26] The basic form of the relationship is:

$$C = M P^{N}$$

where C = fiber mat density (g/cm^3)

M,N = constants

Since this equation predicted that the sheet density approached zero at low pressure, Ingmanson[27] introduced a model of the form:

$$C - C_o = M P^{N}$$

where C_o = mat density at zero bond (g/cm^3)

In an effort to account for creep, Wilder[28] modeled compression with an equation of the form:

$$C - C_o = [A + B \log(t)] P^{N}$$

where t = time (seconds)

A,B = constants

For dynamic compressibility tests, time dependency becomes an important consideration in mat deformation because of water removal and fiber network viscoelasticity. In a recent study by Ceckler et al.,[13] it was concluded that two modes of compression act together which constitute fiber mat compression. In the initial mode, which is time independent, nonlinear and moisture dependent, elastic behavior is observed. This is assumed to be a direct result of fiber bending. The second mode of compression is time dependent and is associated with the viscoelastic deformation of the fiber wall (creep), and the resistance to deformation resulting from the expulsion of water from inside the fibers. This is referred to as the fiber compression mode. Wegner, et al.[17] concluded that expulsion of the water in the fiber cell wall controls the viscous and compressive characteristics of the wet sheet.

Effect of Temperature

Busker and Cronin[29] classify temperature as a primary press variable which is capable of influencing the outgoing sheet dryness by four percentage points or more. This beneficial effect, which has long been known and applied in the paper industry, is independent of other press variables so that its benefit can be achieved in addition to others. A typical set of data[29] which demonstrate the positive influence of temperature on dewatering is presented in Fig. 6.

The most obvious effect of increased temperature is a decrease in viscosity and surface tension. This decrease, in accordance with Darcy's Law, reduces the flow resistance in the fiber network and should result in an increase in flow rate from the sheet. The more rapid dewatering at high temperature, as shown by Francik and Busker,[30] can cause disruption of the sheet structure. Studies of pressing at increased temperatures,[30,31] indicate that the increased dewatering cannot be accounted for by fluid property effects alone.

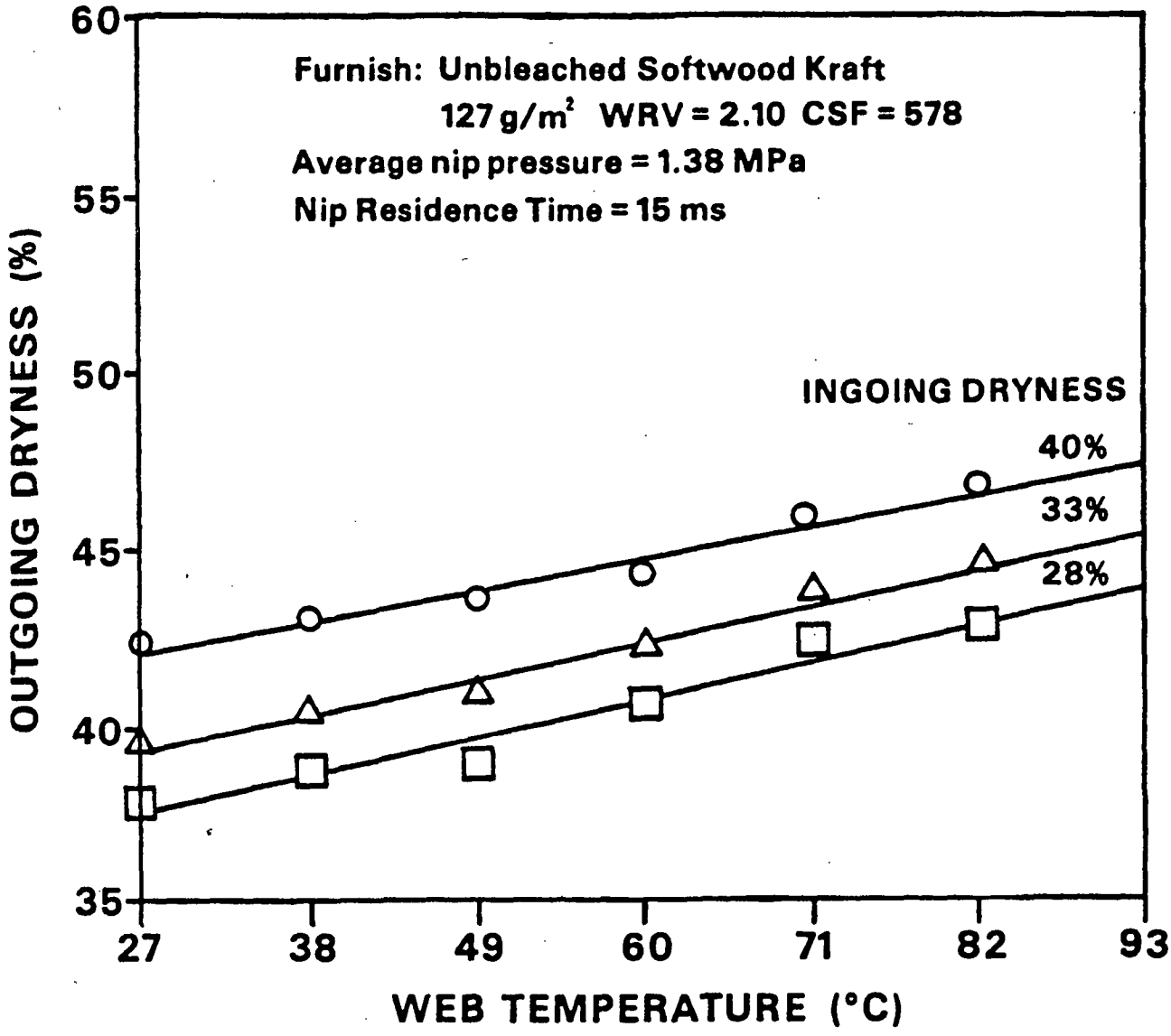

Figure 6. Effect of increased sheet temperature on water removal during wet pressing.[29]

A major effect of temperature is to increase the compressibility of the fiber network through softening of the various fiber components.[30-32] The temperature at which softening becomes important is a function of moisture and dependent on the relative amounts of the particular fiber components.[33] The data in Fig. 7 and 8, assimilated from several studies, show this dependence. Water tends to act as a plasticizer and reduces the softening temperature of the hemicelluloses and lignin. For a moist sheet, the data in Fig. 8 and in

Ref. 33 indicate that the hemicelluloses should soften around 60°C and the lignin at about 100°C.

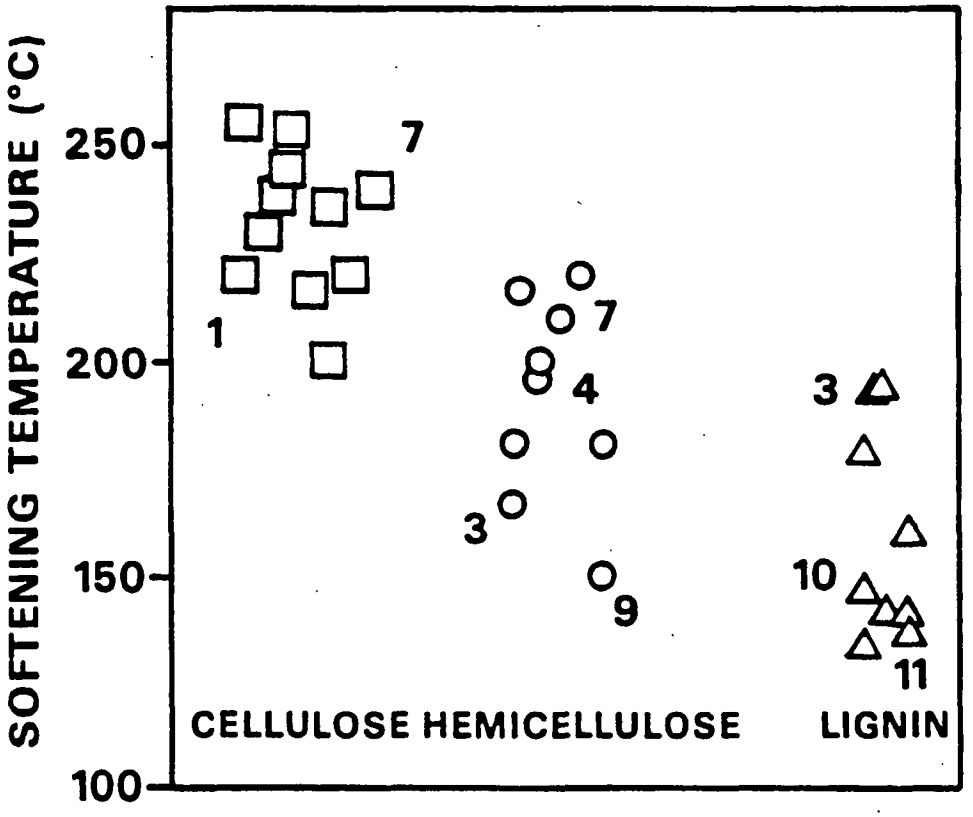

Figure 7. Published data relating to main softening temperatures, i.e., glass transition temperatures under completely dry conditions. The numbers refer to measurements by various authors according to the references in 33.

Another major effect of increased temperature is on the expansion of the fiber network. According to Back,[34] the springback of the web with the release of an applied load falls off rapidly with temperature (Fig. 9). Several pilot studies[35] and commercial applications of hot pressing[36] in which bulk was seen to decrease significantly with temperature support Back's conclusions. Somewhat contradictory evidence was given by Carlsson,[14] who found that sheet expansion in the press nip increases with increasing temperature. Carlsson defended his conclusions with the results in Fig. 10. According to Carlsson, as the viscosity

of the water is decreased with temperature, the back-flow of water into the sheet during expansion is enhanced and the sheet can expand more easily.

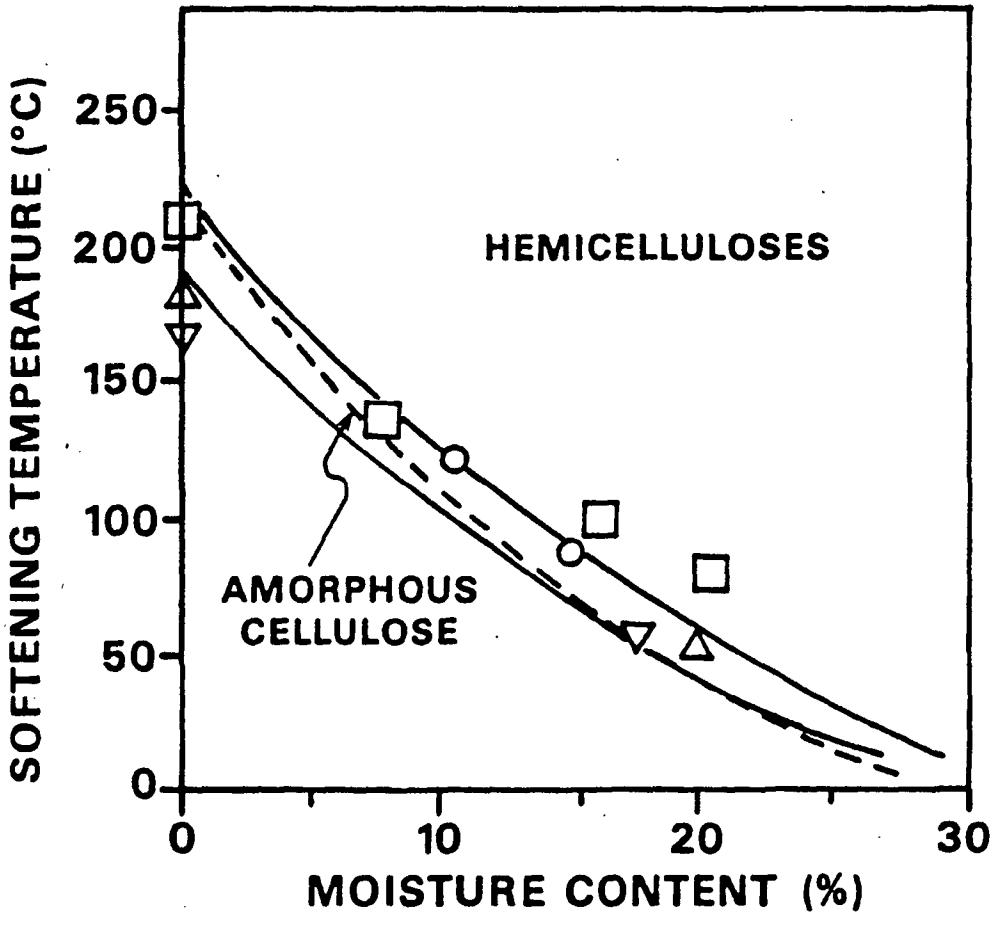

Figure 8. Influence of water on the glass transition temperature of hemicelluloses as calculated using the approach of Kaelble (Ref. 6).[33]

HOT SURFACE DRYING

Hot surface drying is defined as the drying of a moist fiber mat in contact with a hot surface on one side and a cool air stream on the other.[37] Heat is transferred to the sheet by conduction and convection and water vapor is removed from the open surface by the air stream. In conventional paper manufacture, it is estimated that 85% of all paper drying is carried out on cylinder dryers.[38]

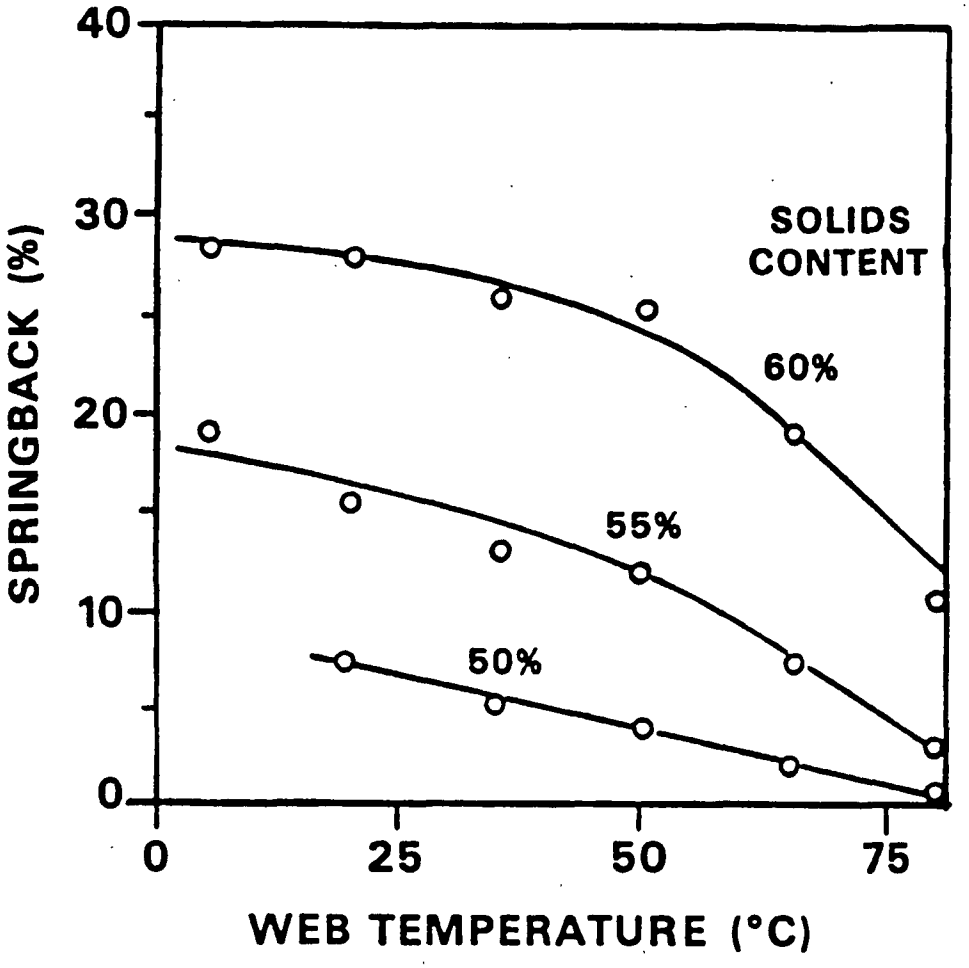

Figure 9. Springback of wet fiber mats on deloading.[34]

In cylinder drying, heat is transferred to the drying cylinder by condensation of steam on the inside surface. Heat is then conducted through an iron wall and out to the paper. Water is evaporated in the sheet at or below the atmospheric boiling point and moves through and out of the sheet by diffusion. Although this process is simple and provides a convenient sink for low pressure steam, it is limited to low drying rates in the range of 15-30 kg/hr-m^2. Use of a low temperature heat source, large thermal resistances to heat transfer, and vapor transport by diffusional flow all contribute to the low drying rates associated with conventional drying. These low drying rates often limit the production of modern high speed paper machines.

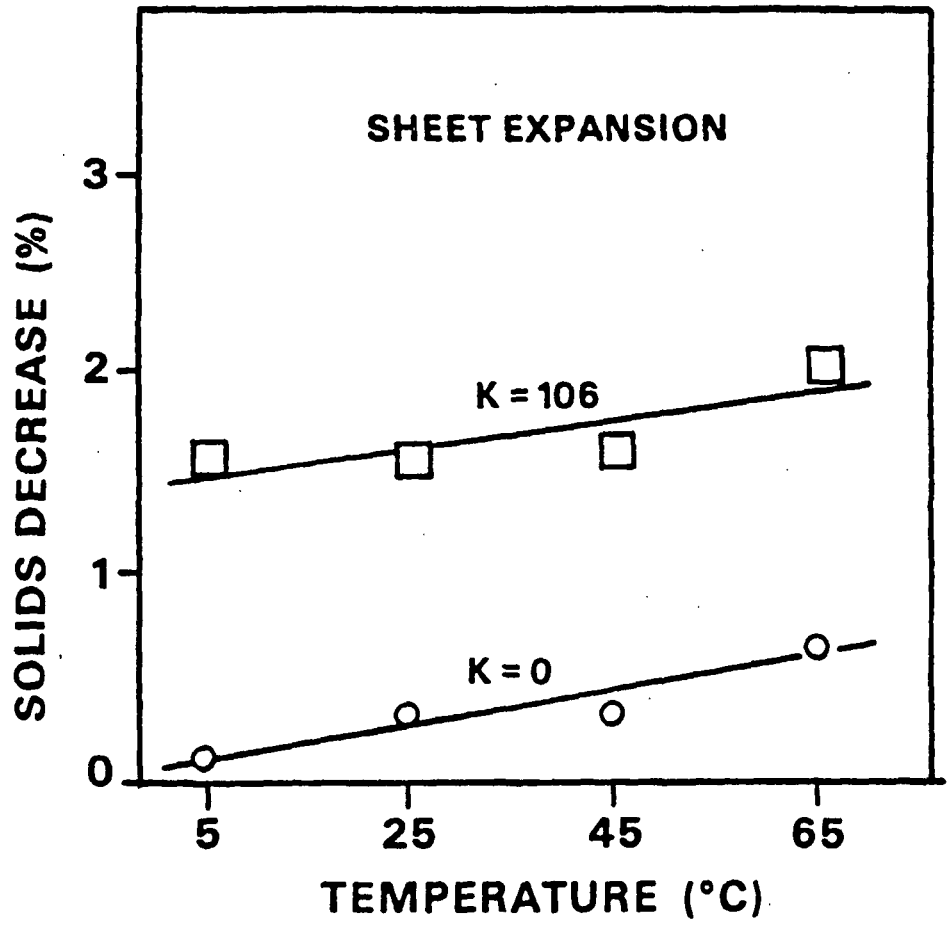

Figure 10. Sheet expansion as a function of temperature for two kraft pulps (kappa = 0, kappa = 106). Initial dryness of 30%, basis weight of 150 g/m^2, and pulse time of 25 milliseconds.

Drying is typically carried out at cylinder surface temperatures of 120-175°C and pressures between 1.5-5.0 kPa. Although mild, the process is effective in retaining the density developed in the press section.

The drying process in conventional cylinder drying is often viewed as consisting of three major periods: a warm up period, a constant rate period, and a falling rate period. Sensible heating of the sheet is the main activity during the warm up period which continues until a maximum evaporation rate has been established. The constant rate period is characterized by a slightly decreasing

evaporation rate. As the surface region of the sheet dries out, the drying rate decreases rapidly. This period is known as the falling rate period.

The Dreshfield-Han Model of Hot Surface Drying

Hot surface drying has been investigated extensively;[39] most notably by Dreshfield and Han,[37] Han and Ulmanen,[40] and Cowan.[41] The most widely accepted qualitative model of hot surface drying is attributed to the work of Dreshfield and Han.[37] Dreshfield showed quantitatively, using a beta-ray transmission technique, the internal movement of water in the web during drying. He also used a dye migration technique as a qualitative tool for identifying the direction of water movement and the zones of evaporation and condensation within the sheet. These studies, combined with measured sheet temperature profiles, provided the basis for developing a qualitative model of the constant and falling rate periods during hot surface drying. Figure 11 is an illustration of the Dreshfield-Han model.

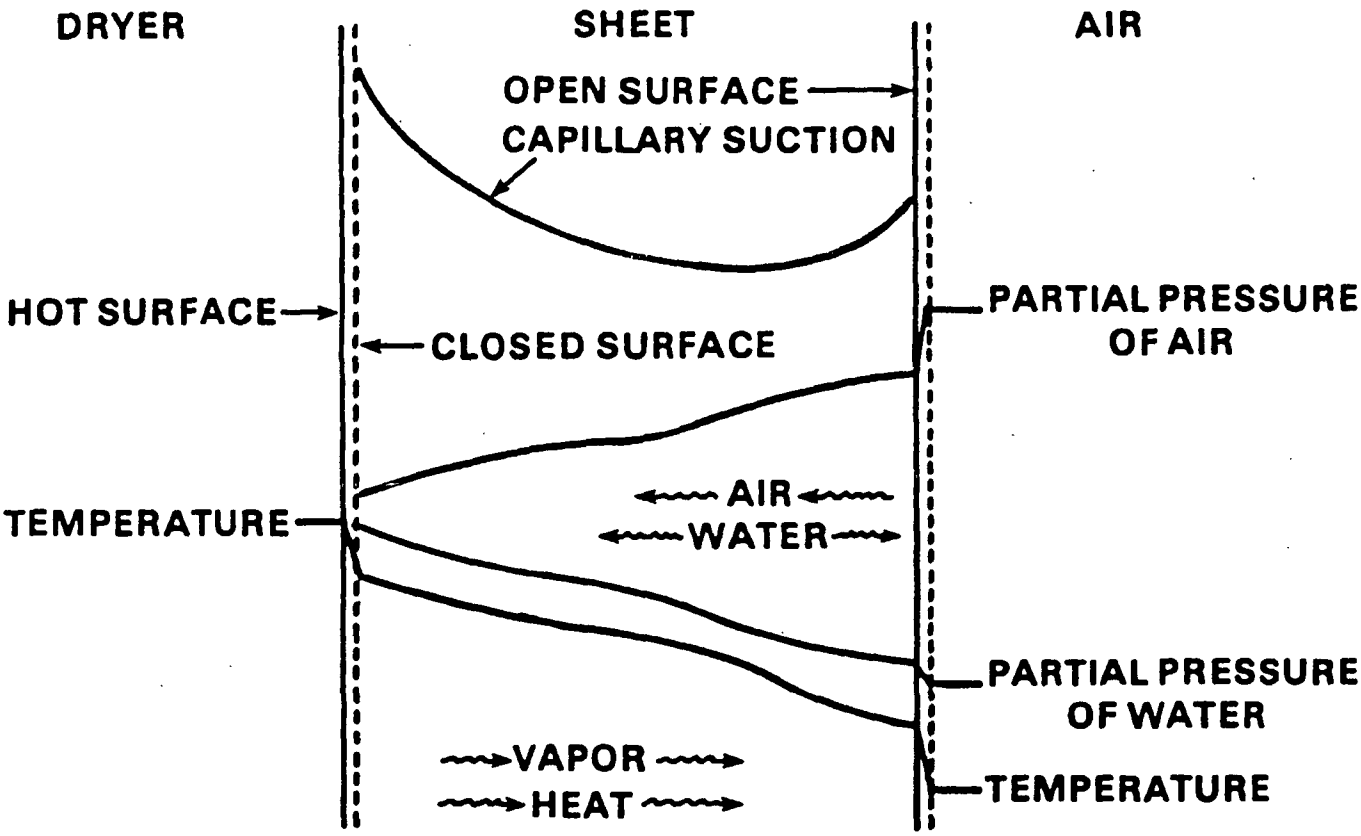

Figure 11. Dreshfield-Han model of hot surface drying during the constant rate period.[37]

During the constant rate period, vaporization occurs at both the heated and open surfaces. The evaporated water diffuses toward the open surface under a partial pressure gradient. As the vapor passes through the sheet it encounters cooler regions and condensation of some vapor occurs. At the same time, water movement is induced by capillary suction toward both surfaces where vaporization takes place. These vaporization-condensation cycles continue to occur throughout the drying process.

The falling rate period starts at a "critical" moisture content due to the presence of a dry layer next to the hot surface. It should be noted, however, that the critical moisture content is not a fundamental property but a parameter which changes with drying conditions as well as with the treatment of the furnish.[39] In this period, the front of vaporization continues to move away from the hot surface. In both periods, heat is transferred through the sheet partly by vapor diffusion and partly by conduction.

Other drying studies[40-41] have further established the Dreshfield-Han model. Cowan,[41] working with a simplified system of glass fibers concluded that during the constant rate period, hot surface, internal, and open surface evaporation contribute almost equally to the overall drying rate. In the falling rate period, however, Cowan found the internal evaporation to account for 60-70% of the overall drying rate.

Contact Resistance

The thermal resistance between the heat source and moist sheet is a major contributor to low drying rates in cylinder drying. Review of literature values for various thermal resistances to heat transfer indicate that the contact resistance accounts for 30-60% of the total resistance to heat transfer.[33]

The contact resistance to heat transfer is a measure of the intimacy of contact between the sheet and the hot surface and the rate at which heat is transferred. If the thermal resistance is high, the heat flux is low and the contact poor. Holm,[42] using a modified Chapman printing smoothness tester, measured the degree of surface contact between a wet web and hot surface at various moisture contents under low pressures. At dryness levels above 50%, he found that only 5% of the sheet surface was in contact with the hot surface. If this holds for conventional cylinder drying, then the actual contact through most of the dryer section is small.

The contact coefficient is not only a function of the surface characteristics of the sheet and hot surface, but also of the air layer between the two. Riddiford,[43] in a mathematical analysis of airflow between a paper sheet and dryer surface, concluded that for low felt-paper tensions, an air gap can exist which would cause a significant reduction in the average drying rate. He estimated that for a 1.5 m diameter drying cylinder running newsprint at 600 m/min and a web tension of 5.2 N/cm, an air gap of approximately 0.15 mm would exist along a distance of about 8 cm.

The contact coefficient can be significantly improved by increasing felt tension, hot surface temperature, and sheet moisture content.[44] Figure 12 is a plot of heat transfer contact coefficient against moisture content for different surface temperatures at two felt tensions. These data, reported by Redfern,[44] show a 50% increase in the contact coefficient when the felt tension is increased from 4.4 to 22.1 N/cm.

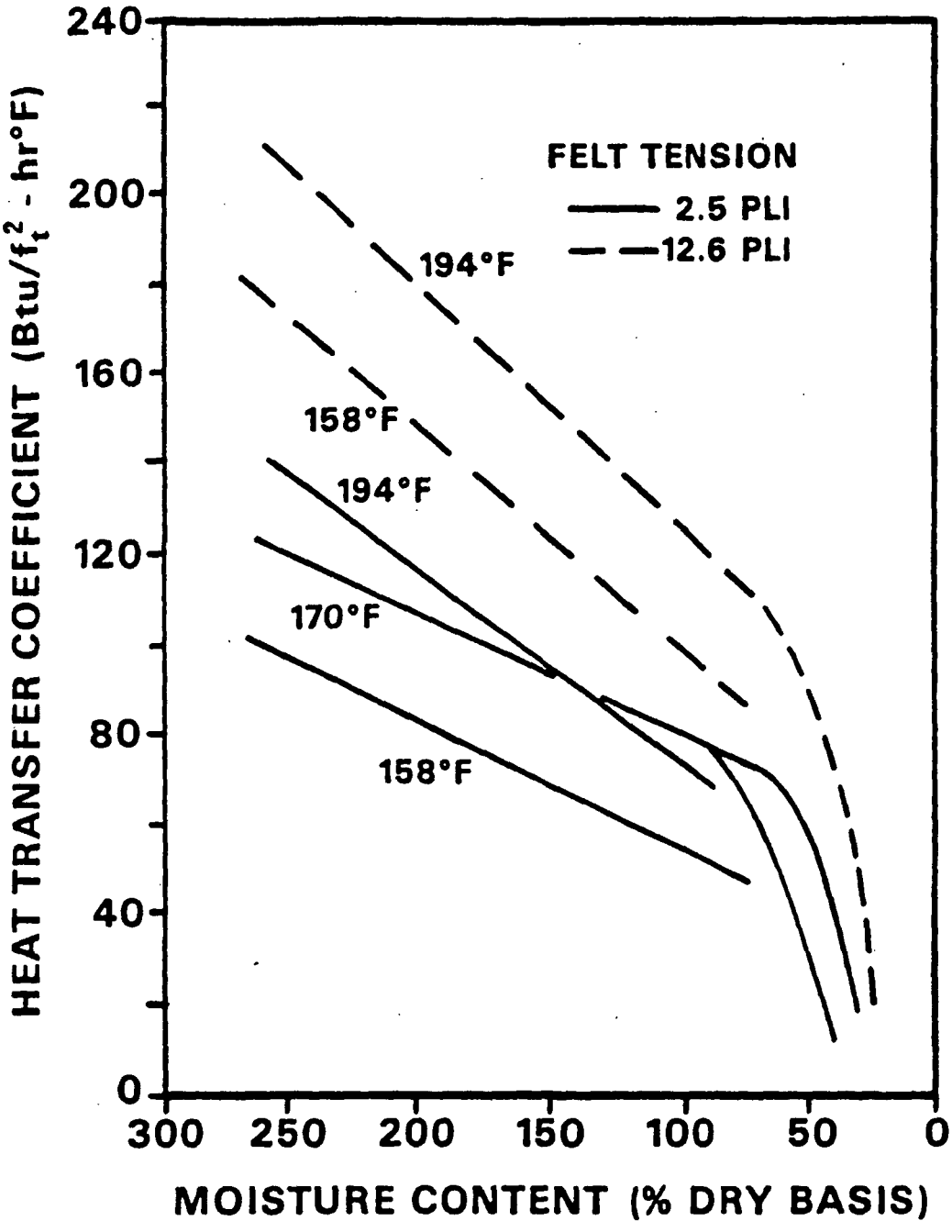

Figure 12. Heat transfer contact coefficient as a function of moisture content for different temperatures at two felt tensions.[44]

Vapor Movement During Hot Surface Drying

Dreshfield[37] viewed vapor movement as a sequence of vaporization-condensation cycles. He assumed that a liquid-vapor equilibrium exists everywhere in the fiber mat. As the vapor moves away from the hot surface it condenses in cooler regions of the sheet, transferring latent heat. Cowan,[41] using experimental techniques similar to Dreshfield but using glass fiber mats, further demonstrated this cycle of internal evaporation and condensation.

Holm, et al.[45] have suggested, based on results of a computer simulation of drying, that bulk vapor flow could be an important vapor transport mechanism. They postulated that when the sheet reaches the saturation temperature during drying, a significant amount of vapor could be transported by bulk, pressure-induced vapor flow through the sheet.

Ahrens, et al.[46] studied hot surface drying temperatures up to 240°C and applied pressures up to 30 kPa. A large increase in the average drying rate was observed as the sheet temperature approached the boiling point. These results are given in Fig. 13. The increase in drying rate was attributed to a change in the vapor removal mechanism from diffusion to bulk vapor flow. They called this drying process, where vapor removal is driven by a total pressure gradient rather than a partial pressure gradient, "high intensity" drying. Recent laboratory studies[47,48] have demonstrated the development of a total vapor pressure driving force at the hot surface-sheet interface.

IMPULSE DRYING

Impulse drying refers to water removal from a moist fiber web as it passes through a high temperature press nip. This new process, which combines elements of both wet pressing and hot surface drying, is usually bounded by nip

temperatures of 150-500°C, pressures between 0.3-7.0 MPa, and residence times up to 100 milliseconds. This combination of intense, short duration conditions produces heat transfer and water removal rates substantially higher than those attained in conventional drying processes.

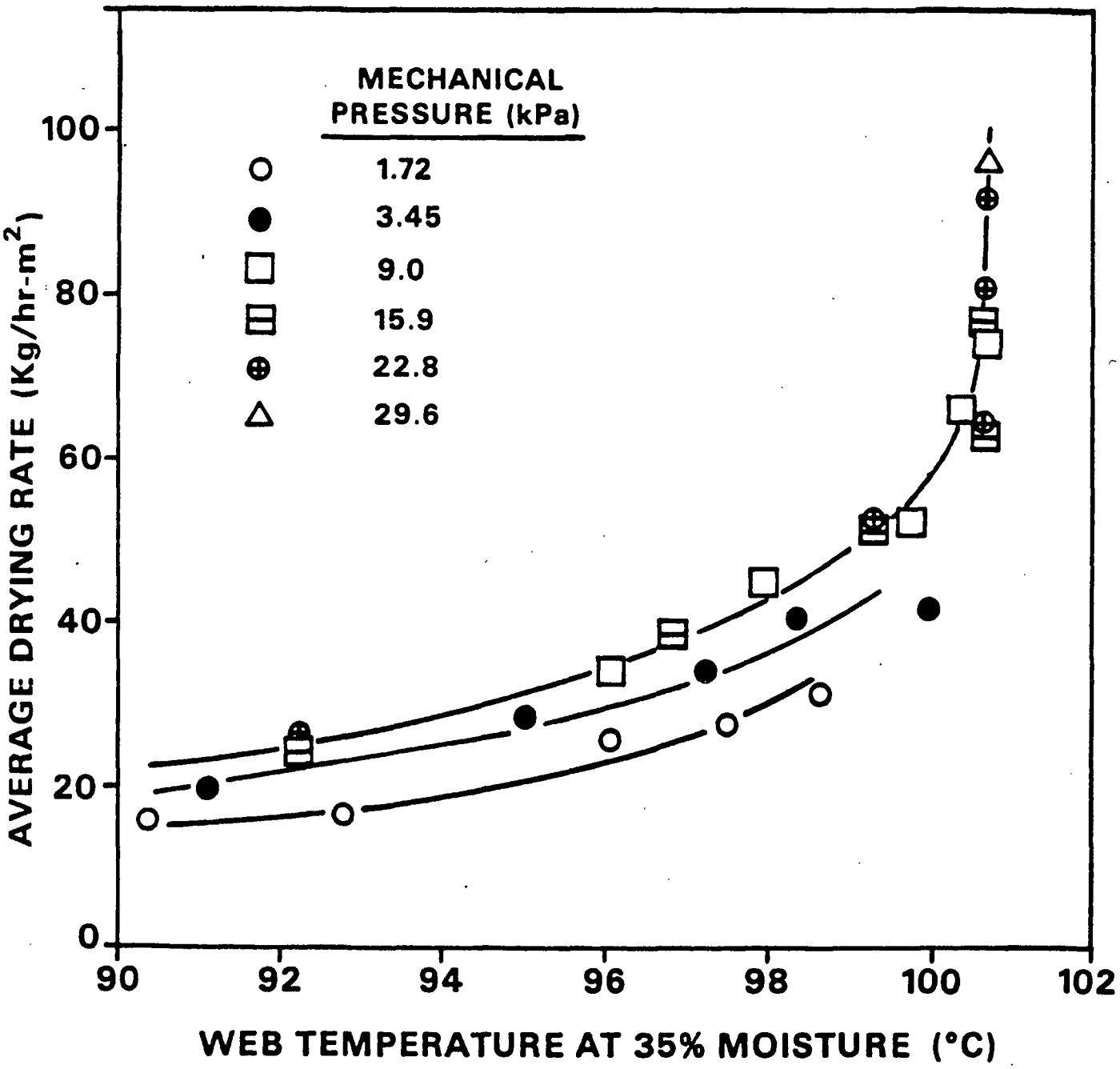

Figure 13. High intensity drying.[46] Increase in drying rate correlated with a typical sheet temperature.

Wahren[49] first proposed the impulse drying process in the late 1970's. However, it wasn't until 1981 that any data were published[5] that demonstrated the potential effectivenes of impulse drying. Further investigative work at The Institute of Paper Chemistry by Burton,[6] and Arenander and Wahren[7] continued to explore this new process. Results from this early work (Fig. 14) included water removal rates up to 50,000 kg/hr-m^2 and dryness increases of 20% or more.

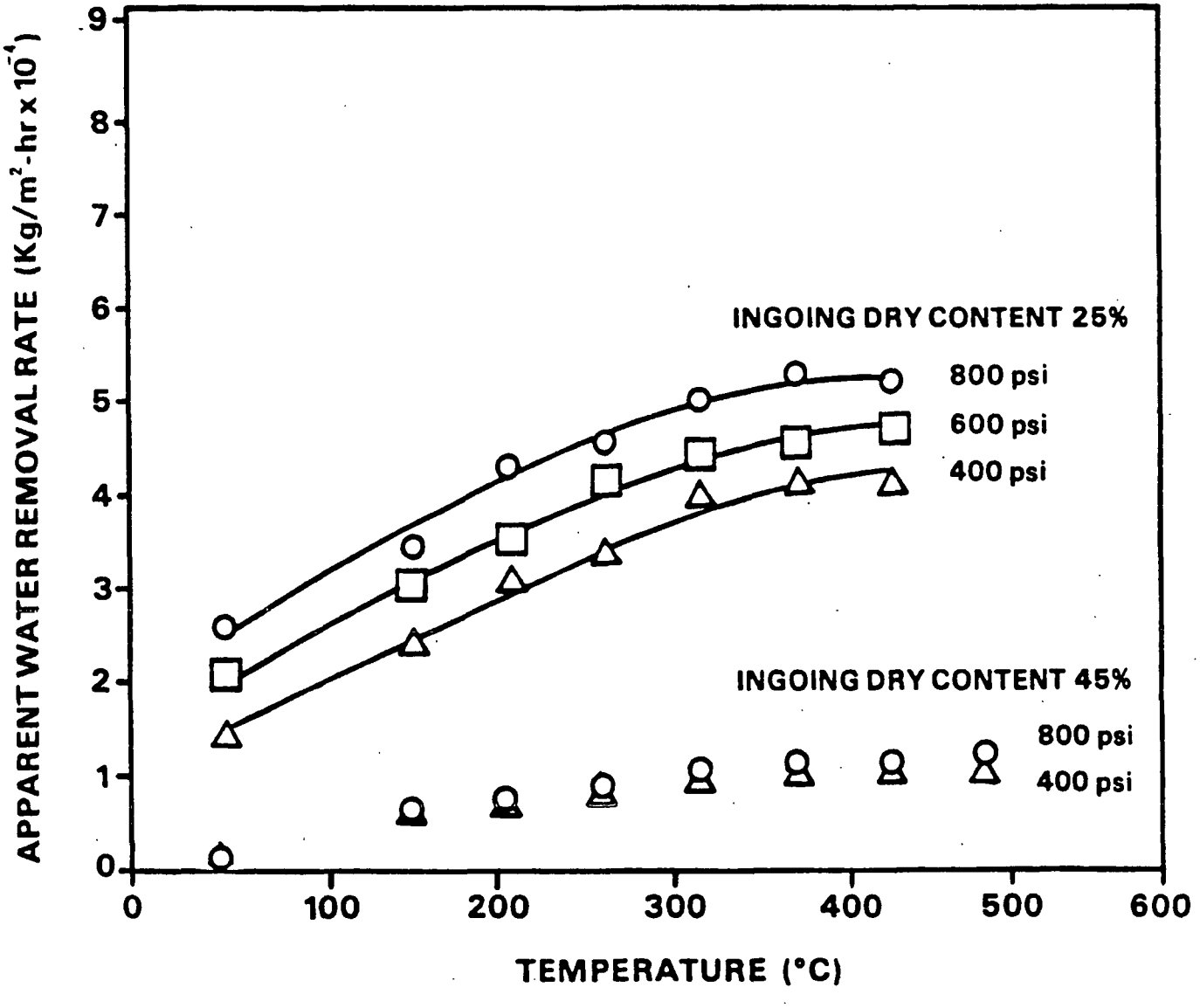

Figure 14. Water removal rates for impulse drying.[7]

In a recent overview of impulse drying, Sprague[1] presented some impressive experimental results: dewatering rates 100-1000 times those for cylinder dryers, specific energy use 1/3 to 1/2 that for conventional drying, and significant improvements in paper properties, particularly strength. The paper property improvements were strongly correlated with the density development.

Sprague noted that the water removal rate is a strong, essentially linear function of the hot surface temperature divided by the square root of the nip residence time. This relationship is shown in Fig. 15. Applied pressure only has a small effect over the range examined (1-5 MPa).

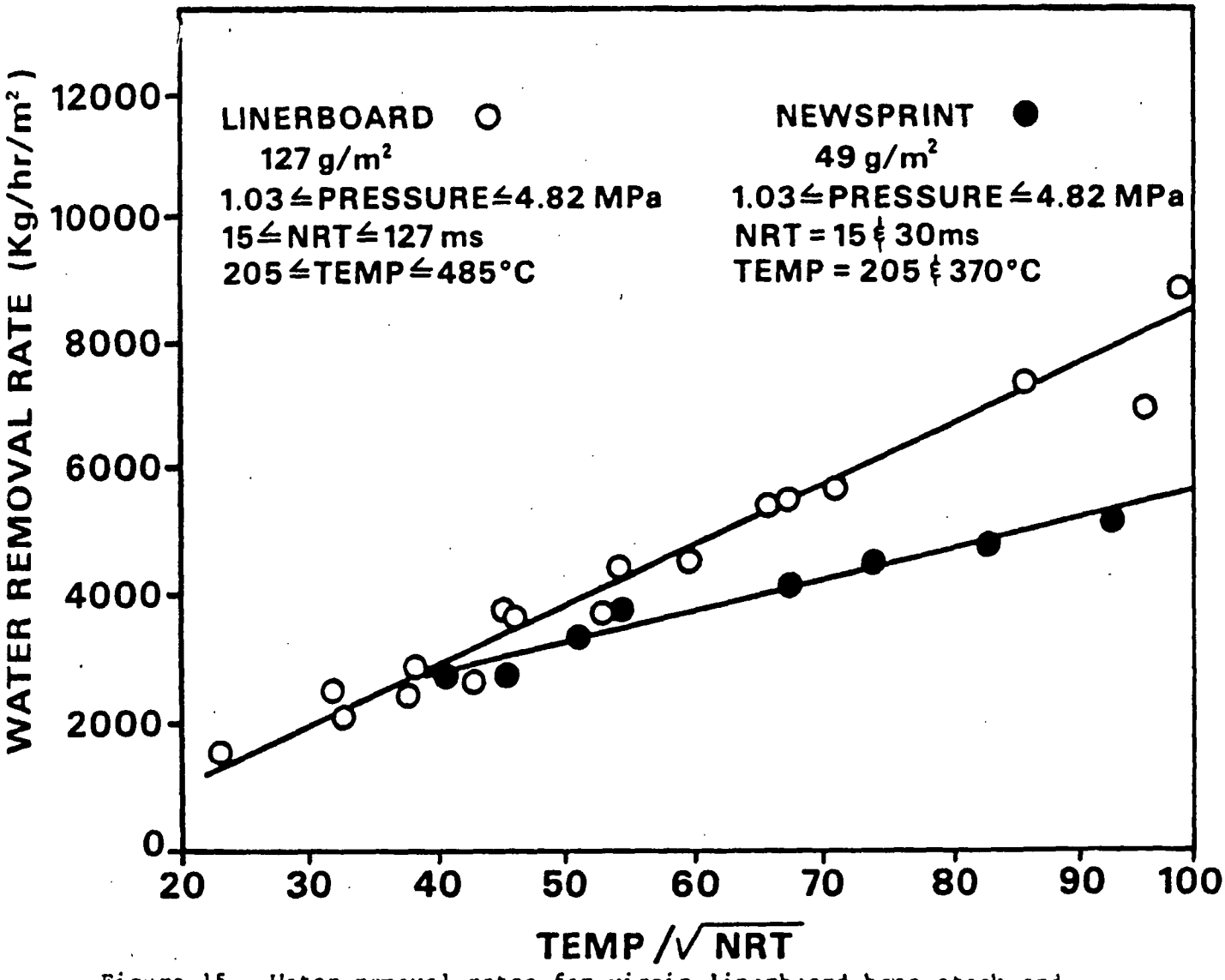

Figure 15. Water removal rates for virgin linerboard base stock and newsprint as a function of $T/(NRT)^{1/2.1}$

Liquid dewatering is seen to comprise a large fraction of the total water removed during impulse drying (Fig. 16). According to Sprague,[1] "a thermally augmented wet pressing effect and displacement or entrainment of liquid water by bulk vapor flow facilitate this liquid removal." Preheating the sheet further increases the total dewatering by as much as 60%, with almost all of the increase occurring as liquid dewatering.

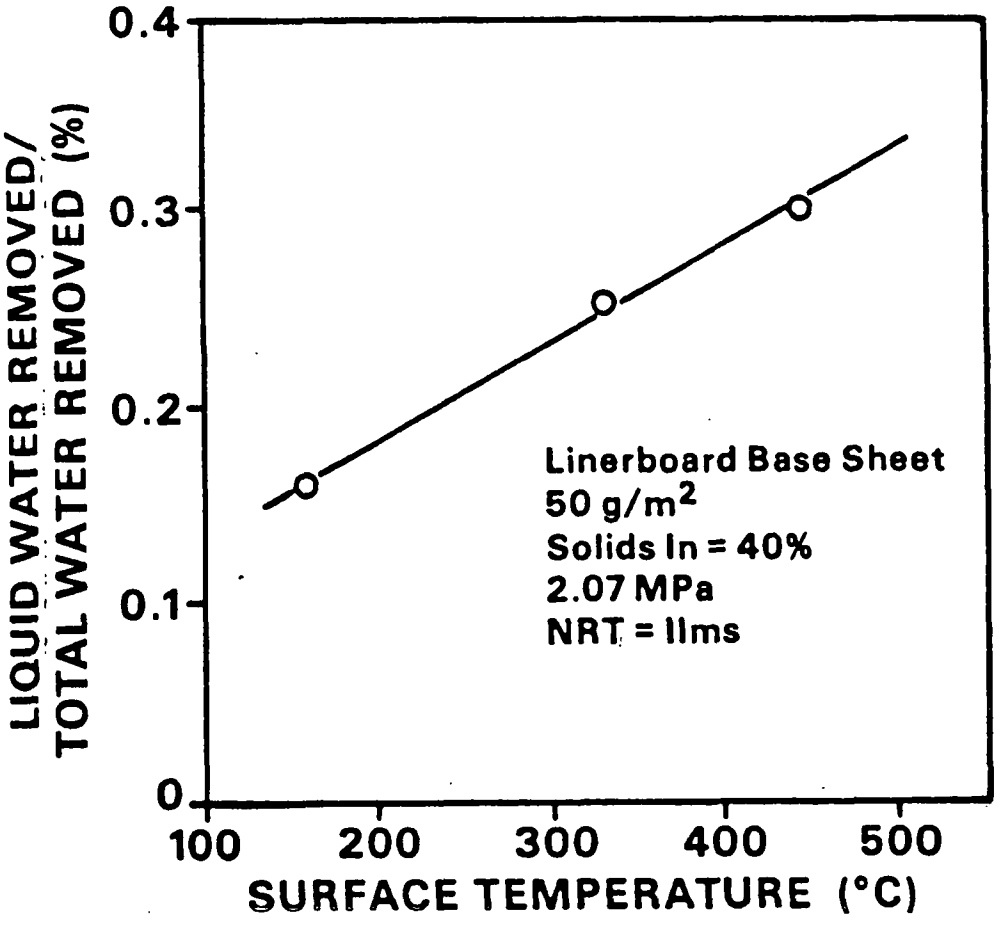

Figure 16. Liquid water removal in impulse drying.[50]

Impulse drying results in high average density values. For impulse dried linerboard, increases in average density of over 40%, compared to conventionally dried linerboard, are observed. As seen in Fig. 17, density development is very

dependent on thermal impulse and applied pressure. Thermal impulse is defined as the area under the temperature-time curve.

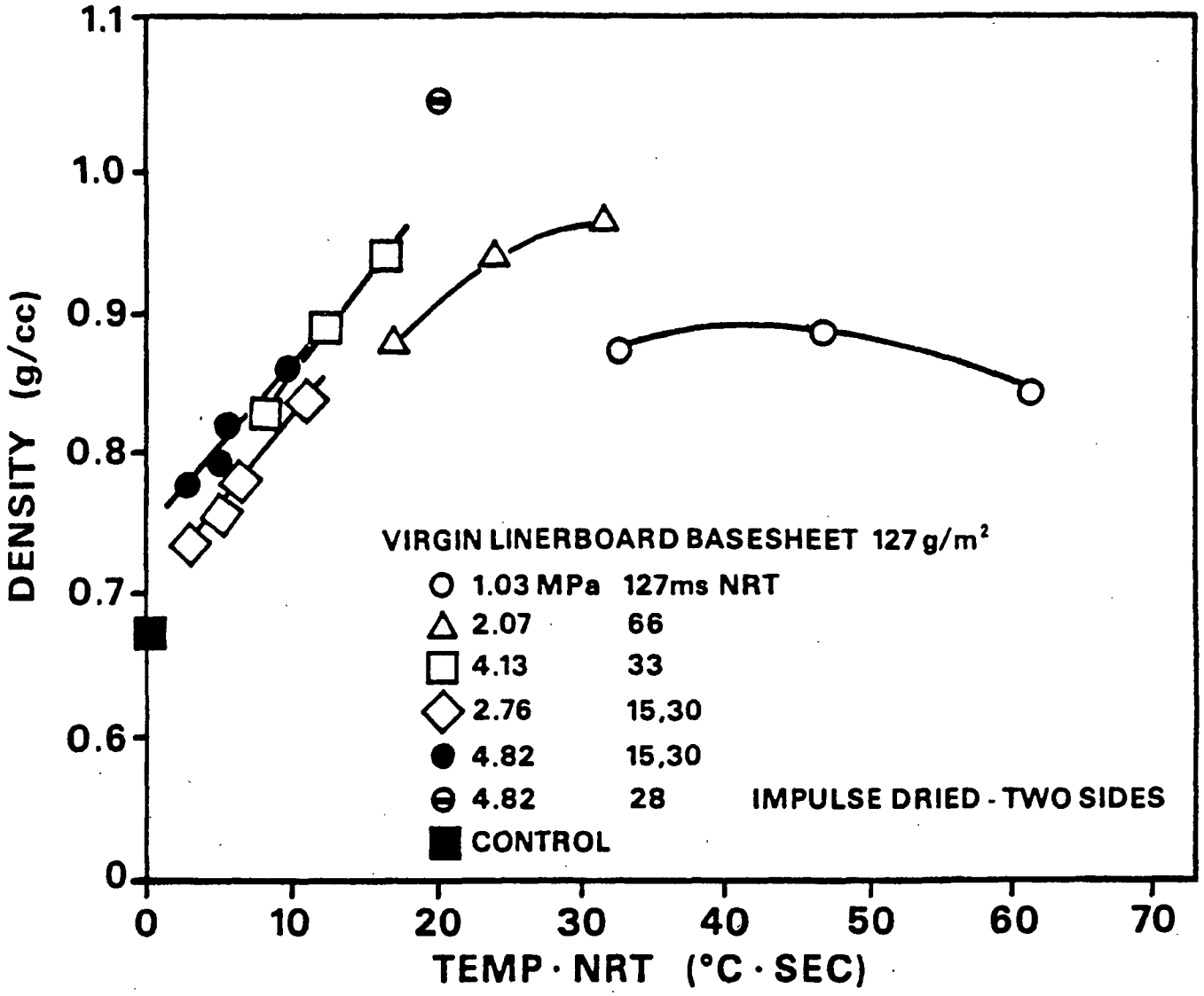

Figure 17. Density development for virgin linerboard base sheet as a function of thermal impulse.[1] Control represents conventional wet pressing and drying conditions.

The improved strength properties reported by Sprague are due to this increase in average sheet density. Increases in strength that usually accompany density increases are well documented. However, the ability of impulse drying to promote bonding, even for high yield or poorly bonding furnishes is unusual.

This ability is illustrated in Fig. 18 in the comparison of three linerboard furnishes;[1] virgin linerboard, recycled linerboard, and 75% yield CMP.

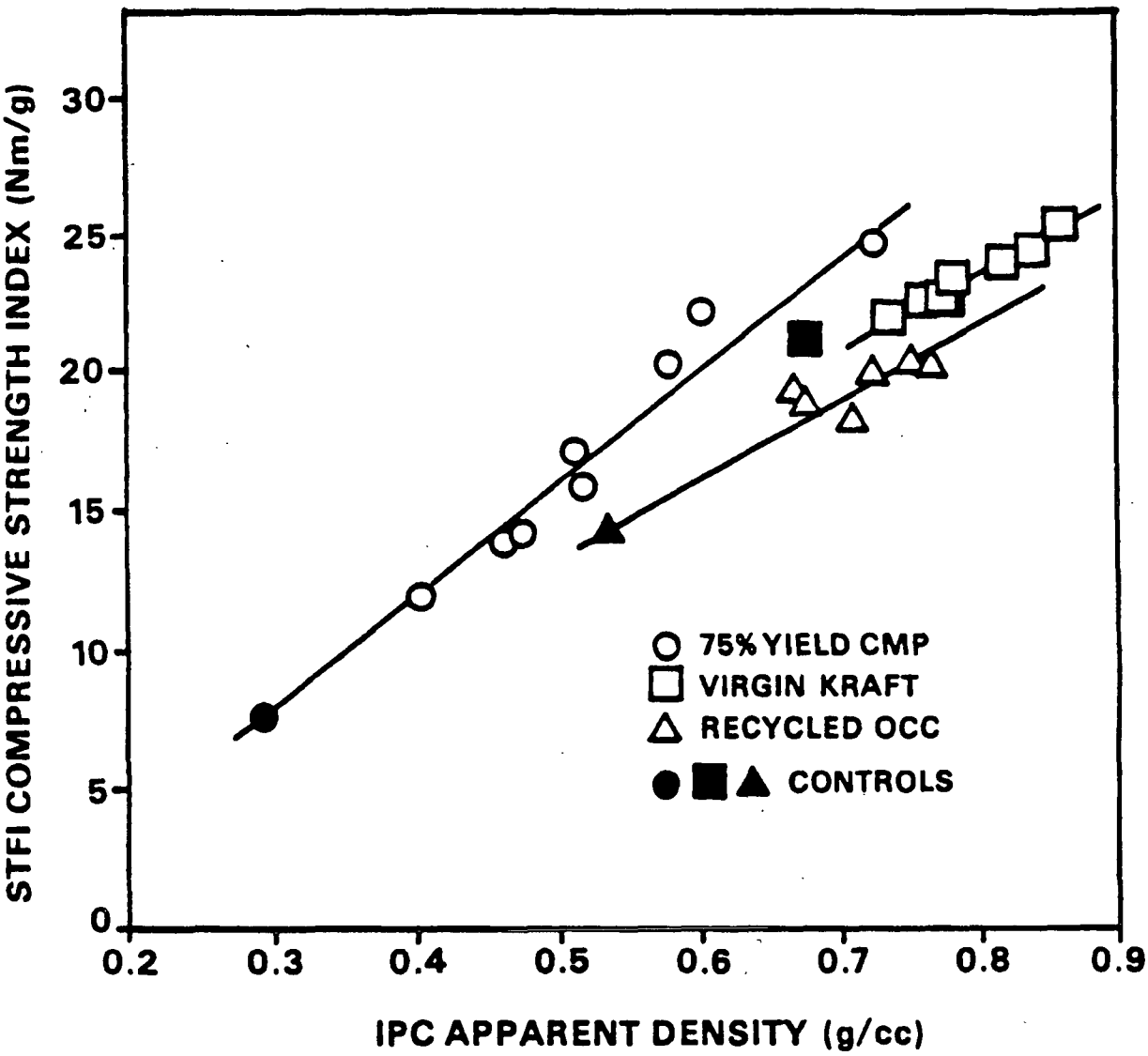

Figure 18. Comparison of compressive strength-density relationships for various linerboard base sheet furnishes, impulse dried.[1] Controls represent conventional wet pressing and drying conditions.

Impulse drying appears to be a promising, commercially viable process with the potential to dramatically alter the current papermaking process. The process appears to involve intense dewatering and densifying mechanisms which result in

high heat transfer and water removal rates, and significant increases in average sheet densities when compared to conventional drying processes. Most of the experimental studies to date on impulse drying have dealt with performance evaluation. A clear lack of understanding of the dynamic physical processes occurring in the sheet during impulse drying is evident.

PROBLEM STATEMENT

Impulse drying results in high average density values and in very nonuniform z-direction density profiles. The densifying forces are believed to create a J or U shaped profile, with the greatest density near the hot surface. The experimental work presented in this thesis is aimed at understanding the process of density profile development under impulse drying conditions and determining the mechanisms responsible.

EXPERIMENTAL

APPROACH

Early exploratory investigations demonstrated that impulse drying was a very effective means of water removal.[5-7] However, there was a clear lack of experimental work being directed at understanding the dynamics of the process. In an effort to help fill this void, this thesis was proposed to investigate the density development in the web during impulse drying and to determine the mechanisms responsible. Because of the unique interdependency between water removal and densification, it was believed that this thesis would also lead to identification of dewatering mechanisms as well.

When this thesis was formulated, it was believed that in order to truly understand the process of density development, the response of the fiber network to densifying forces should be directly observed. This conviction was further strengthened by MacGregor's description of the process he termed stratification.[20] He defined this process as the change in vertical distribution of sheet fiber and filler material resulting from the fluid shear force development during the dynamic wet pressing process. MacGregor described the expected compression response of an idealized sheet divided into twelve regions of equal basis weight. At that time direct observation or measurement of such an event had yet to be accomplished. By combining the experimental results of Chang[12] with fundamental concepts of flow in compressible porous media, MacGregor was able to describe in detail the probable compression response of the individual fiber regions to the mechanical and fluid shear forces that occur during pressing. With this in mind, the development of an experimental system, capable of measuring what MacGregor visualized, was planned. This system would include the direct

measurement of the instantaneous compression response of three individual sheet regions from which information on dewatering and densifying mechanisms would be derived.

To accurately determine a density profile in a moist sheet of paper which is being compressed to thicknesses ranging from 0.125-0.635 mm, under compressive loads of 7 MPa or more, and at time intervals as small as 4 ms, is a considerable undertaking. The measurement system should be fast, precise, thermally stable, and should not interfere with the fiber network or the fluid flow. Furthermore, the system should differentiate between various regions in the sheet to obtain a suitable profile.

Realistically, possible methods for determining dynamic density profiles would interact with the sheet and would, to some extent, disrupt the fiber network. In order to differentiate between sheet regions, thicknesses of fiber regions of known basis weight would have to be accurately determined. Only one measurement system was considered capable of approaching the requirements of the ideal system outlined above. This was the inductive measurement system used by Chang[51] for total sheet thickness measurements. Chang's measurement system is illustrated in Fig. 19. The transducers, mounted in the pedestal, track the displacement of targets placed on either side of the sheet. These targets include a flat steel disk on the open felt surface and a flat steel screen between the felt and paper. Total sheet density is calculated from target separation and sheet basis weight.

It was believed that Chang's technique could be extended to determine a density profile by using multiple targets placed at various levels in the sheet. A major problem of the method is that the target thickness is large in comparison

to the sheet. This introduces an unknown amount of error into the sheet thickness determination.

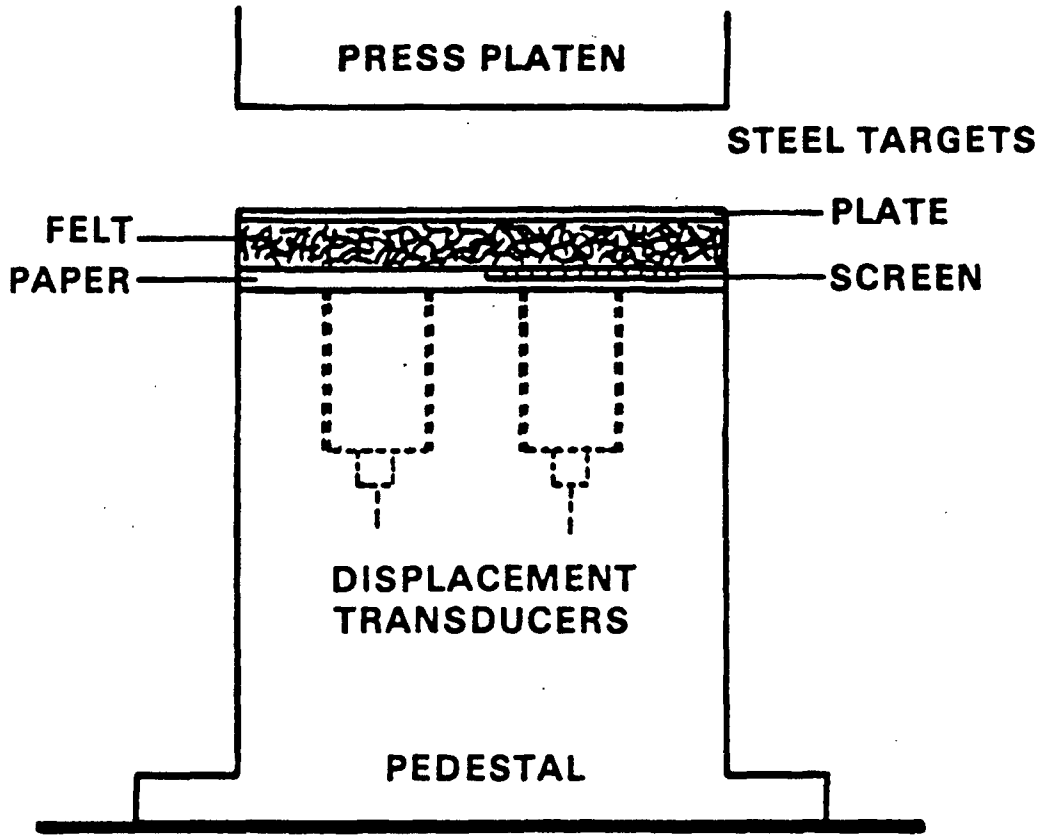

Figure 19. Experimental nip used by Chang in the instantaneous measurement of sheet thickness during wet pressing.

In addition to the density profile determination, instantaneous measurements of platen surface temperature, sheet temperature profiles, hot surface vapor pressure, and applied mechanical pressure were planned to aid in understanding the densifying forces. The applied mechanical pressure would give the total compressive force being applied to the sheet. Recall that this force is borne by both the fiber network and fluid within the fiber network. The instantaneous heat flux to the sheet would be calculated from the platen surface temperature history during impulse drying, and the total energy transferred to the sheet would be calculated from the integral of the heat flux determination.

These data should contribute to a better understanding of heat transfer mechanisms. Similarly, instantaneous sheet temperature profiles should give detailed information on heat transfer and moisture movement within the sheet. The hot surface vapor pressure would provide a direct measurement of a driving force for water removal and densification.

An outline of the research program that was followed in this thesis is presented in Fig. 20. Development of the experimental system constituted a major portion of the program. Once the system was determined to be working properly a dynamic density development study was initiated to investigate the density development under impulse drying conditions. As a basis for comparison, wet pressing runs were also made. The density development study consisted of determining density profiles as a function of sheet moisture, hot surface temperature, flow resistance, basis weight, nip residence time and applied mechanical pressure. The sheet structure was then studied by determining static density profiles in the sheet after impulse drying and by qualitative examination of the sheet structures on the fiber level with the Scanning Electron Microscope (SEM). The last phase of the research program consisted of the measurement of sheet temperature profiles in the web as a function of hot surface temperature. A compilation of the experimental conditions examined is presented in Appendix II.

EXPERIMENTAL SYSTEMS

Impulse Drying Simulation

Impulse drying is considered an extension of wet pressing in which one of the press rolls is elevated to a high temperature. Hence, a simple wet pressing simulator operated with one heated pressing surface (Fig. 21) suffices for the study of impulse drying. The press, known as a Wahren-Zotterman falling-weight

press-nip simulator,[52] has been shown in a comparative study to accurately duplicate press nip impulse characteristics.[53] Pressure profiles, pressure rise rates, impulses, rates of caliper change, and stress strain comparisons all show good agreement between the pilot press and the simulator.

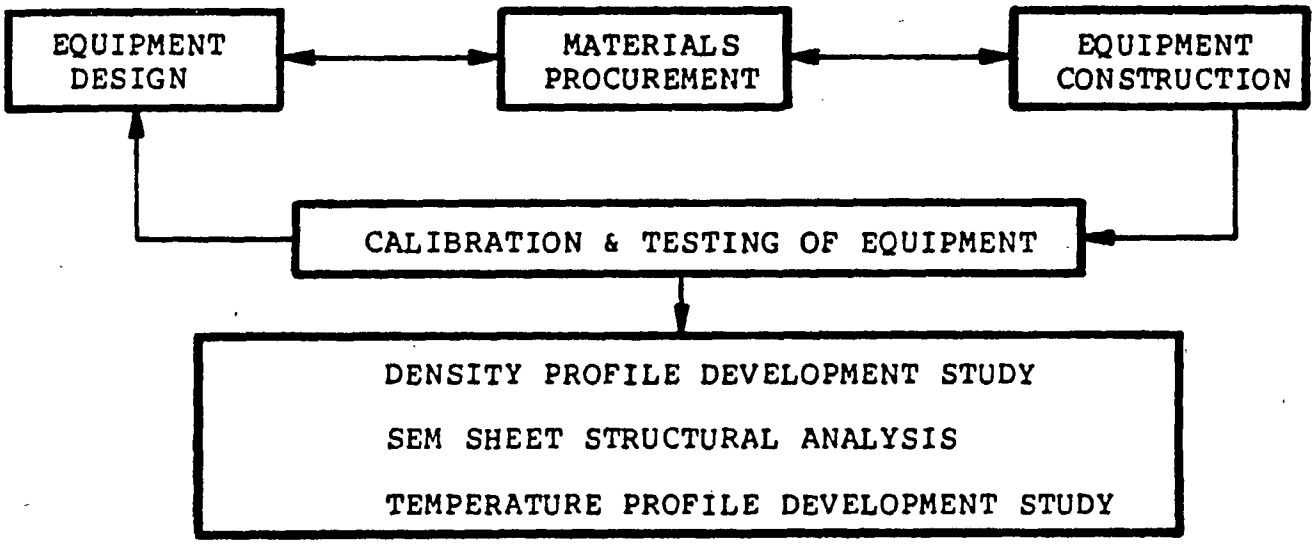

Figure 20. Outline of research plan followed in thesis.

The major differences between the simulator and roll press lie in the geometries of the two systems. In the roll press nip the caliper is forced to be symmetrical around a point of minimum clearance between press rolls.[51] As a consequence, the direction of water flow in the sheet is a combination of lateral and transverse movement. For the simulator, the entire sheet is pressed between parallel plates so the water flow is predominantly in the transverse direction.

Operation of the apparatus depicted in Fig. 21 is simple; the heated platen is released from a specified height, falls and impacts a wet sheet, compressing it against the stationary pedestal. The platen rebounds and is caught on the rise by an air driven brake system to prevent a second impact. The resulting

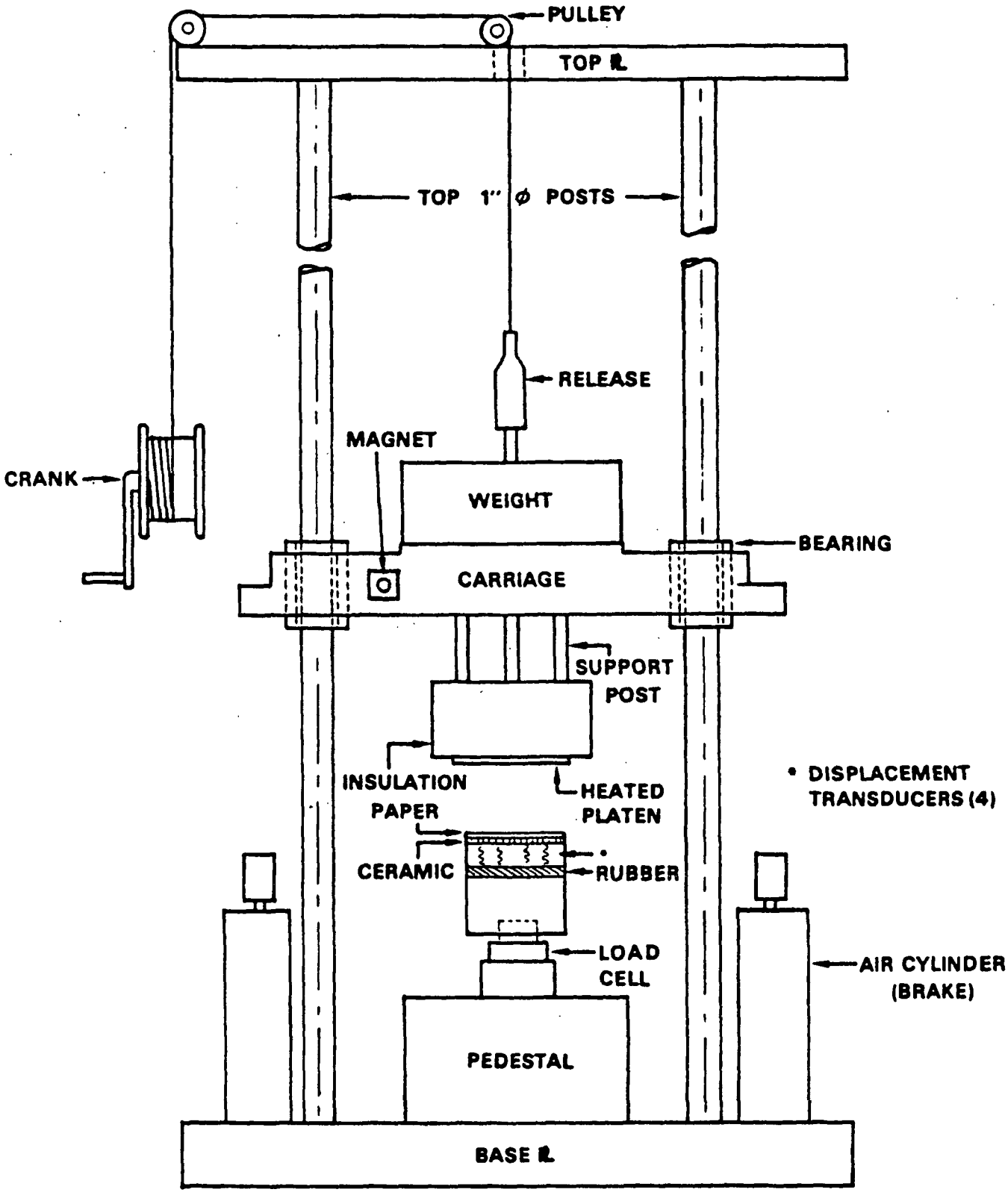

Figure 21. Schematic of impulse drying simulator used in experimental studies.

pressure-time relationship is typical of that seen in a roll press nip. This relationship may be altered by adjusting the drop height and weight and by the choice of elastic material placed in the pedestal.

Press Platens and Instrumentation

Two separate data acquisition systems are used. A schematic of the electronics system is shown in Fig. 22. Signals from the displacement transducers and sheet thermocouples are acquired with a Tracor Northern TN-1710 system, while signals from the surface thermoprobe, vapor pressure transducer, and force transducer are acquired with a Tec Mar A/D system. Both systems are interfaced with an Apple computer for data storage and manipulation. All data are eventually stored on a Burroughs B6900 mainframe for further plotting and analysis. Data collection by both systems is initiated simultaneously by a magnetic sensor activated by the falling carriage.

Figure 23 is a schematic of the press platens used in the impulse drying simulation. The upper platen is electrically heated and is attached to the falling carriage assembly. It is constructed of a high purity iron (99.63% Fe) and insulated with 2.5 cm thick Marinite XL structural insulation. The surface of the head is plated with a 0.76 μm layer of chromium. The calculated temperature drop across this layer is small compared with the total temperature drop of the hot surface during a typical impulse drying event. The platen is instrumented with a vapor pressure transducer and a surface thermoprobe. The entire system is designed for temperatures up to 500°C.

The vapor pressure transducer, a Kaman KP-1910 high temperature series which can operate at temperatures to 540°C and pressures to 7.0 MPa, is used to measure the vapor pressure at the hot surface/paper interface. The sensor is an

eddy current type that utilizes impedance variation to measure either static or dynamic pressure. Output is an analog voltage that is directly proportional to the applied pressure. The sensor is mounted in the heated platen approximately 3.2 mm from the hot surface. Twenty 0.38 mm diameter holes connect the measurement chamber to the platen surface. Sizing of the measurement chamber/holes was based on the results of a compressible flow model. The model, which considered frictional effects of compressible flow into the measurement chamber, is presented in Appendix I.

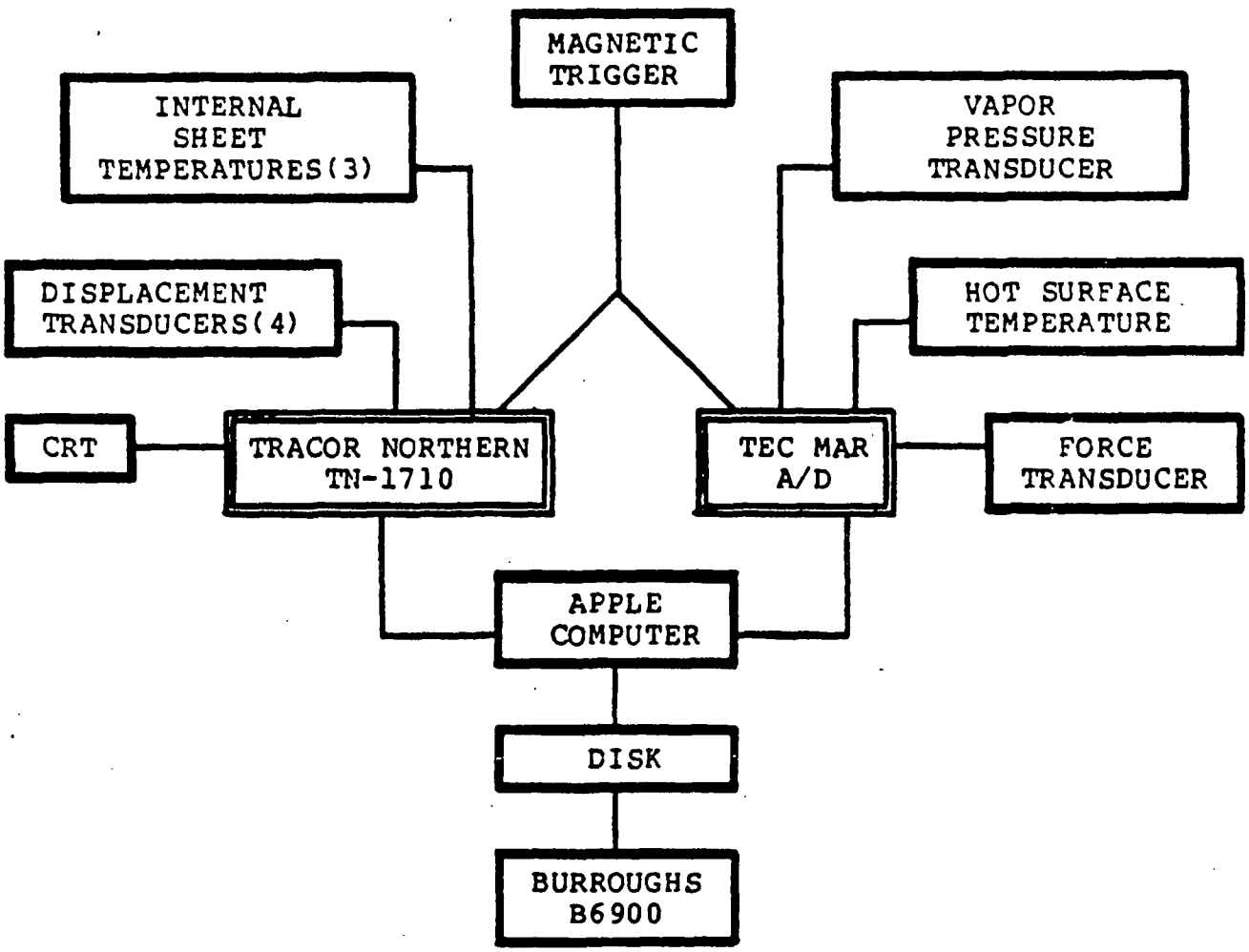

Figure 22. Schematic of electronics system.

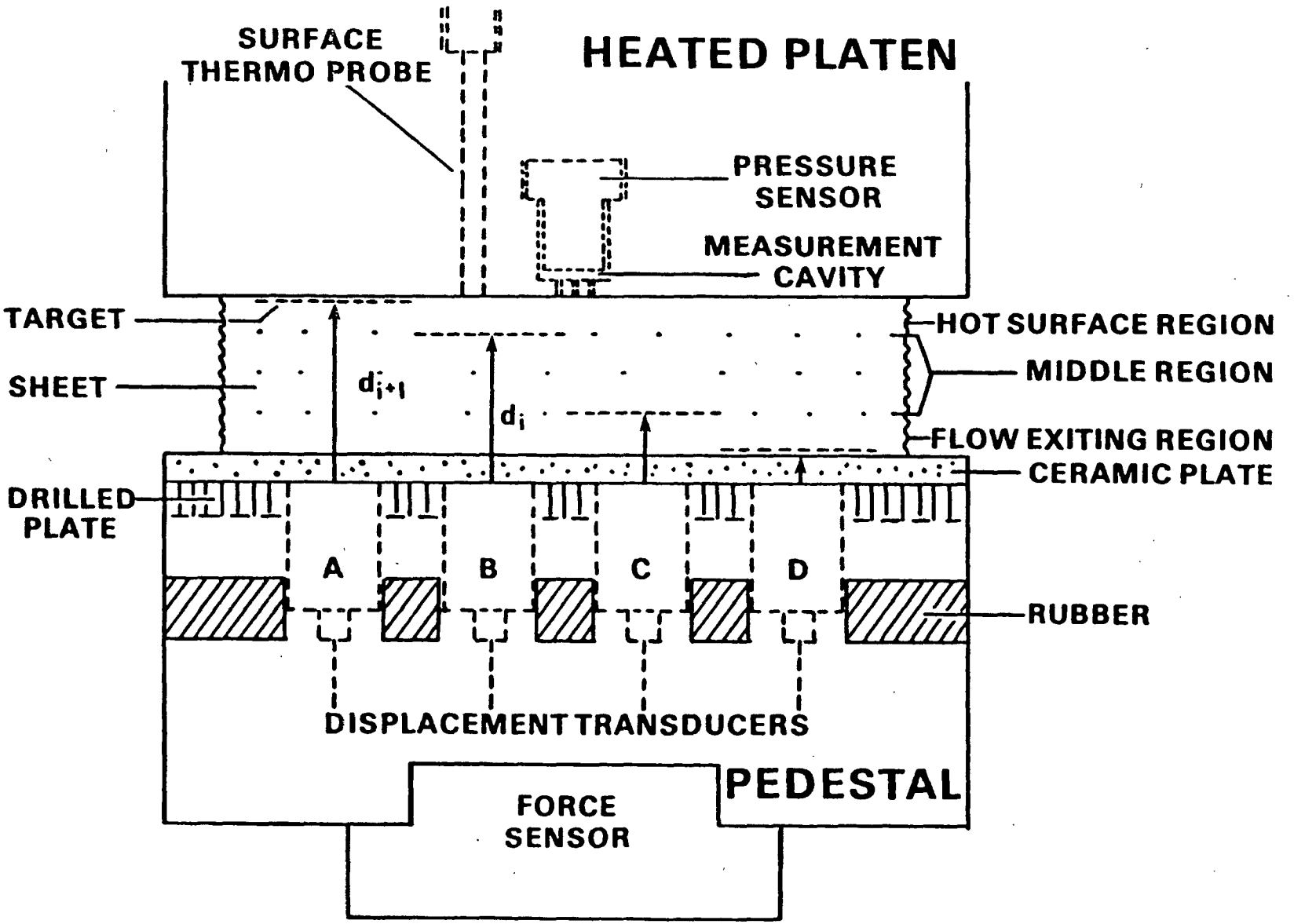

Figure 23. Schematic of the press platens used in the impulse drying simulation.

A Medtherm fast response coaxial thermoprobe is used for the dual purpose of temperature control and measurement of the instantaneous surface temperature for heat flux calculations. The iron-constantan probe, depicted in Fig. 24, has a response time on the order of 1 to 5 microseconds. It is coaxial, consisting of a small internal constantan wire coated with a 1.3 μm layer of ceramic insulation and an extended iron tube. The thermocouple junction at the end of the probe is made with a 1 μm thick plating of constantan and is positioned flush with the heated platen surface.

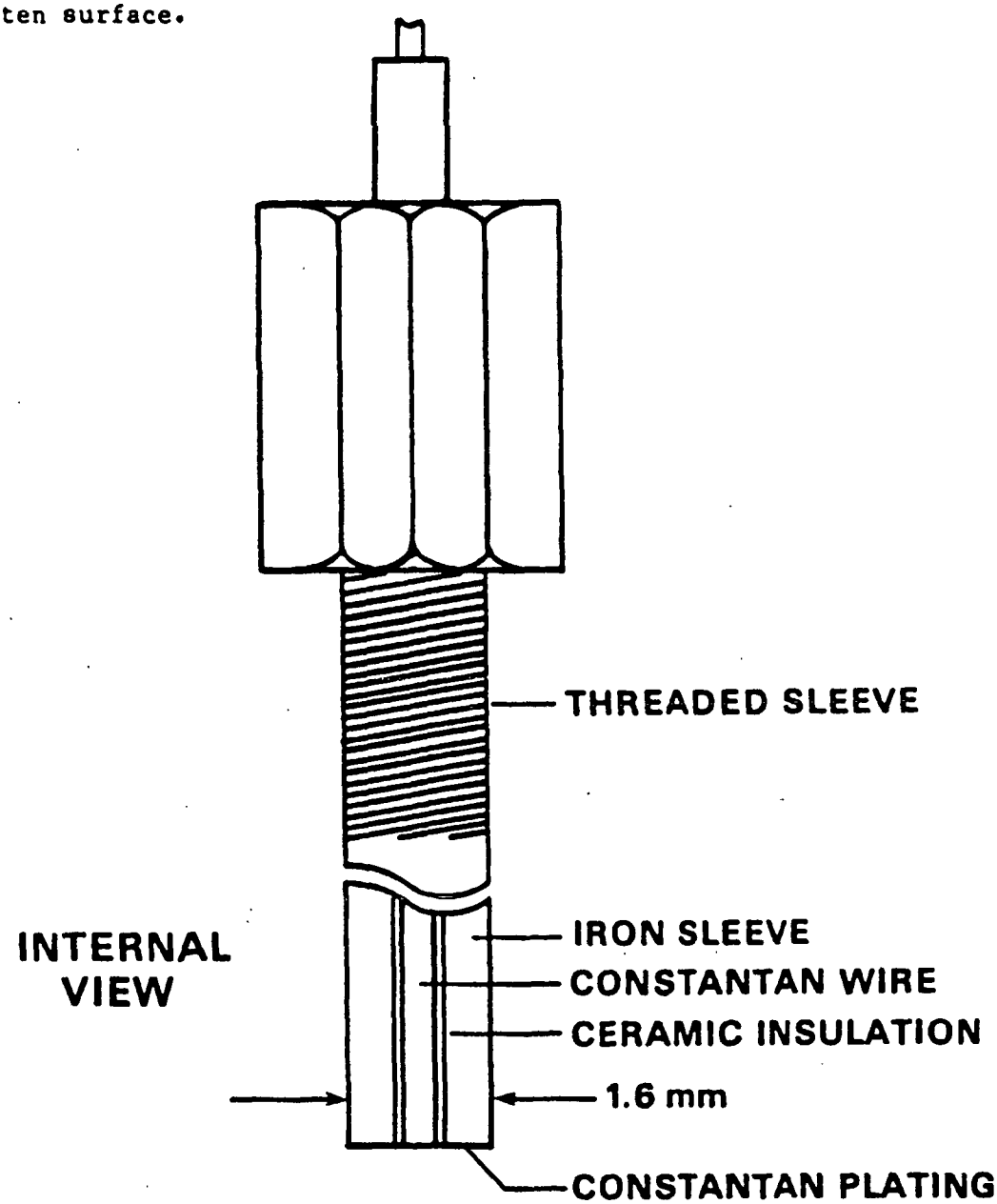

Figure 24. Schematic of a coaxial thermoprobe used to measure surface temperature history of the heated platen during impulse drying.

The lower platen or pedestal (Fig. 23) is fixed and supports the web as the falling head compresses it. Water is expressed from the sheet into a ceramic flow receiver which has an average pore size of 40 μm. A vented drilled plate under the ceramic accepts excess water. Use of the rigid ceramic limits the press nip to one compressible material (the sheet) and contributes to a uniform pressure distribution on the sheet.

Rubber is placed in the pedestal to manipulate the pressure-time relationship in the press nip. Four adjustment bolts (Fig. 25) are used to control the compressive force initially placed on the rubber and to control the levelness of the water receiving surface. The pedestal is instrumented with a force transducer which measures the impact force of the falling upper head, and four displacement transducers which provide data necessary for the determination of the sheet density profile.

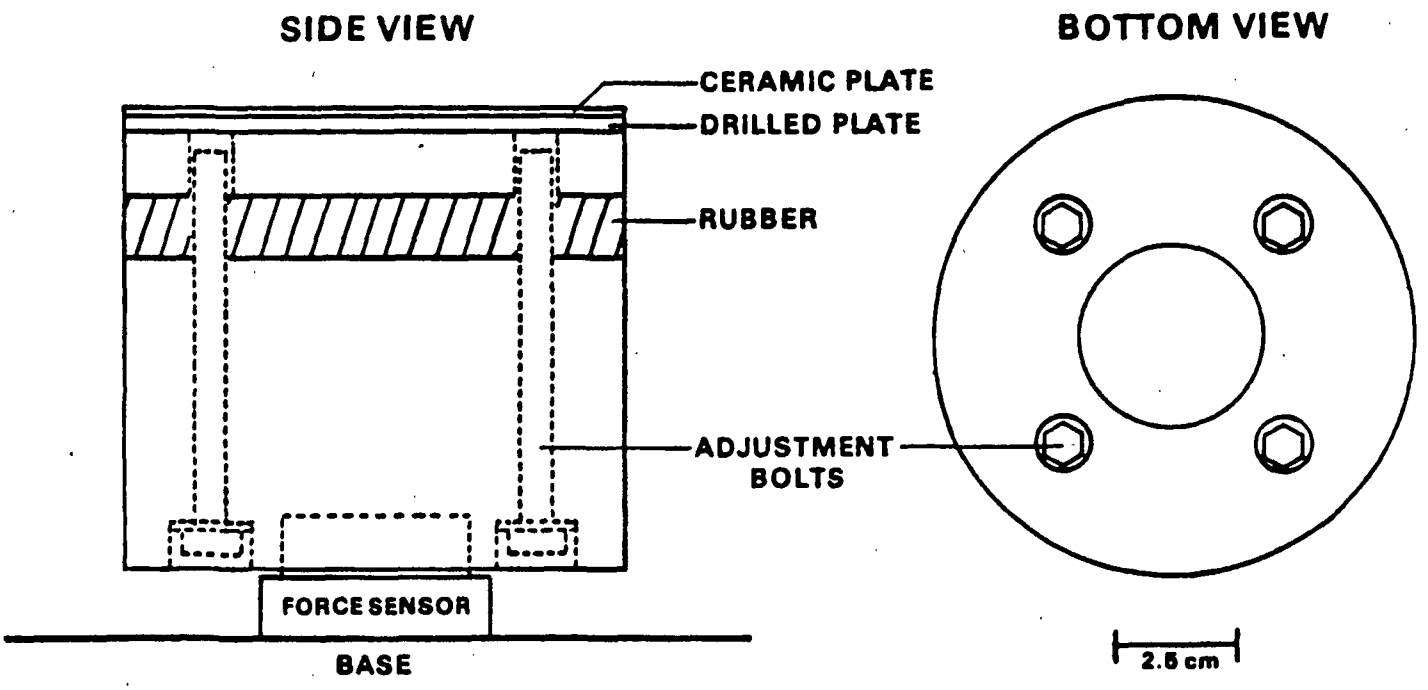

Figure 25. Schematic of lower platen depicting adjustment bolts used to control compressive force on rubber and surface level.

An impact-force transducer (PCB Piezotronics, Inc.) senses the total force applied to the pedestal by the falling platen. The factory calibrated load cell is capable of measuring up to 225 kN. The pedestal is constructed of a high strength aluminum alloy (7575) to minimize the mass resting on the load cell.

The four displacement transducers are of the eddy current type (KD-2310S series) manufactured by Kaman Instrumentation Corp. and are used to track the motion of metal targets during compression (see Fig. 23). The basic principle of operation of these probes involves inducing electrical current on the surface and within the metal target. These "eddy" currents produce a secondary magnetic field which reduces the intensity of the original magnetic field produced by the exciting coil of the transducer. Changes in impedance of the exciting coil are sensed and converted into a signal directly proportional to the distance between coil and target.

The transducers have a measuring range of 4.0 mm with a resolution of 0.01% of full scale calibration. Accurate calibration over a measurement span of 1.25 mm is done with a special micrometer (Fig. 26), accurate to within 6.35 μm, to which a sample target is attached. The transducers are calibrated while rigidly mounted in the lower head, prior to each set of compression tests (5-15 tests/set). Figure 27 is a typical calibration curve of displacement vs. voltage. It is linear with a correlation coefficient of 0.99999.

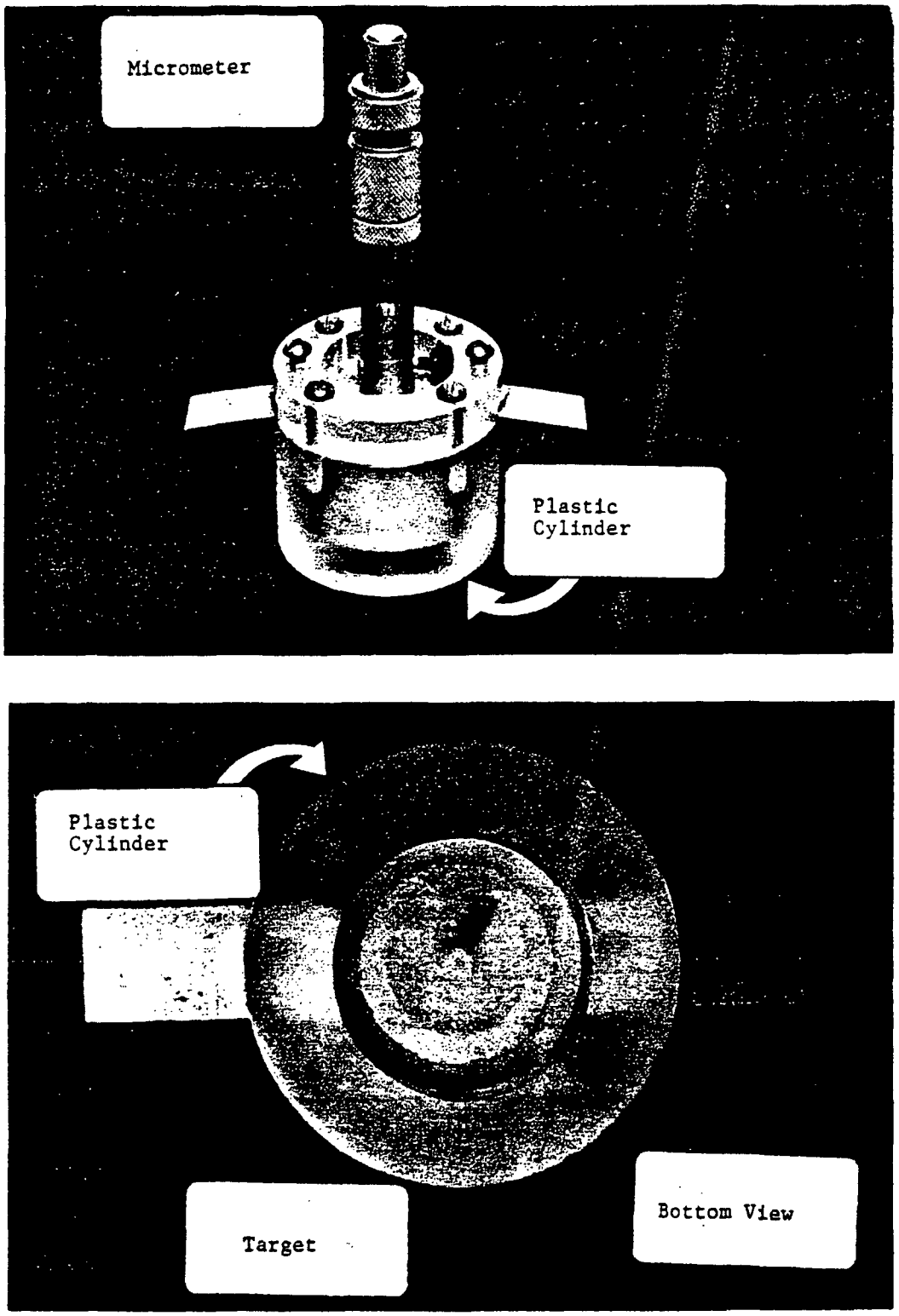

Figure 26. Calibration micrometer used for calibrating displacement transducers.

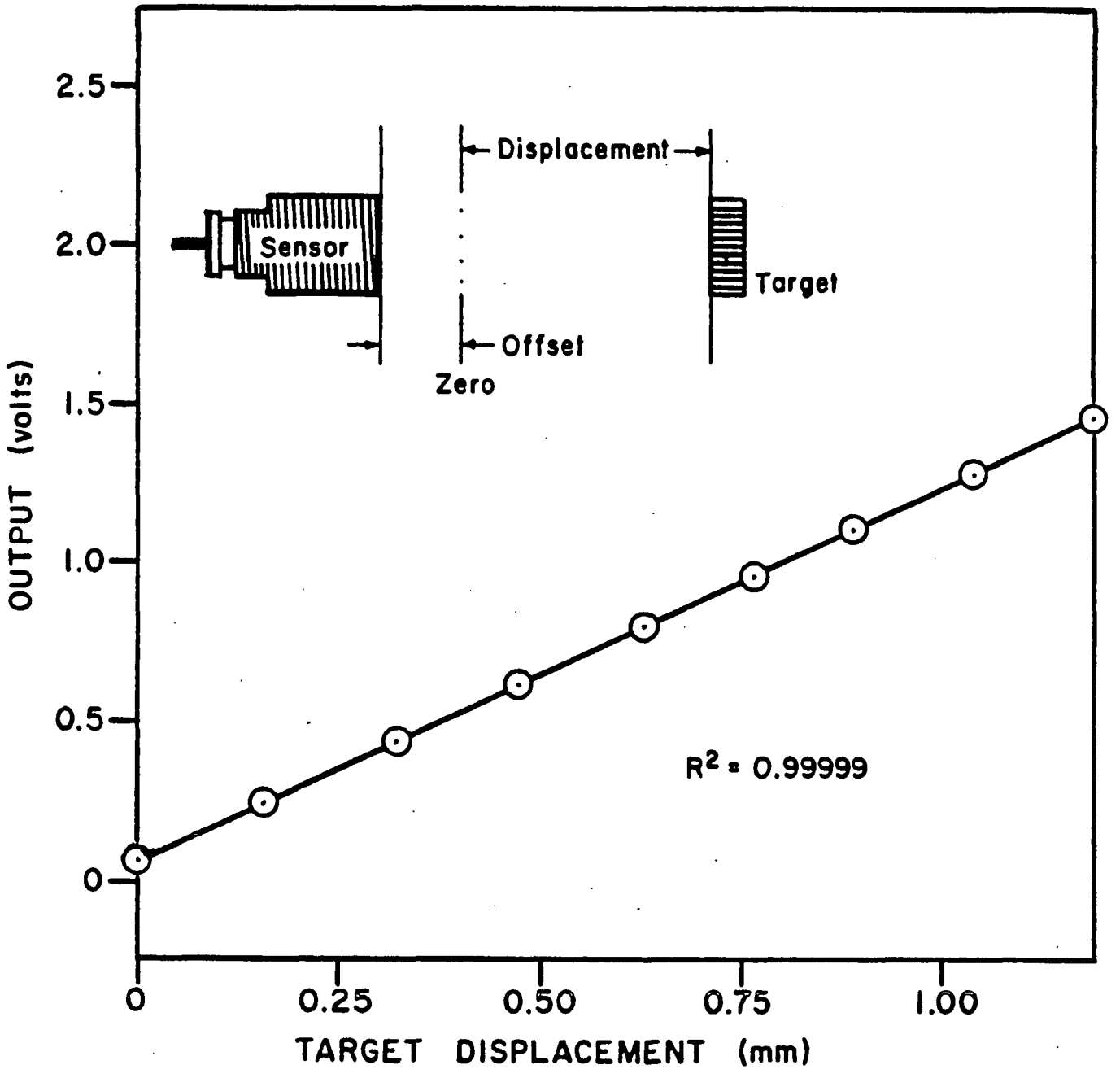

Figure 27. Typical linear calibration curve of displacement vs. voltage.

DYNAMIC DENSITY PROFILE DETERMINATION

The instantaneous density profile is calculated from the dynamic thickness measurements of specific sheet regions of known basis weight. The targets used in the method are embedded in the sheet at various levels during sheet formation (see Fig. 23) and are thin relative to total sheet thickness. During consolidation, the targets move with the surrounding fiber network in response to dewatering and densifying forces. The displacements of the targets are recorded from the transducers mounted in the lower head. The instantaneous density of a region is then calculated from adjacent target separation and region basis weight, as indicated in Fig. 23, such that:

$$\rho_i = W_i/(d_{i+1} - d_i)$$

where, ρ_i = apparent density of the ith web region (g/cm^3)

W_i = basis weight of the ith web region (g/cm^2)

d_{i+1}, d_i = distance to targets above and below ith web region, respectively.

Figure 28 is a typical set of displacement data with the applied pressure included for reference. Before the "nip" closes and after it opens, the sheet is unrestrained so the signals may not accurately reflect the true positions of the targets in the sheet. For wet pressing conditions, this can be corrected by placing a piston on the sheet surface which slightly precompresses the web and does not leave the web after pressure application. For cases where the top platen is heated, as in impulse drying, sheet restraint is not possible. The data in Fig. 28, as well as other raw, unfiltered displacement data obtained under restraint, have proven to be very clean and reproducible.

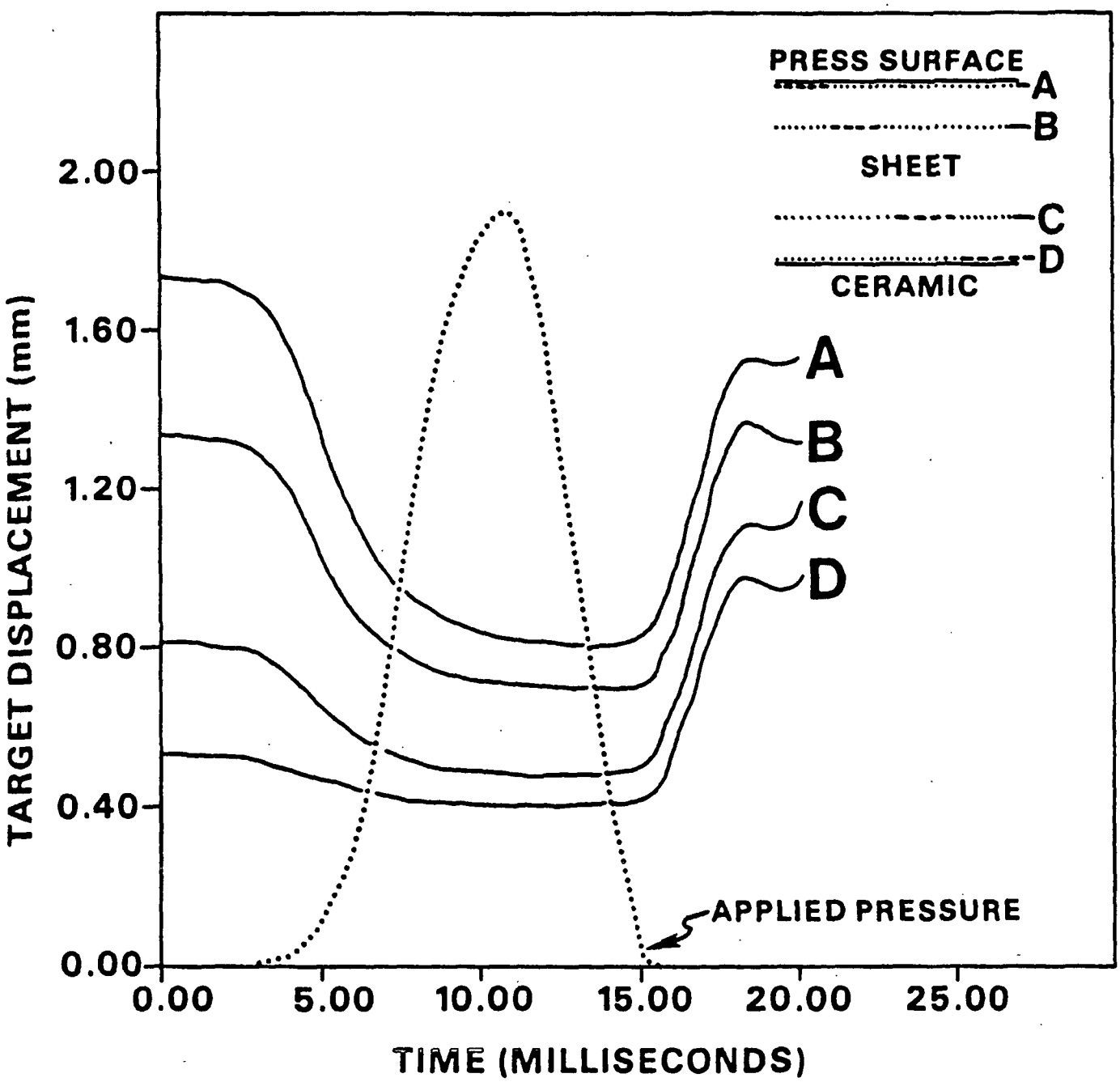

Figure 28. Typical unfiltered recordings of the target displacement histories (A-D) used in the calculation of dynamic density profiles, and the total nip pressure for wet pressing conditions at 20°C. Pmax = 4.8 MPa.

Factors Important to Density Profile Determination

A number of factors are critical to accurate density determinations. These include proper transducer calibration; target material, thickness, and temperature; target embedding method; basis weight variation; and parallelism between pressing surfaces. To achieve a high degree of accuracy, each of these factors must be addressed.

Under some severe drying conditions, such as in impulse drying, it was assumed that the target would experience temperatures up to about 250°C. Since it was known that changes in target resistivity and magnetic permeability with temperature could result in significant displacement measurement error, a series of experiments was performed to determine how this problem could be reduced or eliminated. Some typical results are plotted in Fig. 29 as measurement deviation (percent deviation from true value) versus target temperature for several thicknesses of nickel and copper mesh. Based on measurements of this type, it was apparent that increasing target thickness and use of a nonmagnetic material would enhance the thermal stability of the system to the point where the effects could be ignored. Over the range of temperatures used in impulse drying, it was determined that a 38.1 μm thick copper mesh material could be used without significant measurement deviation resulting from thermal effects. For wet pressing conditions at constant temperature, it was found that target thicknesses as low as 12.7 μm could be effectively used.

While increasing target thickness improves the thermal stability of the measurement, it increases the amount of fiber network disturbance associated with the target's presence. To minimize this problem, the ratio of target to sheet thickness must be kept small. It is also essential that the target be embedded in the sheet in a manner which minimizes fiber network disturbance. A

method to accomplish this is described in the section entitled "Handsheet Forming Techniques."

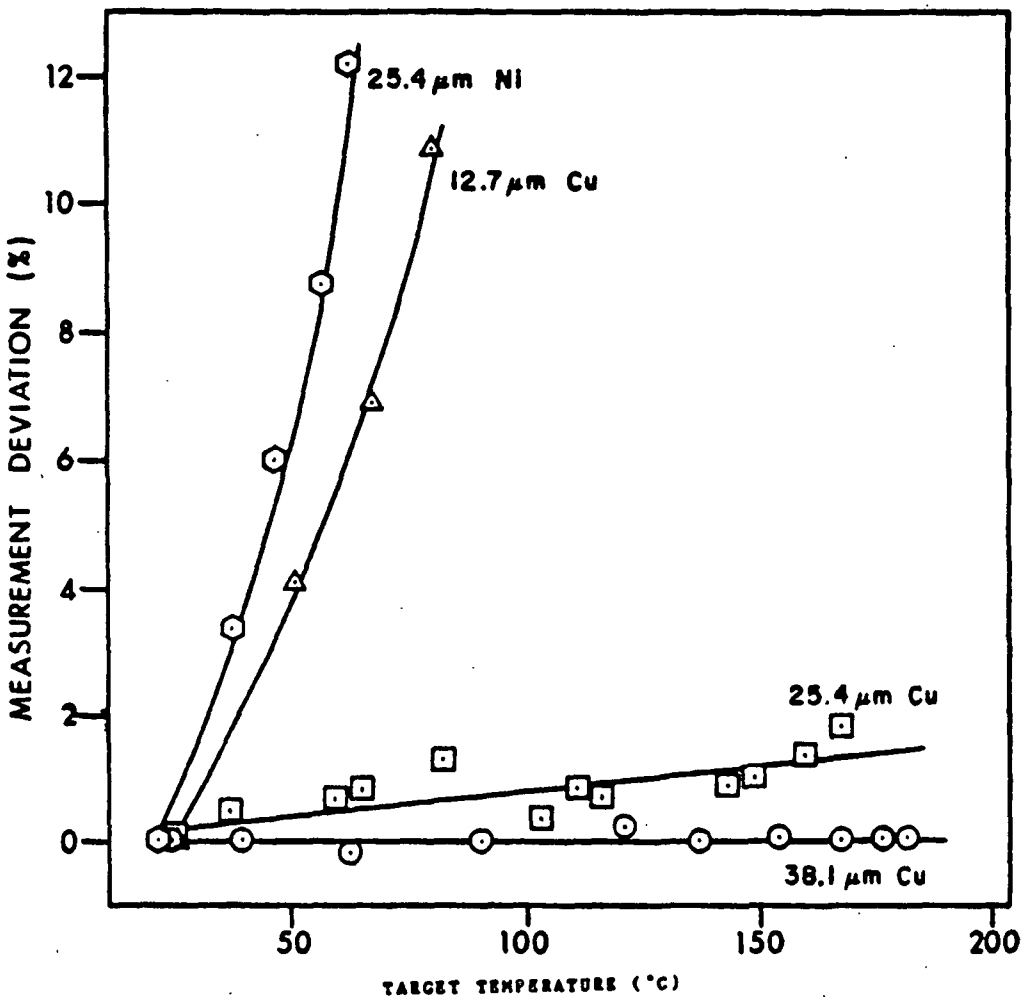

Figure 29. Displacement measurement deviation (percent deviation from true value) as a function of target temperature for copper and nickel mesh.

The openness of the target should be large enough to minimize flow resistance and interfacial effects. In addition, it is desirable for interaction between fibers on opposite sides of the target to be possible. This would allow the target to be bonded on and within the sheet, reducing disturbances associated with its presence. Figure 30 is an SEM photograph of a 25.4 μm thick copper target on the surface of a dry sheet. It is readily apparent that the open area is large in relation to the sheet pores and that its thickness is small relative

to the sheet. The open area of the copper mesh varies between 65 and 75%, depending on target thickness.

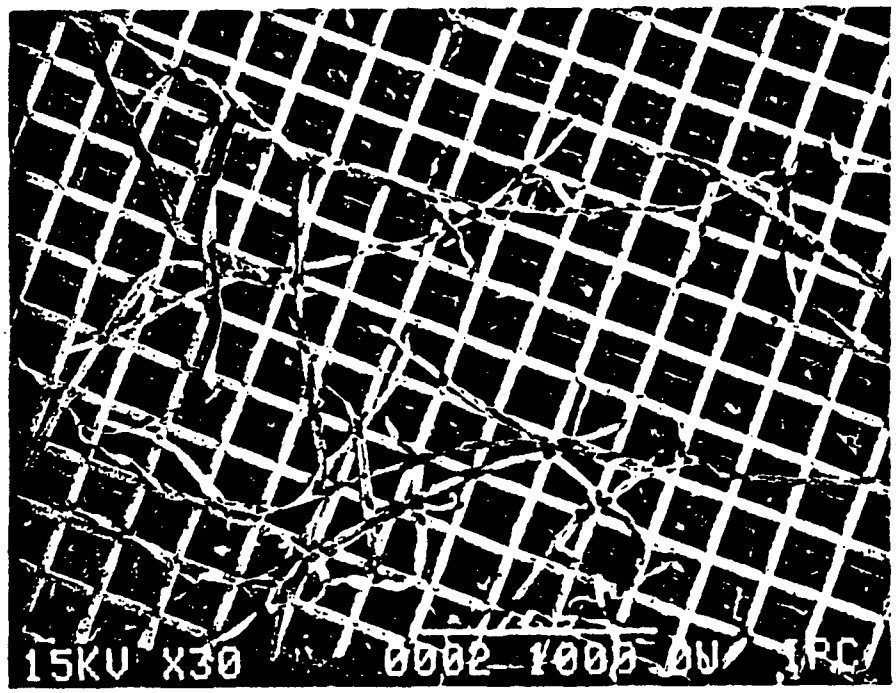

Figure 30. SEM photograph of a 25.4 μm thick copper target on the surface of a handsheet.

An error analysis showed that parallelism between pressing surfaces could be the largest potential source of error in the density profile measurement. This error may vary over a wide range, depending on the severity of the misalignment. In order to achieve an acceptable degree of parallelism, a number of corrective measures had to be taken. The press heads had to be machined and surface-ground as flat and parallel as possible. The pressing apparatus had to be designed and constructed to ensure parallel contact of the press surface. For the falling weight simulator, this required proper alignment of guidance shafts, close tolerance bearings, and balancing of the falling head. Fine adjustment of the press surface level was accomplished in most cases by shimming but was also controlled by the adjustment bolts shown in Fig. 25. The four displacement

transducers were used to track the displacement of the pressing head to determine if parallel contact was being made dynamically. If not, then adjustments were made accordingly. Nip impressions were also performed to determine uniformity of pressure application.

In preliminary experiments it became apparent that the manner in which targets were embedded in the sheet significantly affected the density determination. Placing the targets between previously formed fiber layers and then pressing them together yielded displacement histories that were not realistic or repeatable. Figure 31 is one example of this type of anomalous data in which the sheet appears to first compress and then expand as the pressure is applied. In some cases, expansion would be seen to occur through the central part of the press nip.

A handsheet forming method was developed in which the targets were embedded in the sheet during formation. This greatly improved the density profile measurement. Apparently, when layered handsheets with targets between layers are used, the targets disturb the fiber network and result in areas of locally increased thickness. In contrast, when the target is embedded during formation, fibers are displaced by the target and layer interfaces are eliminated, resulting in a more uniform structure. This concept is illustrated in Fig. 32.

STATIC DENSITY PROFILE DETERMINATION

Several methods were used as an alternative means for determining density profiles of sheets after being pressed or impulse dried. These profiles provided data for evaluating the dynamic method and for determining the degree to which the density profiles attained dynamically were retained in the final sheet structure. Three methods were utilized. These include:

1. Static determinations using the dynamic system described above.
2. Surface grinding layers of fiber off the sheet and calculating the density from the remaining thickness and basis weight.
3. Qualitatively determining the density profile by a gold mapping technique on the Scanning Electron Microscope (SEM).

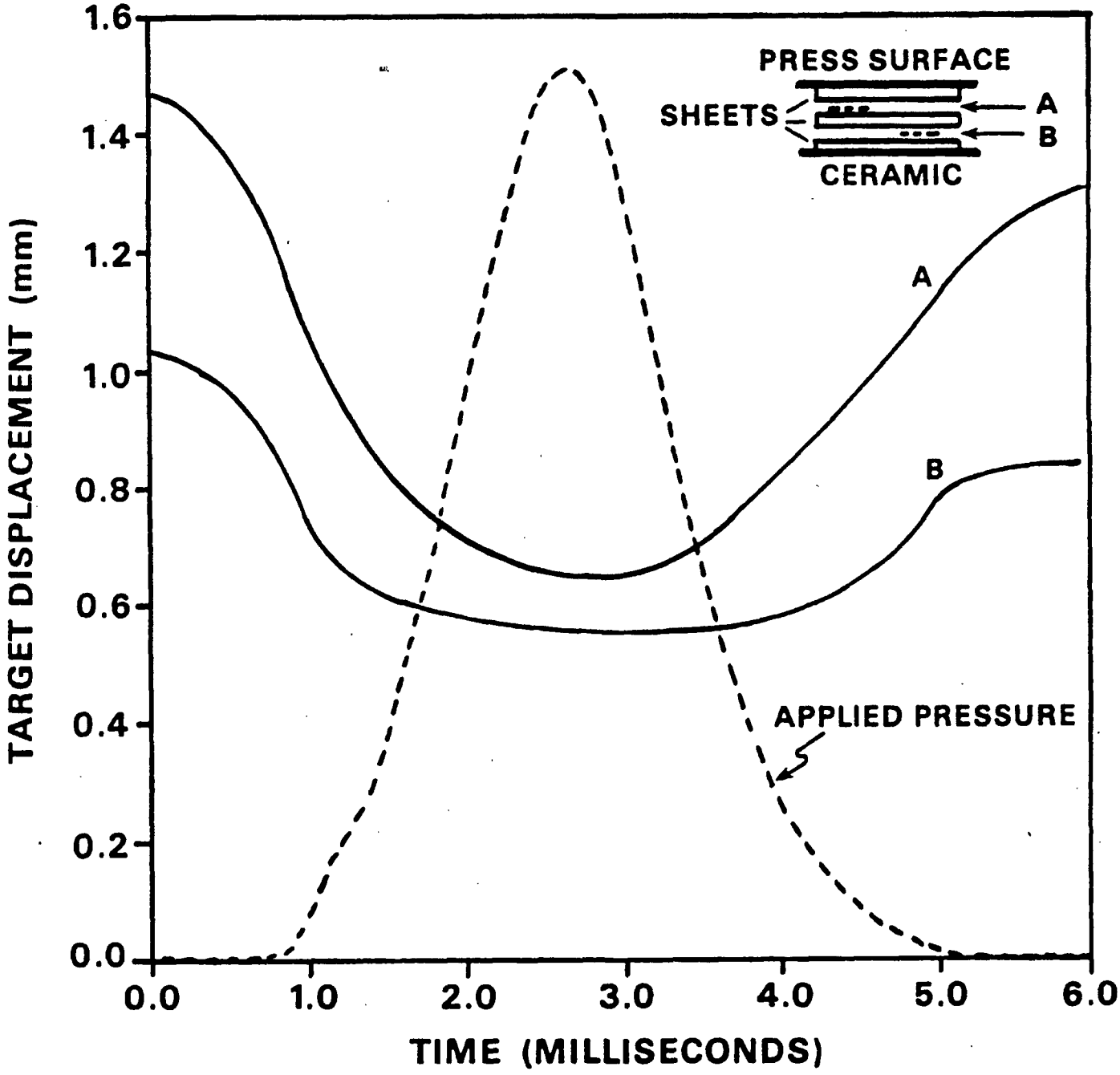

Figure 31. Target displacement histories (A, B) in which the targets were inserted between layers.

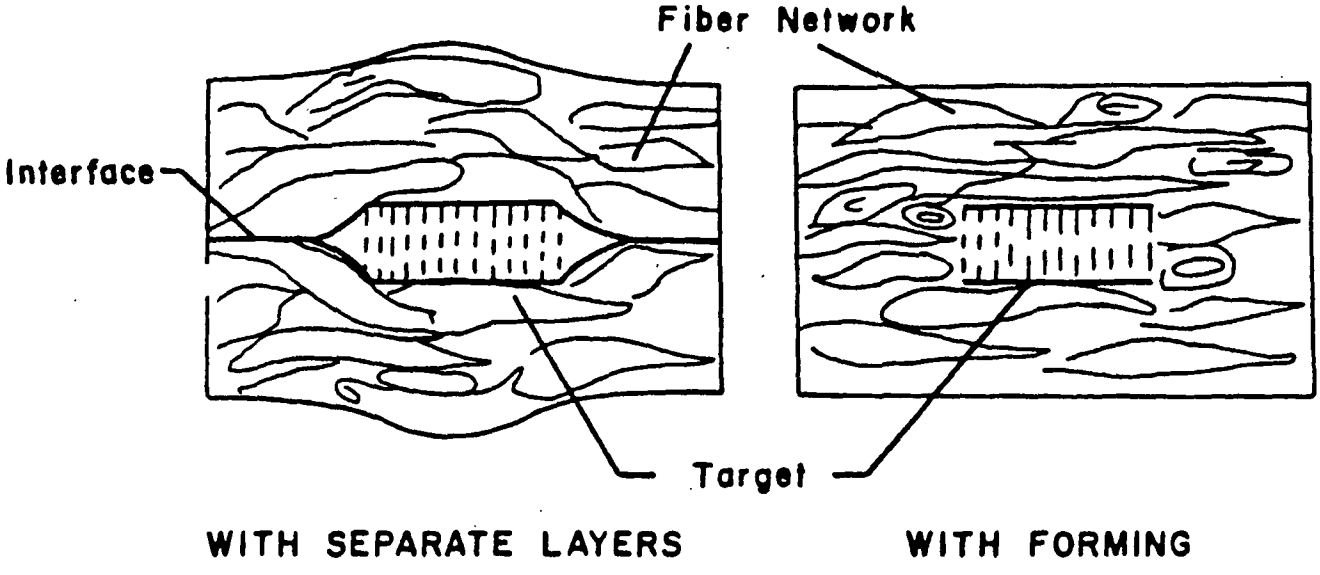

Figure 32. Comparison of two types of target placements; placing target between layers and forming target in the sheet.

Static density profile determination with the dynamic system was done by leaving the sheet on the pedestal after being pressed or impulse dried, measuring the target separations, and calculating the density profiles as before. A plastic plate weighing 65 grams was placed on the sheet surface to restrain the sheet lightly during the measurements, which were performed within one minute after pressing. One potential problem with this method is the moisture transfer between the ceramic and the sheet during the postnip period. At lower moisture ratios (< 1.5), however, this problem is probably small.

Surface grinding of paper is a process where successive layers of fibers are removed by grinding away the paper surface. The method used in this study was based on the work of Beckman and Plucker[54] in which the sample was held by a special vacuum plate while an ordinary machine shop grinder ground off a certain thickness of material. The paper sample can be ground to a thickness as low as 13 μm, depending on sample structure. Unfortunately, the technique is destructive and the degree of disturbance to the density profile is not known. Another

problem in using this method is that the sheet must be dry for grinding. Thus, immediate postnip evaluation is not feasible.

The density profile determined using the surface grinding method required three replicate runs for each set of conditions considered. Each sample was ground to a specific thickness corresponding to the region of interest. Thicknesses were determined using the IPC rubber platen caliper instrument and the apparent density was calculated directly from the layer thickness and basis weight. A density profile was obtained by combining the measured layer densities of the three replicate runs.

The last method utilized in evaluating the sheet density profile was a qualitative SEM mapping technique suggested by Litvay.[55] The method involves coating a cross section of the paper sample with a gold-palladium plating and then x-ray mapping the gold distribution. Since the gold plating resides on the solid surfaces, the gold distribution is indicative of the mass distribution across the sheet thickness. Figure 33 is an example of the mapping obtained by this method.

The SEM mapping technique is subject to a number of errors and its degree of accuracy is not yet known. According to Litvay,[55] a better way to make the measurement would involve mapping the sheet structure directly from the video signal rather than the x-ray signal. This would eliminate the errors associated with the SEM x-ray mapping technique. The procedure of sample preparation is also considered to be very important. Care must be taken not to disturb the density profile when preparing the sample. The sample preparation and mapping techniques still require further work to improve the methods although the results presented in this thesis are encouraging as they qualitatively agree with the density profiles evaluated by the other two procedures.

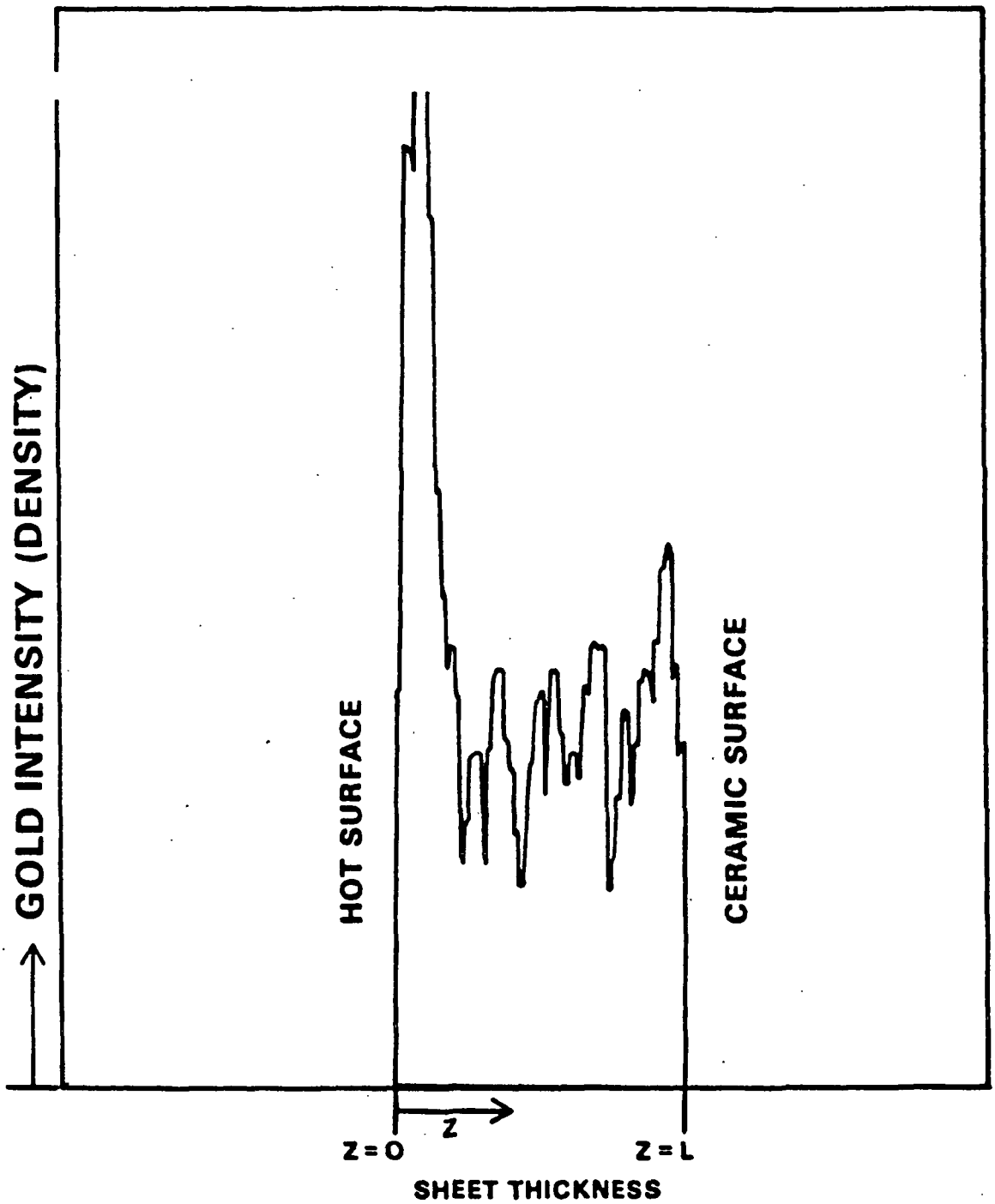

Figure 33. Typical x-ray mapping of gold x-ray backscatter intensity versus sheet thickness. Qualitatively this represents apparent density.

HANDSHEET FORMING TECHNIQUES

Handsheets are formed from an unbleached, softwood kraft furnish. Some of the pulp was beaten to 420 CSF while the rest remained unbeaten. All fines were removed from the unbeaten stock by screening the stock through a 150 mesh vibrating screen to give a freeness of 735 CSF. Fines removal was done to eliminate density development in the sheet that may arise from fines migration during impulse drying.

A constant rate forming apparatus, similar to that described by Cowan[56] and later used by Fang,[57] was used to form handsheets with uniform and reproducible fiber distributions. Experiments showed the basis weight variability within paper samples to be relatively small, with a coefficient of variation of 0.94%. Circular samples, 2.5 cm in diameter, were randomly cut from each handsheet. Variability between samples was somewhat poorer, with a coefficient of variation of 3.2%. This is attributed to the error involved in separately weighing out the fiber required for forming each sheet.

The steps involved in forming the handsheets are lengthy and require great care. Since the basis weight in three regions of the sheet must be known for calculating the density profile, the amount of fiber required for each region is weighed out separately. Next, the pulp for each region is disintegrated in a mixer and diluted to 0.01% consistency. After allowing the stock to mix for several minutes, handsheet forming is initiated in the forming apparatus depicted in Fig. 34.

Before forming takes place, however, a forming filter must be present on the surface of the septum and the forming tube must be clean and free of air bubbles.

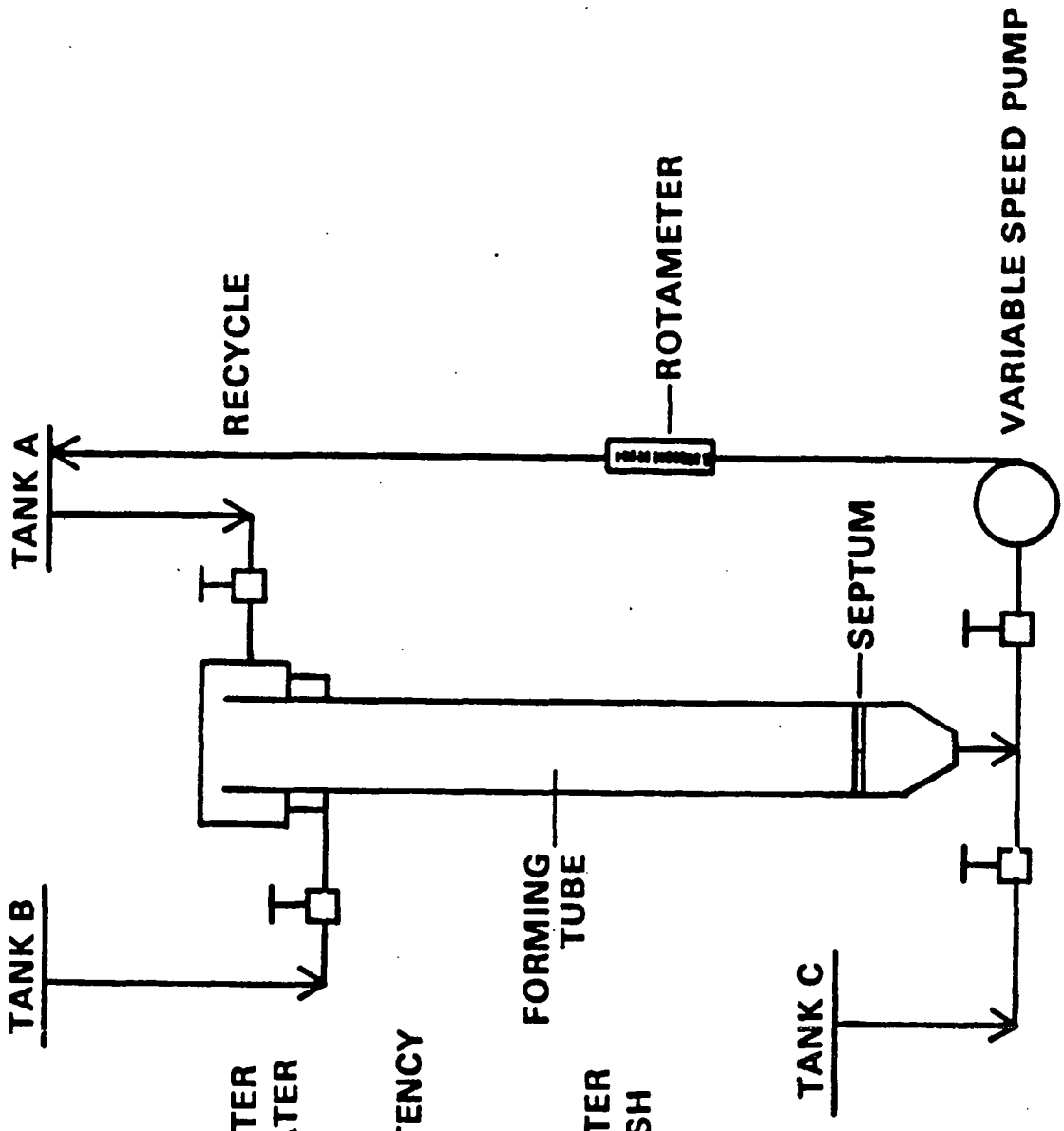

Figure 34. Forming apparatus for forming handsheets used in density profile measurements.

The forming filter (Kendall nongauze milk filter) facilitates the removal of the wet sheet from the septum and contributes to the uniformity of fiber deposition. It is important to soak these filters for 24 hours prior to forming to soften and thoroughly wet the filter material.

With distilled water from Tank A flowing through the forming tube at a constant rate of 6 L/min, forming is initiated by introducing approximately 500 mL of stock from Tank B into the forming tube. These fibers are allowed to settle before placing a target, shiny side down, onto the mat surface. These few fibers are used to help hold the surface target on the sheet. Target positioning is accomplished in the presence of a continuous flow of distilled water with a specially designed insertion tool. This allows the target to be positioned without disturbing the fibers or interrupting fluid flow. The tool is illustrated in Fig. 35.

The tool is positioned in the forming tube slightly above the mat surface with the target in the desired deposit tube. A rod is used to push the target gently from the deposit tube so it can settle onto the mat surface. After the target is positioned, the insertion tool is slowly removed and forming can continue. The flow of stock is initiated at a rate of about 3 L/min. The flow of distilled water is reduced to maintain a constant flow rate of 6 L/min. After all the stock has entered the tube, distilled water flow is increased back to its previous rate. The second target is positioned as before and the process is repeated until all four targets are deposited. After the last target has been deposited on the mat surface, a final 500 mL sample of stock is drawn through the tube in the same manner as for the first surface target. In the final step, the water flow is stopped and the water level in the forming tube is drawn below the septum and the pump is shut off.

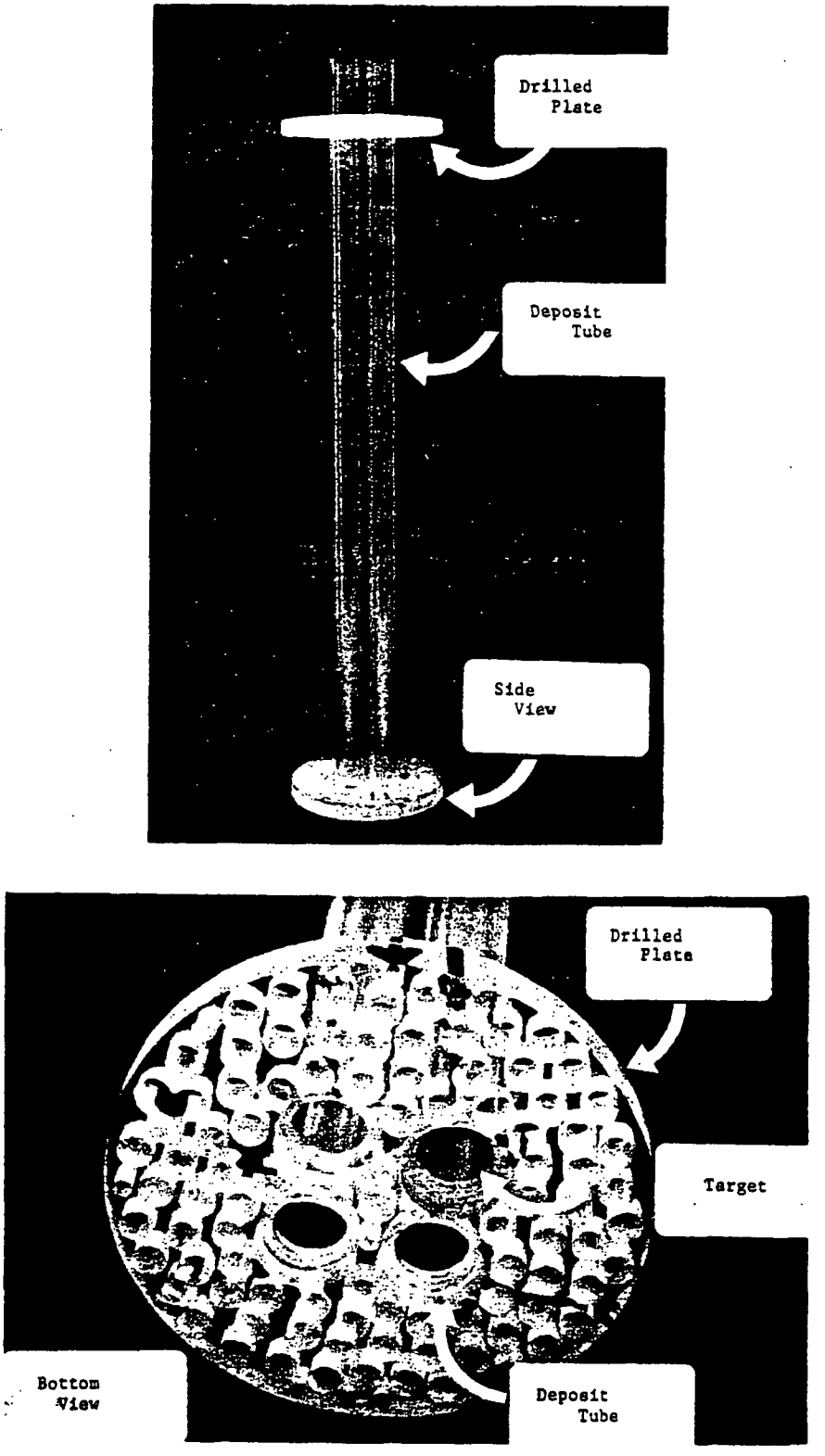

Figure 35. Insertion tool used for positioning targets on the mat surface during handsheet forming.

The forming tube is removed and the filter/sheet combination is removed from the septum. Another filter is placed on the open sheet surface and the sheet/filter composite is couched between blotters. The sheet is then pressed between blotters in a standard hydraulic press to achieve the desired moisture level. After pressing, the handsheets are stored overnight and tested the following day. Long-term storage is avoided because it was found that oxidation of the target material can affect the displacement measurement.

Handsheets ranging from 50 to 200 g/m^2 were made. Four targets were usually embedded in the handsheet as illustrated earlier in Fig. 23. However, for basis weights of 50 g/m^2, only three targets were used to give a 50/50 basis weight split. This method produces uniform handsheets without the interfaces that develop when separate fiber layers are conjoined.

Some tests required internal sheet temperature measurement. For these cases, it was necessary to conjoin individual fiber mats. Fine wire chromel-constantan thermocouples (25 μm diameter) were placed between fiber mats, and the resulting composite sheet was pressed to the desired moisture content.

RESULTS AND DISCUSSION

DENSITY DEVELOPMENT IN WET PRESSING

Impulse drying is considered an extension of wet pressing in which one roll is at a high temperature. Thus, a number of density profile measurements were performed under wet pressing conditions to serve as a basis of comparison for impulse drying studies. Although limited in scope, these density profile measurements offer a unique view of some of the various phenonema of wet pressing. These include the effects of flow resistance and press roll temperature on densification as well as new information regarding crushing and rewetting.

Figure 36 shows the maximum sheet density achieved in the press nip correlated with ingoing moisture ratio. The maximum density, which corresponds to the minimum sheet thickness, is a direct indication of the degree of water removal in the nip. Three sets of conditions are given to show the dependence of the maximum density attained in the nip on ingoing sheet moisture, basis weight, and impulse.

As discussed in a previous section on wet pressing, flow controlled pressing behavior is typical of high moisture, high basis weight and high flow resistance sheets, and is highly dependent on press impulse. This behavior is consistent with the lower densities attained by the 170 g/m^2, high moisture sheets, together with the density increase with impulse of these sheets (Fig. 36). In contrast, the high densities developed by the low basis weight sheets, particularly in the low moisture range, are consistent with a compression controlled pressing situation.

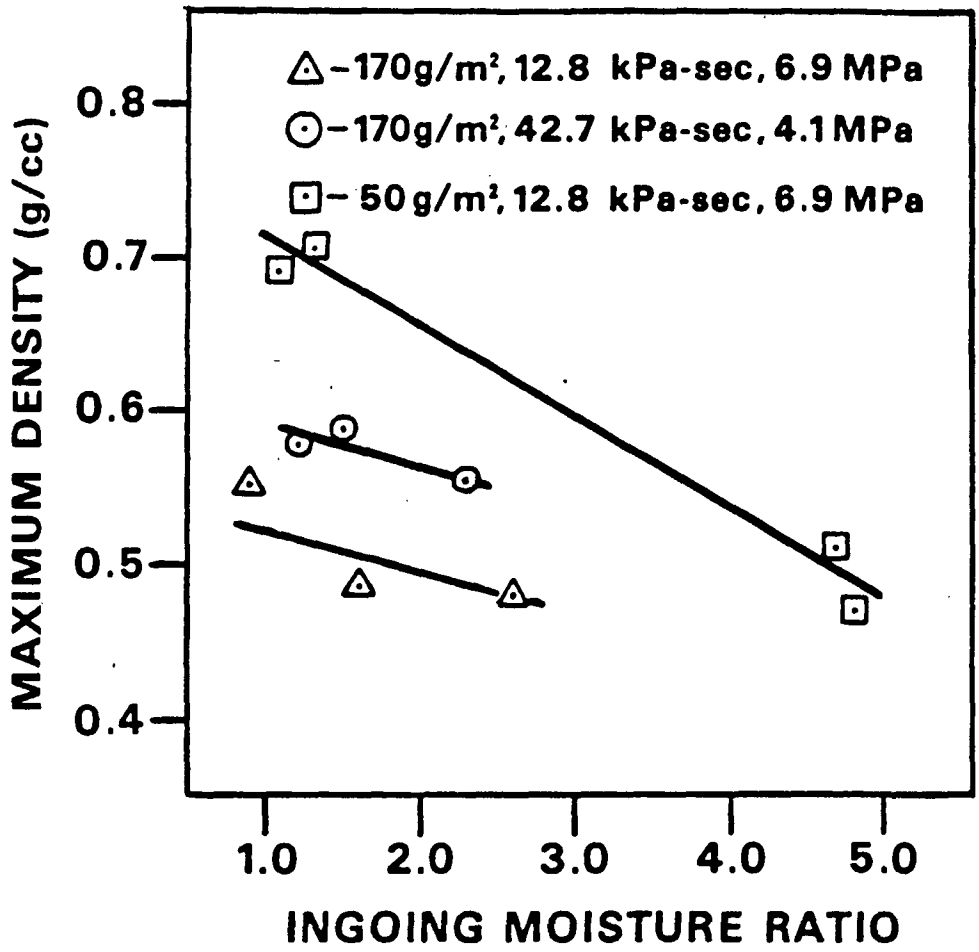

Figure 36. Correlation of maximum sheet density achieved in the press nip with ingoing moisture ratio for various basis weights and impulses.

Effect of Flow Resistance

The effect of flow resistance on density development was examined by testing sheets of different degrees of refining with variable ingoing moisture ratios. Sheets of low flow resistance were made from an unbeaten, 735 CSF, fines-free furnish, while sheets of high flow resistance were made using a beaten, 420 CSF furnish.

Figure 37 shows the total sheet density-time relationships for two wet pressing conditions. Both sheets were of a basis weight of 53 g/m^2, and a freeness of 420 CSF, but of varying ingoing moisture ratio. Initially, the sheets are of

different densities because of moisture differences and the method used to attain those moistures. The high moisture sheet was conditioned by lightly pressing between blotters, while the low moisture sheet was more heavily pressed between blotters in a standard hydraulic press.

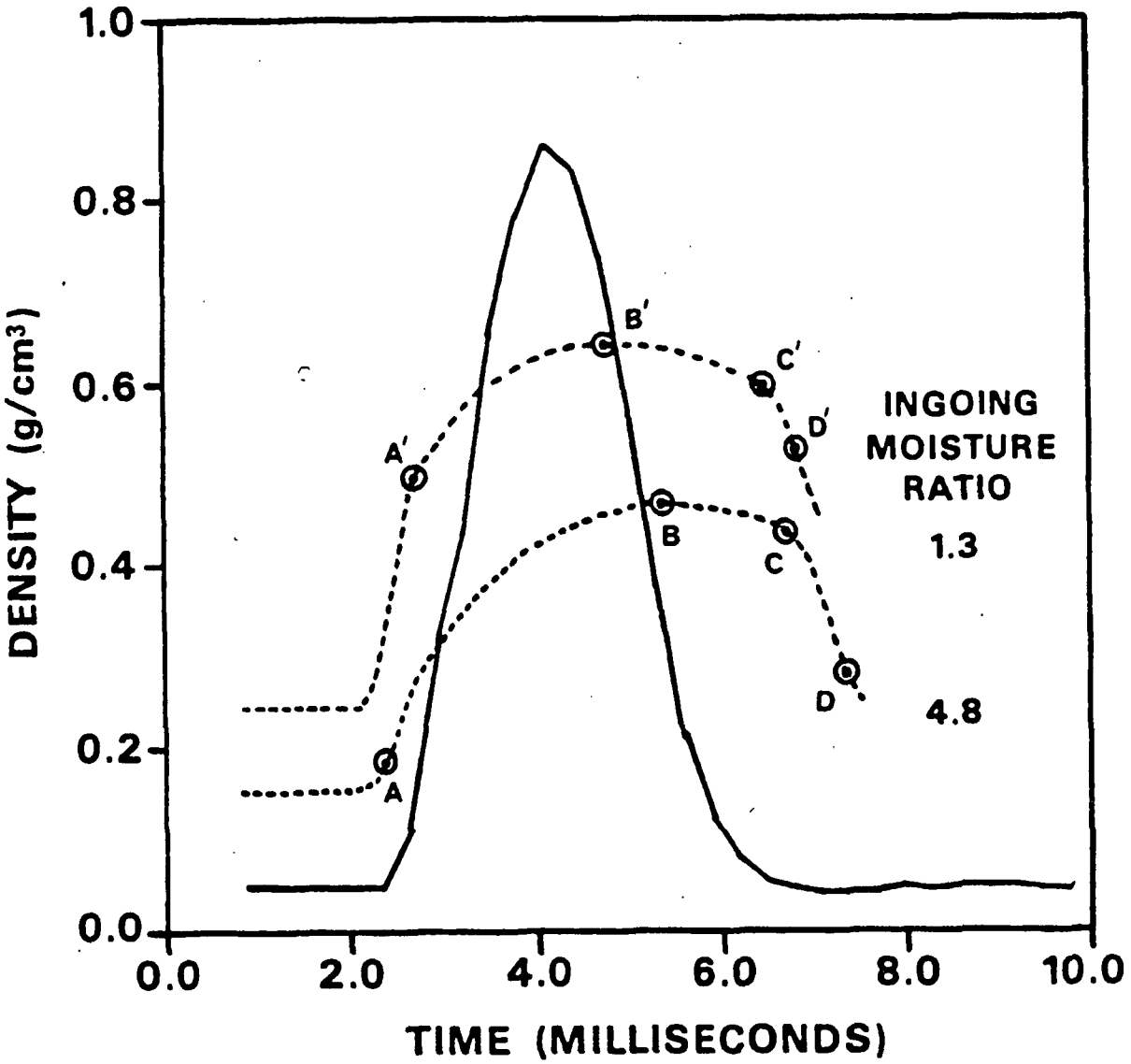

Figure 37. Sheet density-time relationships for wet pressing of sheets with different initial moisture ratios. Basis weight = 53 g/m^2, Freeness = 420 CSF, Moisture ratio = 1.4, 4.8, Peak pressure - 6.9 MPa.

As the sheets enter the nip (Fig. 37), each undergoes some unsaturated compression during which the fiber network is compressed and air is driven out. For the high moisture sheet this represents only a small amount of compression. Once the calculated saturation density is reached (Points A,A'), a hydraulic pressure develops which resists further compression. This resistance is signaled by a change of slope in the density-time curve. Continued dewatering and compression is controlled to a large extent by the flow resistance of the fiber network. These results are consistent with the Wahlstrom-Nilsson-Larsson wet pressing theory and with the detailed work of Carlsson. However, published work in this area deals with saturated fiber mats. In Fig. 37 the flow effects on unsaturated sheets are demonstrated. The detail seen in the nip opening process offers a potential means for investigating this portion of the press nip.

According to the Wahlstrom-Nilsson-Larsson theory,[9-11] the maximum density in the nip (Points B,B') corresponds to the point at which the hydraulic pressure decays to zero. In Fig. 37, the low moisture sheet reaches a higher maximum density, and reaches it earlier than the high moisture sheet. This behavior is reasonable, since the hydraulic pressure generated in the low moisture sheet should start later in the press nip and develop to a lower value when compared to the high moisture sheet. After reaching the peak density the sheet undergoes a period of constrained expansion (Points B,B' to Points C,C'). As indicated by the density data, the expansion during this period is not very great. At Points C,C' the applied pressure is released, the nip opens, and the unconstrained sheet expands more rapidly. Points D,D' denote the last points of sheet saturation, calculated from the gravimetrically determined exiting moisture ratio and measured sheet thickness. It is apparent that a considerable amount of water is reabsorbed by the sheet between Points B,B' and D,D'.

The differences in the density-time relationships in Fig. 37 demonstrate the heavy dependence of density development on sheet moisture content. The more moisture in the sheet initially, the more moisture that must be removed to attain a given density level during the nip residence time of a particular press nip. Unfortunately, the flow resistance of the sheet inhibits this dewatering, requiring longer pressing times and/or higher press loads to reach the density level attained at lower initial moisture levels.

If the sheet flow resistance is increased by refining the furnish to a lower freeness, densification, as well as dewatering is reduced. Figure 38 shows the density-time relationships for two wet pressing conditions of the same initial moisture ratio (MR = 4.8) but different freeness levels (420 and 735 CSF). The press conditions are the same as in Fig. 37. Although both the 420 and 735 CSF sheets have the same initial saturation density (Points A,A'), the times at which the hydraulic pressure development resists compression (Points B,B') differ greatly. Because of its lower flow resistance, the high freeness sheet densifies to a greater magnitude before its compression is significantly resisted by the hydraulic pressure development. The slope change is also more gradual, suggesting a more gradual rise in the hydraulic pressure. The high freeness sheet, in a manner similar to the low moisture sheet in Fig. 37, reaches the point of maximum density (Point C') first and achieves a greater density than that of the 420 CSF sheet.

Although Fig. 37 and 38 demonstrate the effects of initial moisture content and flow resistance, respectively, on average sheet density development, questions remain as to how this density is distributed across the sheet thickness. Figure 39 shows the density-time relationships for two internal regions

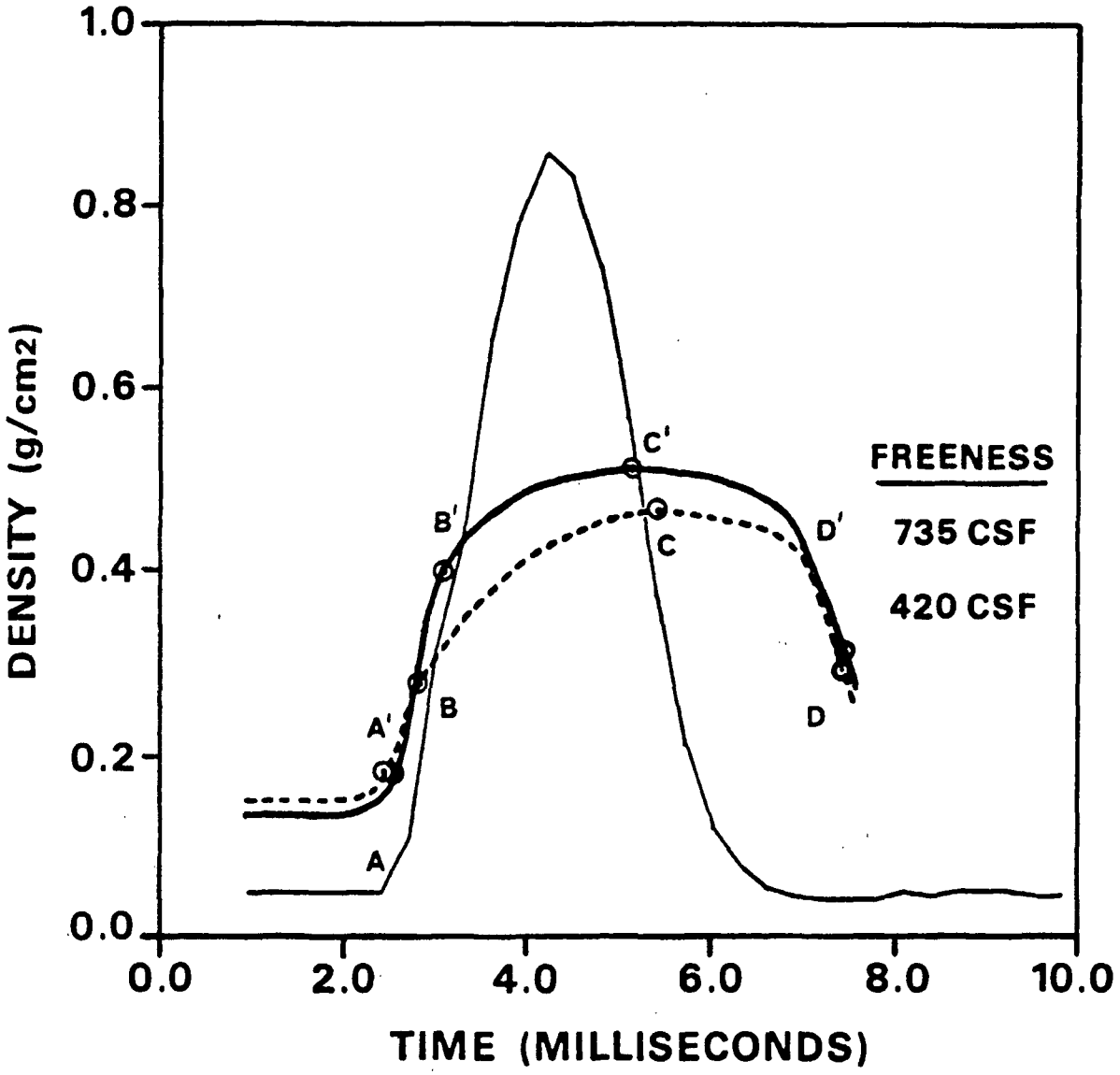

Figure 38. Density-time relationships for two wet pressing conditions of different freeness levels. Basis weight = 53 g/m^2, Moisture ratio = 4.8, Freeness = 420, 735 CSF, Peak pressure = 6.9 MPa.

corresponding to the total sheet densities plotted in Fig. 38. Region 1 represents 50%, by weight, of the sheet adjacent to the press surface, while Region 2 represents the 50% next to the ceramic plate. For the 735 CSF sheet, both regions densify similarly over the entire press nip. In contrast, Regions 1 and 2 of the 420 CSF sheet densify similarly only until the saturation density is reached. At that point, the density of Region 1 breaks away from that of Region 2, indicating a growing resistance to compression which develops from an increase in the hydraulic pressure in Region 1. The difference in density

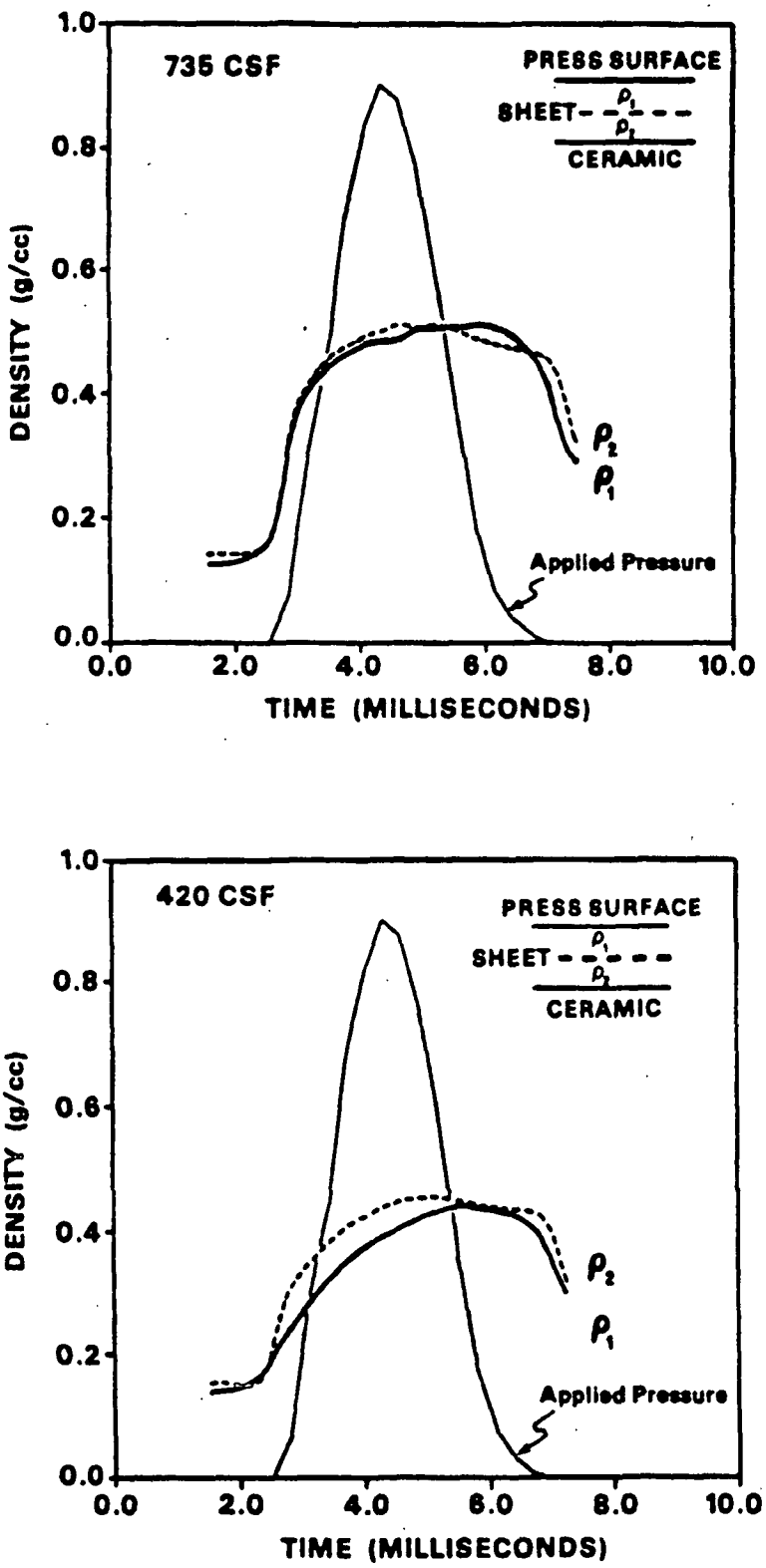

Figure 39. Density-time relationships for the internal regions corresponding to the sheet densities plotted in Fig. 38. Each region, 1 and 2, represents 50% by weight, of the total sheet thickness (about 25 g/m^2 for each region). Moisture ratio - 4.8, Peak pressure - 6.9 MPa.

response between the two regions results from the development of a z-direction hydraulic pressure gradient in which the hydraulic pressure, and therefore compression resistance, is greatest at the impermeable surface and lowest at the flow exiting surface. Although the density of Region 2 increases at a high rate initially, it slows to match the rate of density increase of Region 1. Region 2 density reaches a maximum value somewhat past midnip, then starts slowly decreasing, while the density of Region 1 peaks later and then starts decreasing in accordance with Region 2 density. This behavior results from the rapid development of a z-direction hydraulic pressure gradient which rapidly decays. This allows the structural pressure to distribute more uniformly in the z-direction, resulting in a more uniform density distribution.

Since the basis weights of the sheets in Fig. 39 are only about 50 g/m^2, one would not expect the freeness to have much influence on density development. In fact, it is surprising that any significant difference was observed at all. If heavier basis weight sheets are examined, the observed differences are more evident. Figure 40 shows the total sheet density-time relationships for wet pressing of two 100 g/m^2 handsheets of different freeness levels. The effect of freeness on density development for the heavier basis weight sheets is essentially the same as that observed in Fig. 38. If, however, the internal region densities of the high basis weight sheets are compared as in Fig. 41, much greater differences are observed in z-direction density development.

For both freeness levels, Region 3 densifies similarly while Regions 1 and 2 densify to a lesser extent for the 420 CSF sheet. In contrast to the density profile for the 50 g/m^2 sheet (Fig. 39), a more nonuniform density profile develops in the z-direction. By increasing the basis weight, more moisture is available for removal and also a thicker fiber mat effectively increases the

flow resistance to water flow. Thus, a larger hydraulic pressure in the sheet develops in the press nip. For both cases in Fig. 41, it appears that the hydraulic pressure gradient, and therefore the compression gradient, is greatest across the flow exiting Region 3.

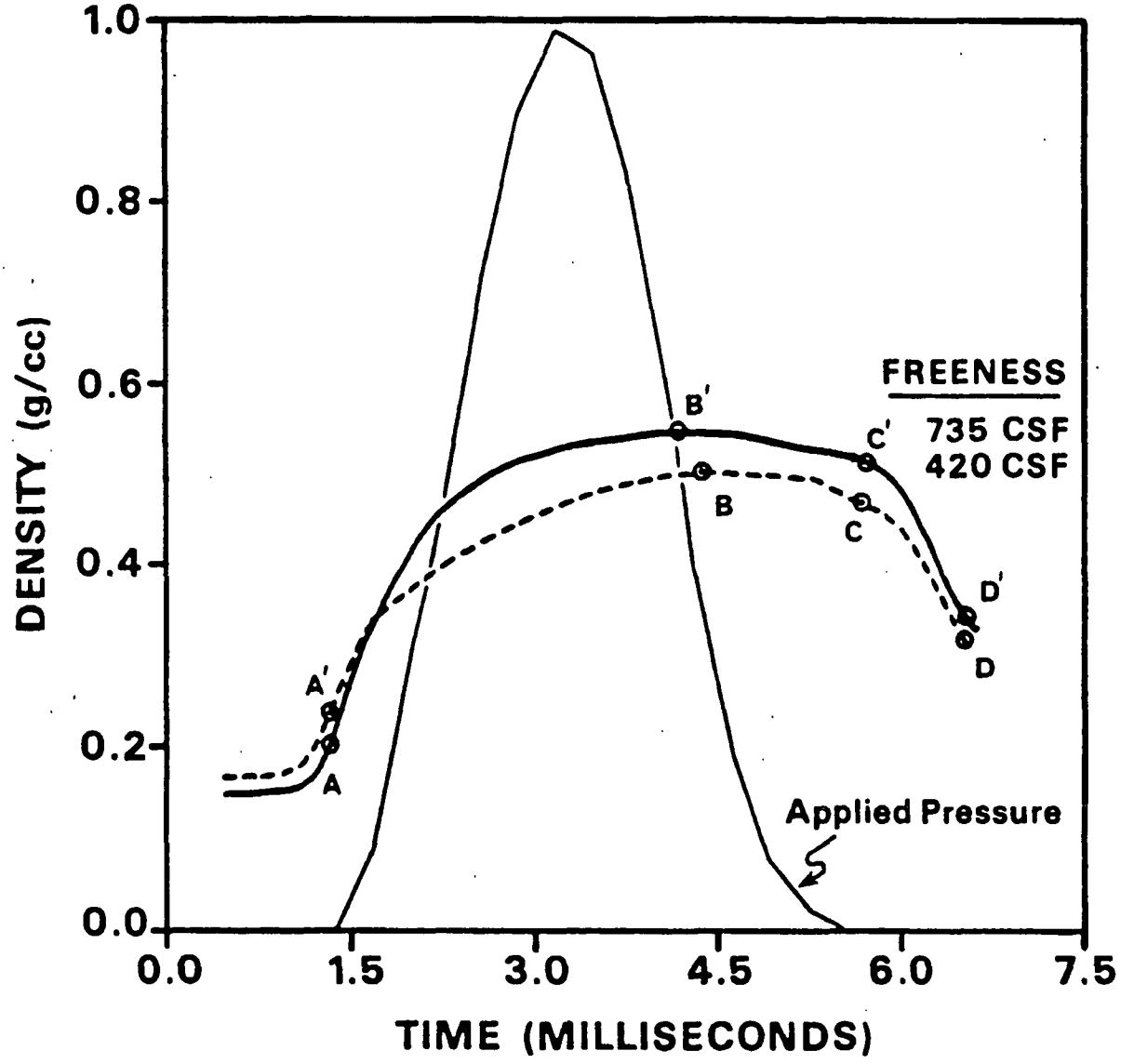

Figure 40. Total sheet density-time relationships for two wet pressing runs using 100 g/m^2 handsheets of differing freeness levels. Moisture ratio = 4.0, 3.6 Freeness = 420, 735 CSF, Peak Pressure = 7.0 MPa.

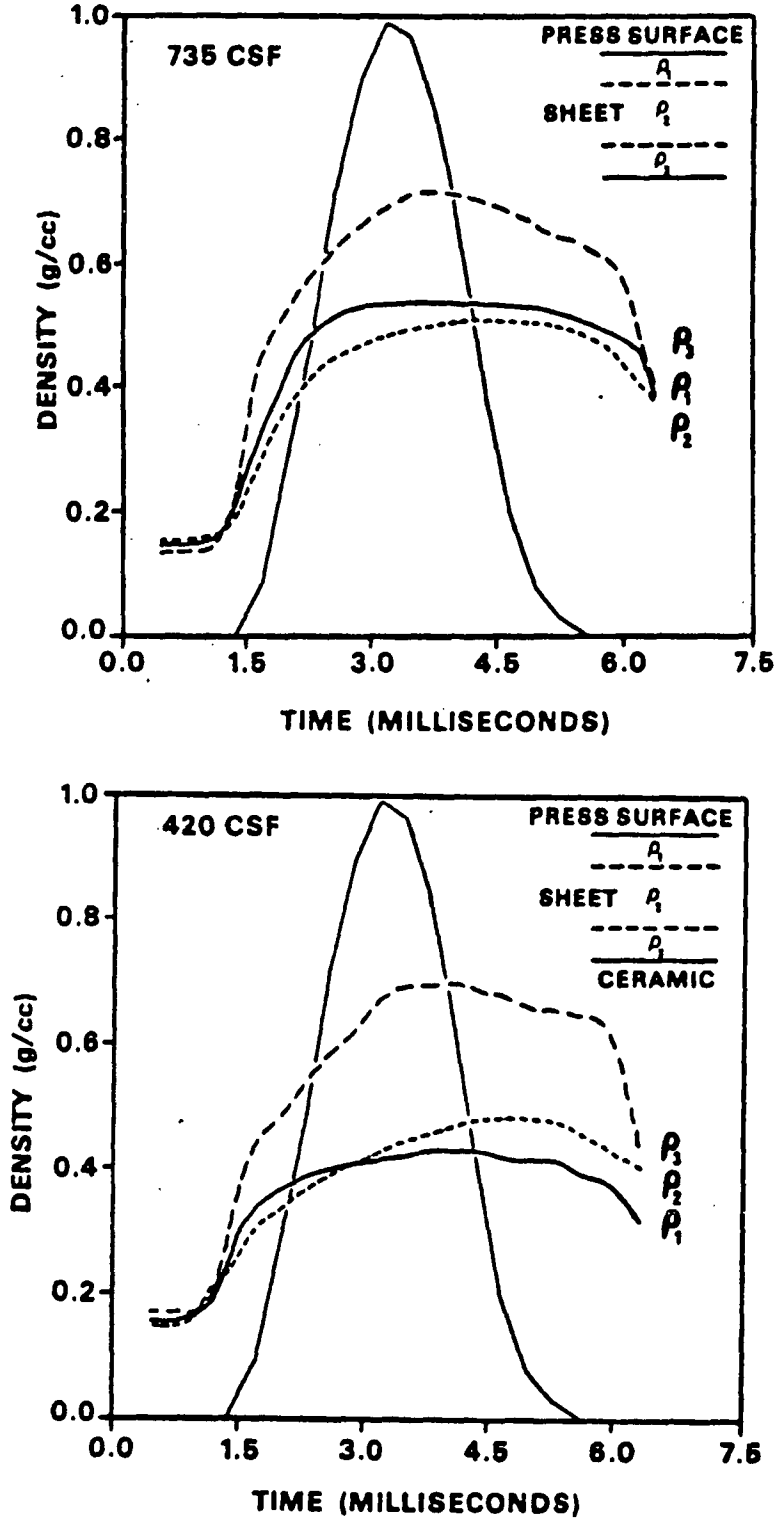

Figure 41. Internal region densities corresponding to sheet densities plotted in Fig. 40. The densities of three sheet thickness regions are depicted with a 25-50-25 split in basis weight for Regions 1-3. Basis weight = 100 g/m^2, Moisture ratio = 4.0, Pmax = 7.0 MPa.

Rewetting

The difference between the water removal at maximum density (Points B,B', in Fig. 37, 40, and Points C,C' in Fig. 38) and that at the exiting saturation density (Points D,D'), indicate a significant amount of water being reabsorbed into the sheet. Table 1 is a tabulation of the calculated water removal at the maximum density in the nip and the exiting saturation density, with the corresponding amount of reabsorbed water for each of these runs.

Table 1. Water removal at maximum density in the press nip and exiting the press nip with reabsorption values for runs plotted in Fig. 37, 38, and 40.

Basis Weight, g/m^2	Freeness Level, CSF	Ingoing Moisture Ratio	Water Removal, g/m^2		Water Reabsorbed, %
			Midnip	Exiting Nip	
55.6	420	4.8	185 (1.47)	105 (2.91)	43.2
52.8	735	4.8	185 (1.30)	100 (2.91)	45.9
56.3	420	1.3	31 (0.75)	11 (1.10)	64.5
53.5	735	1.1	17 (0.78)	7 (0.97)	58.8
102.2	420	3.6	232 (1.33)	131 (2.32)	43.5
105.2	735	4.3	328 (1.18)	191 (2.48)	41.8

[a]Moisture ratios in parentheses.
[b]Water reabsorbed = (midnip - exiting nip)/(midnip).

It should be noted that these data were determined from a nip in which the flow receiver was a ceramic plate with an average pore size of 40 μm. Experiments with felts show a lower degree of water reabsorption, particularly at high moistures.

Three possible major rewetting mechanisms are believed to contribute to the reabsorption of water by the sheet in wet pressing.[58] These include capillary absorption in which water redistribution is due to differences in capillary structure between the flow receiver and paper; film splitting in which a water

film at the sheet-flow receiver interface is split as the two structures separate; and mechanical absorption in which the water redistribution results from a pressure gradient. The lack of dependence of reabsorption on freeness is not consistent with the mechanism of capillary absorption. The large difference in reabsorption for the 100 g/m^2 sheets arises from the difference in initial moisture ratio. The percentage reabsorbed is about the same. The rapid decrease in density exiting the nip, particularly the flow exiting Region 3 (Fig. 41), does support the theory of rewetting by mechanical reabsorption.

Stratification and Crushing

MacGregor recently discussed the theoretical aspects and practical implications of a wet pressing phenomenon he called "sheet stratification."[20,21] Stratification is defined in this thesis as the development of a nonuniform z-direction density profile in which the flow exiting region is the most dense. According to MacGregor,[20] ".... in the process of establishing flow, the sheet must deform first at the flow exiting surface. This causes a greater flow velocity and fluid shear forces here, which in turn cause even more deformation. This creates a sheet which can be more densified at the flow exiting surface, depending on the extent of pressing." This is what is observed in Fig. 39 and 41.

Figure 42 shows density measurements for each of three sheet thickness regions taken over a high moisture wet pressing event. Prior to pressing, the 170 g/m^2 handsheet was at a moisture ratio of 6.33 and was made from a 735 CSF fines-free furnish. The initial compression of the sheet compares well with the nonuniform density development predicted by MacGregor.[20] Since the sheet is initially saturated, pressurization of the liquid water begins immediately. The hydraulic pressure gradient required for fluid flow develops first in the flow

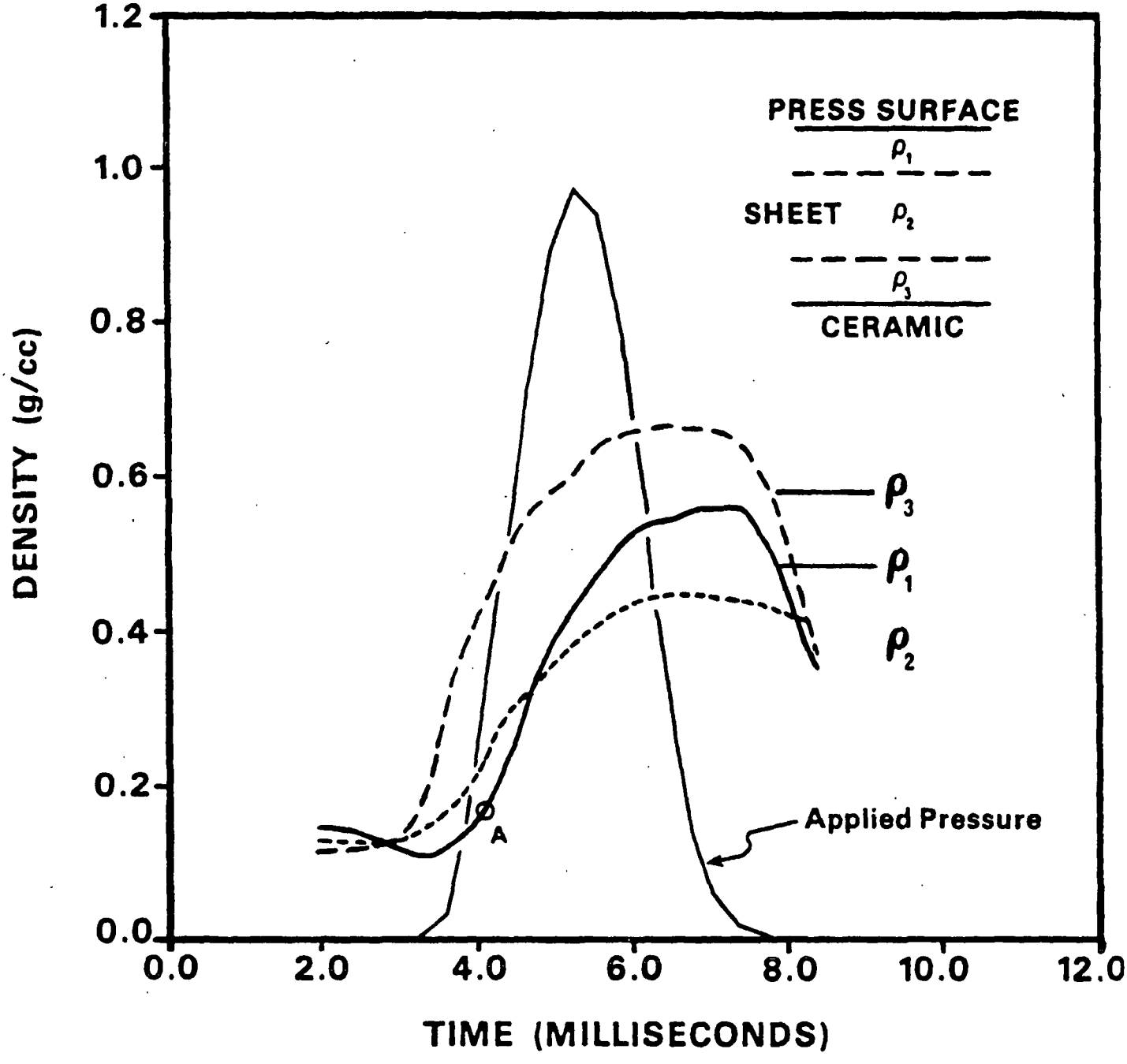

Figure 42. Density-time relationships for each of three sheet thickness regions taken over a single wet pressing event. Basis weight = 170 g/m^2, Incoming moisture ratio = 6.33, Freeness = 735 CSF, Peak pressure = 6.5 MPa.

exiting Region 3. Consequently, this region densifies first. As the compression continues, the hydraulic pressure gradient extends upward toward the press surface. Thus, the middle region densifies next followed by the press surface region. The degrees to which the regions densify during this time depend on the

hydraulic pressure drop across each region which develops in response to the flow resistance of the fiber network. Since flow from the press surface region encounters the greatest cumulative flow resistance, and the flow exiting region the least, it follows that the flow exiting region densifies to the highest degree followed by the middle and press surface region, respectively.

The sheet in Fig. 42 was of very high moisture. The density measurements in Fig. 39, 41, and 44 were made using sheets of moisture ratios more typical of wet pressing. However, the same general densification behavior holds, as described for Fig. 42, once the saturation densities are reached.

Since the sheet in Fig. 42 crushed in the nip, the density profile measurement offered an unusual view of the crushing phenomenon. The abrupt change in slope of the press surface region (Point A) is believed to signal the onset of crush. It appears that the rapid increase in density of the flow exiting region led to a large hydraulic pressure in the press surface region which could not be reduced through the transverse flow of water from the sheet. Thus, the liquid followed the path of least resistance, resulting in the lateral flow of water in the press surface region. The density of the region at Point A (0.17 g/cc) suggests that a cohesive fiber network had yet to develop which could resist the shear forces arising from the lateral water flow. Consequently, crushing occurred in this region through disruption of the fiber network by fluid shear forces. The rapid increase in density of the press surface region results from the lateral flow of both fiber and water out of the nip. It should be noted that the crushing that occurred in the press surface region, as indicated by Fig. 42, could also be verified by visual examination of the crushed sheet.

Effect of Press Roll Temperature

Preheating the sheet prior to pressing has been shown to significantly increase both the absolute water removal in the press nip[29-36] and the average density of the final sheet. These increases with temperature have been attributed to an increase in compressibility due to thermal softening of fiber components and to a decrease in flow resistance due to reduced water viscosity and surface tension forces. In these experiments, the initial sheet temperature was always at room temperature while the press surface temperature was increased up to 150°C.

Elevation of the press surface temperature probably has a similar effect on density development as preheating the sheet prior to pressing. However, since the sheet is being heated in the press nip from one side, it is likely that the cumulative effects are less and depend on the location in the z-direction of the sheet.

Figure 43 shows the total sheet density-time relationships for three 50 g/m^2 handsheets pressed with the press surface temperature at three different levels. As the press temperature is increased, the maximum density obtained in the press nip increases. The fact that the relative shapes of the three curves do not change with temperature suggests that the same densifying forces are in action. The increased temperature accentuates these forces, however, resulting in an enhanced wet pressing effect which leads to higher sheet densities and greater water removal. Examination of the z-direction density profile development of these low moisture, low basis weight sheets does not show significant differences in the magnitudes of the density gradients developed, or in the shapes of the region density-time curves. Considering the low initial moisture,[1,2] it is reasonable that flow effects would not play an important role in the development

of z-direction density profiles. Instead, it is likely that thermal softening plays a more important role.

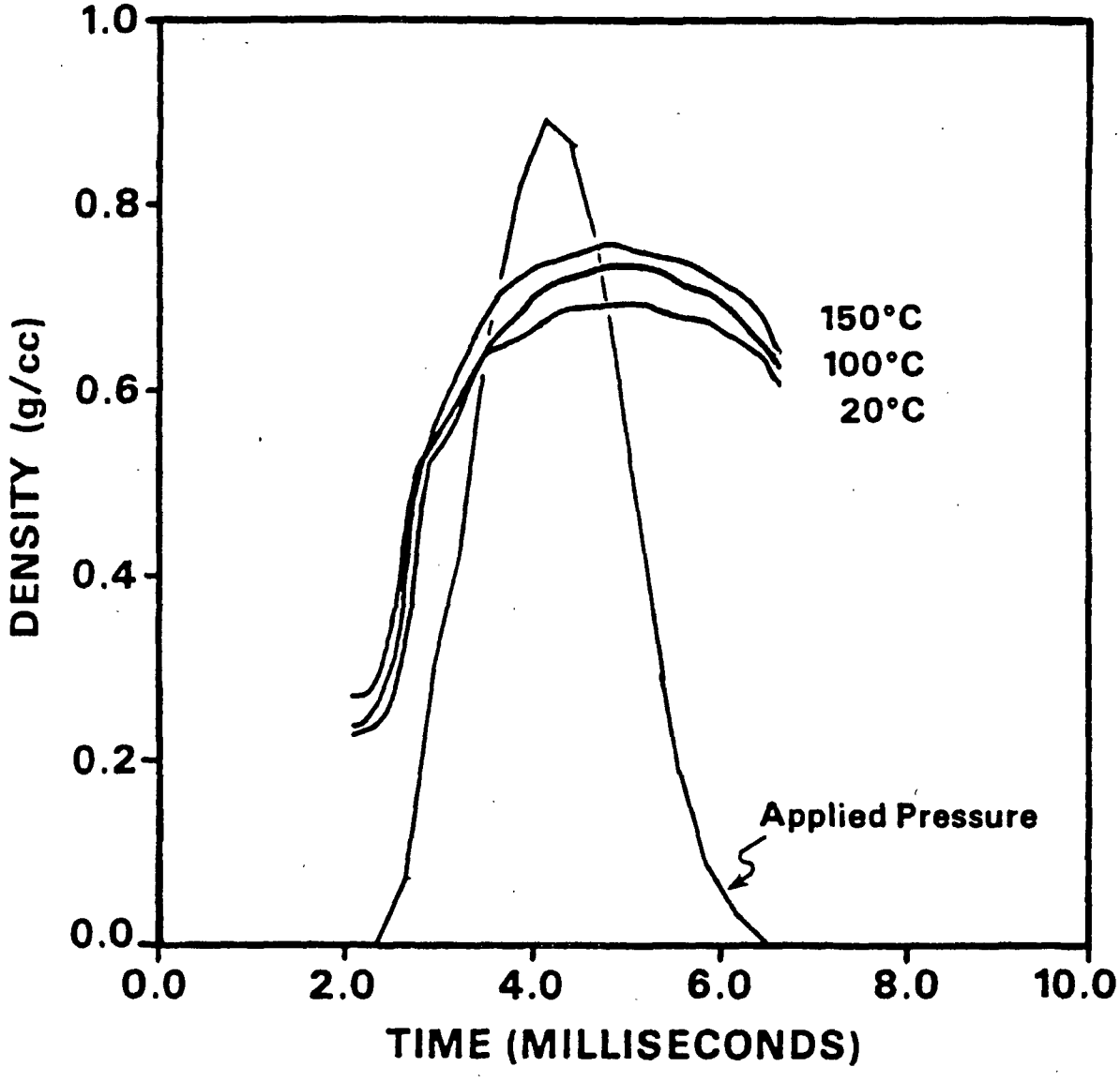

Figure 43. Sheet density-time relationships as a function of platen temperature. Basis weight = 50 g/m^2, Freeness = 735 CSF, Peak pressure = 6.9 MPa, Ingoing moisture ratio = 1.2.

If the density responses of high moisture, high basis weight sheets are examined, definite differences in the z-direction density profiles are evident.

Figure 44 shows the density-time relationships for three thickness regions at press temperatures of 20 and 150°C. The 150°C sheet appears to develop the largest density gradient across the sheet thickness. In light of Darcy's law, it is reasonable that the lower flow resistance associated with the increased water temperature should cause a greater flow velocity out of the sheet, which in turn would result in more nonuniform density development as described by MacGregor.[20]

DENSITY DEVELOPMENT IN IMPULSE DRYING

The average density values of impulse dried handsheets may be 40% or more greater than those developed through conventional processes.[1] However, when compared to wet pressing conditions, the average sheet density developed "dynamically" during impulse drying does not always reflect this large difference. Furthermore, the manner in which that density is achieved is markedly different, as is the degree to which it is retained after leaving the nip. Figure 45 shows a comparison of the average sheet densities obtained during wet pressing at 20°C and impulse drying at 260°C. With the exception of hot surface temperature, the tests were performed under the same pressing conditions. Both cases show similar density development through most of the compression and expansion cycle. However, the impulse dried sheet densifies to a somewhat higher magnitude and reaches its maximum density value slightly before the peak mechanical pressure.

After peaking, the sheet density declines as the applied pressure decreases. The wet pressed sheet densifies to a maximum value slightly past the mechanical pressure peak and subsequently expands as one would expect for such a low initial moisture ratio. In contrast, the impulse dried sheet expands until the

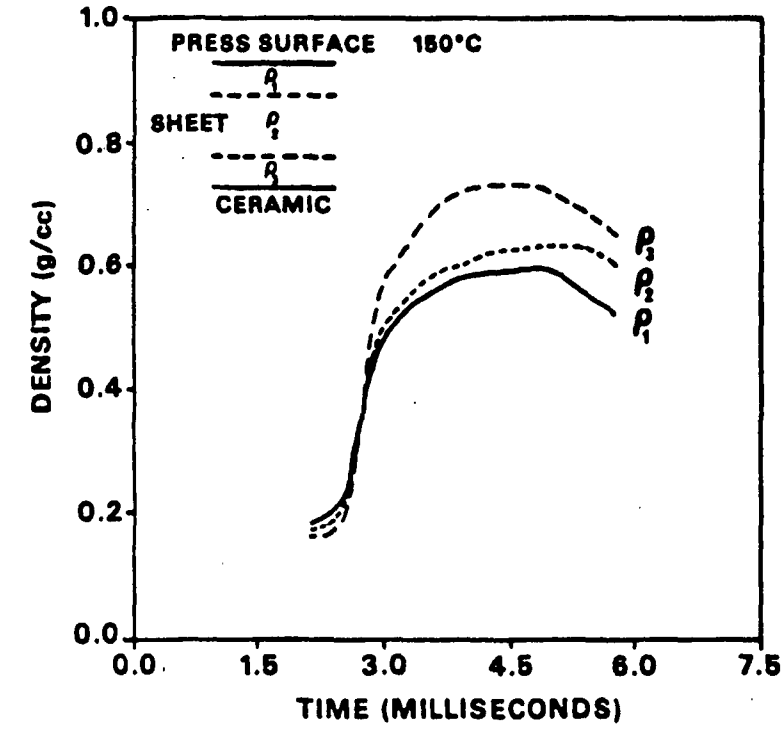

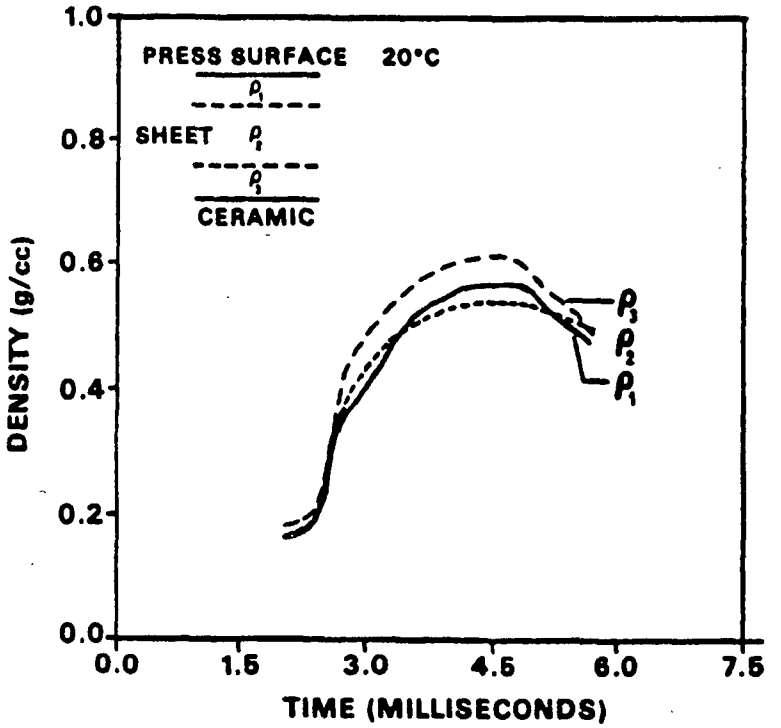

Figure 44. Density-time relationships for each of three internal sheet thickness regions for two wet pressing events. Press surface temperature = 20°C, 150°C, Basis weight = 100 g/m^2, Freeness = 735 CSF, Ingoing moisture ratio = 1.8, Peak pressure = 7 MPa.

applied pressure is at a low value and then increases in density as the applied pressure decreases to zero. These major differences in sheet density response arise from dewatering and densifying forces present in impulse drying but not in wet pressing.

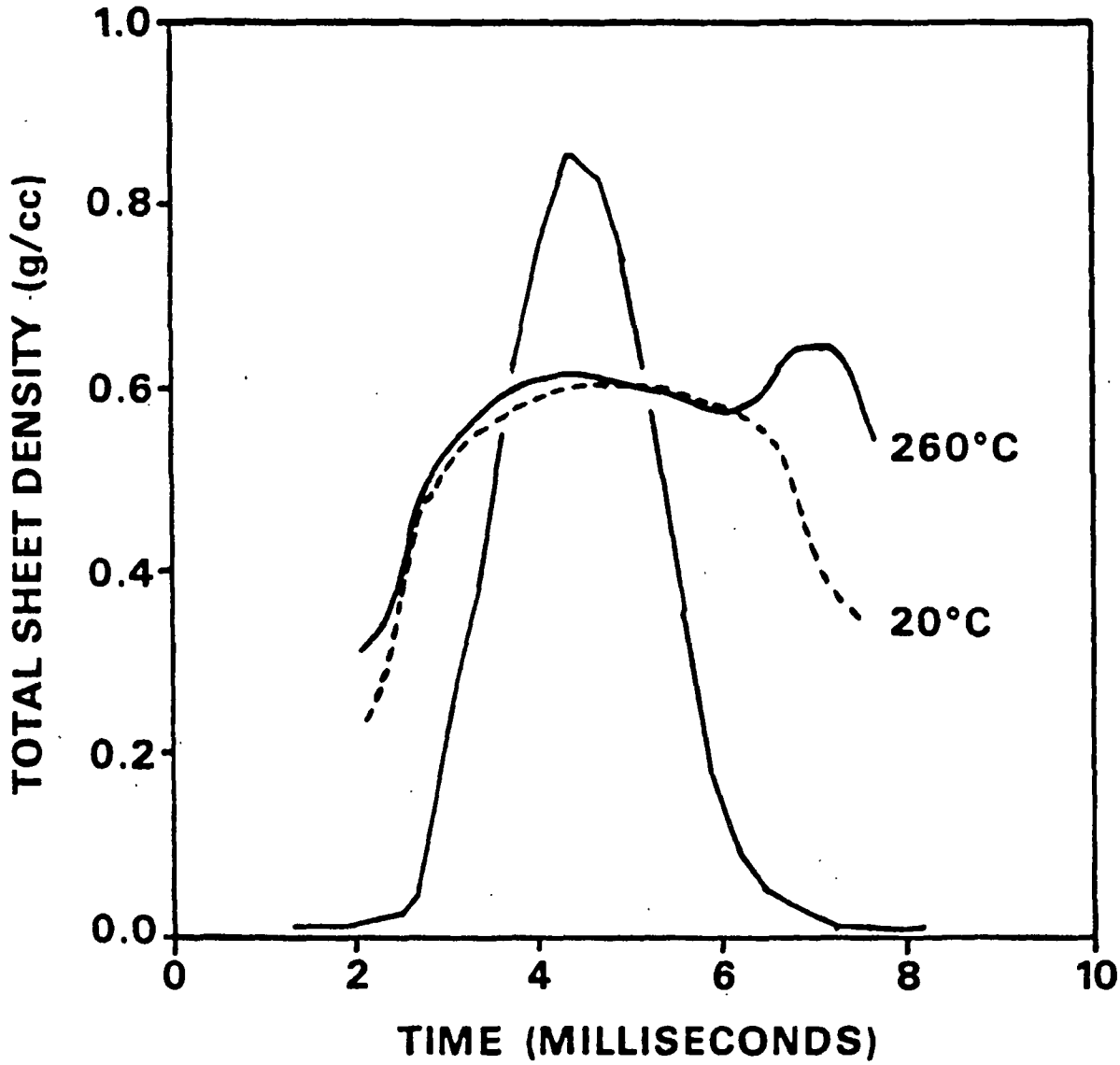

Figure 45. Applied pressure and sheet density-time relationships for impulse drying at 260°C and wet pressing at 20°C. Initial moisture ratio = 1.2, Basis weight = 55 g/m^2, Freeness = 735 CSF, Peak pressure = 7.2 MPa, NRT = 4.5 sec.

Measurements of the internal sheet temperature and z-direction density profile development provide a means for investigating the unusual dynamic physical processes which occur during impulse drying. Figure 46 shows density measurements for each of the three web thickness regions taken over a typical impulse drying event. Figures 47, 48, and 49 show internal sheet temperature measurements, instantaneous heat flux to the sheet, and the instantaneous vapor pressure at the hot surface-sheet interface, respectively, for the same experimental conditions. Figures 46-49 will be referred to in the ensuing discussion on densification during impulse drying. In order to describe the densification process in detail, the impulse drying event has been divided into five time intervals numbered 1-5.

Interval 1 begins when the hot surface contacts the sheet. During this period, the initially unsaturated sheet densifies fairly uniformly throughout its thickness as it would in wet pressing. Temperature measurements (Fig. 47) indicate that rapid sensible heating of the hot surface region of the web occurs at the same time. Because the sheet remains unsaturated, and at temperatures below the ambient boiling point over much of Interval 1, there is little opportunity for liquid or vapor removal. Near the end of Interval 1, however, the average temperature near the hot surface is well beyond the ambient boiling point, giving rise to a rapid increase in evaporation. The heat flux at this point is 0.568 MW/m^2 and rapidly increasing.

During Interval 2, boiling at or near the hot surface rapidly produces water vapor which flows into the still unsaturated sheet. The vapor quickly reaches cooler sites where it condenses, raising the local temperature and degree of liquid saturation. The internal sheet temperature data suggest that this process moves progressively through the web, raising the temperature (T2 during

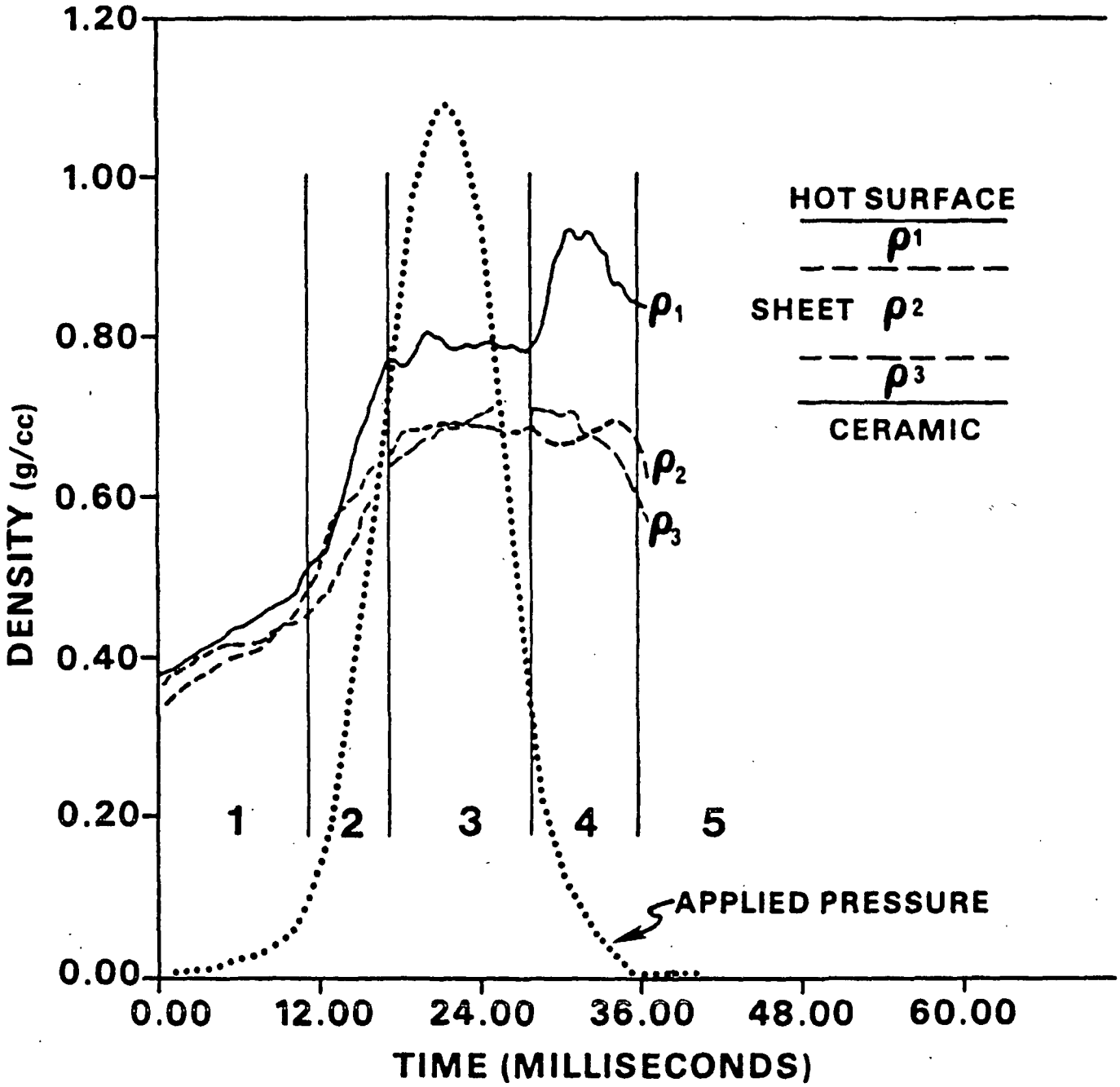

Figure 46. Applied pressure and regional densities for impulse drying of 100 g/m^2, 735 CSF sheet at an initial moisture ratio of 1.3. Hot surface temperature = 260°C, Peak pressure = 3.8 MPa.

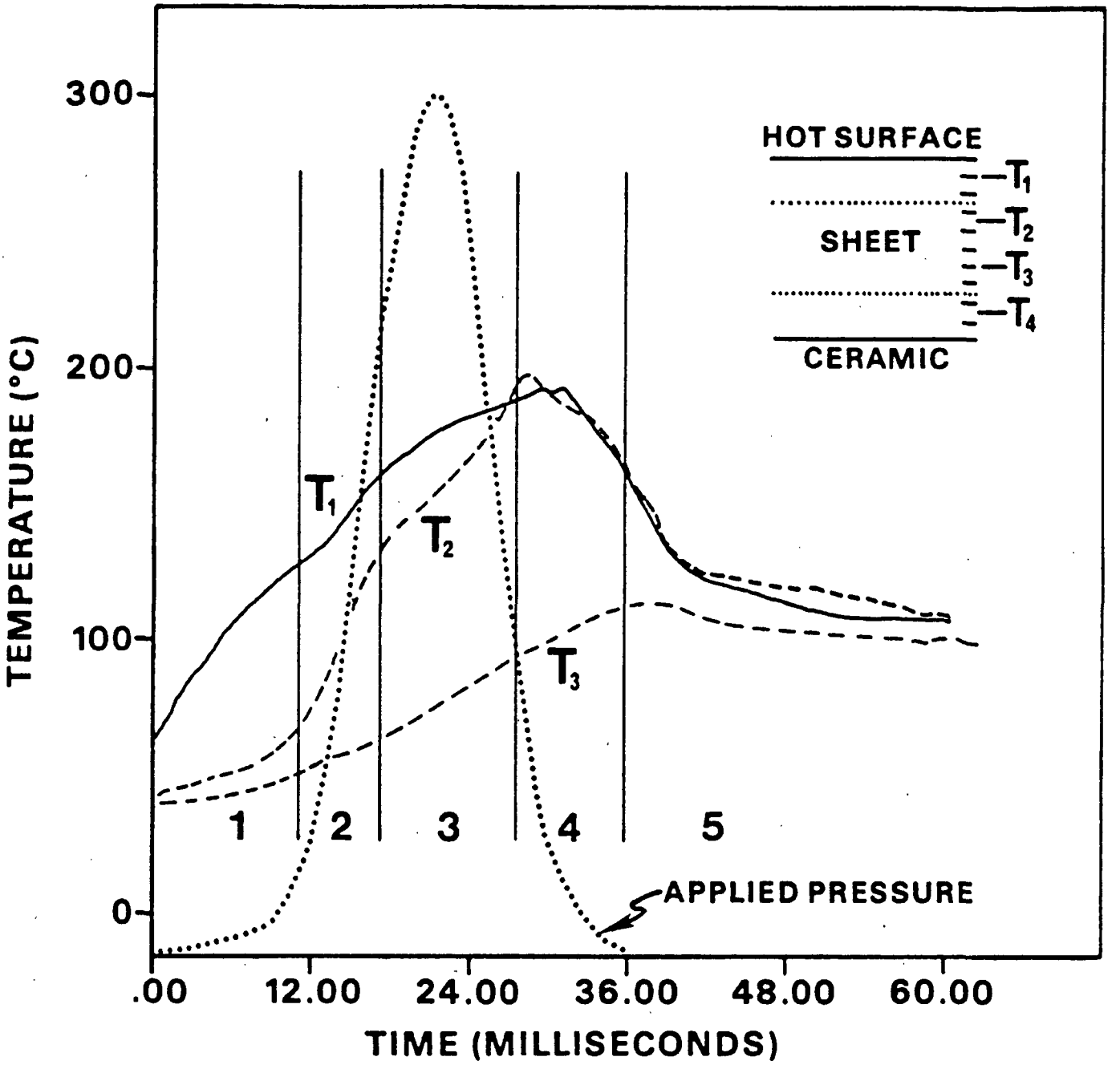

Figure 47. Applied pressure and internal sheet temperatures for impulse drying of a 100 g/m^2, 735 CSF sheet, at an initial moisture ratio of 1.4. Hot surface temperature = 260°C, Peak pressure = 3.8 MPa.

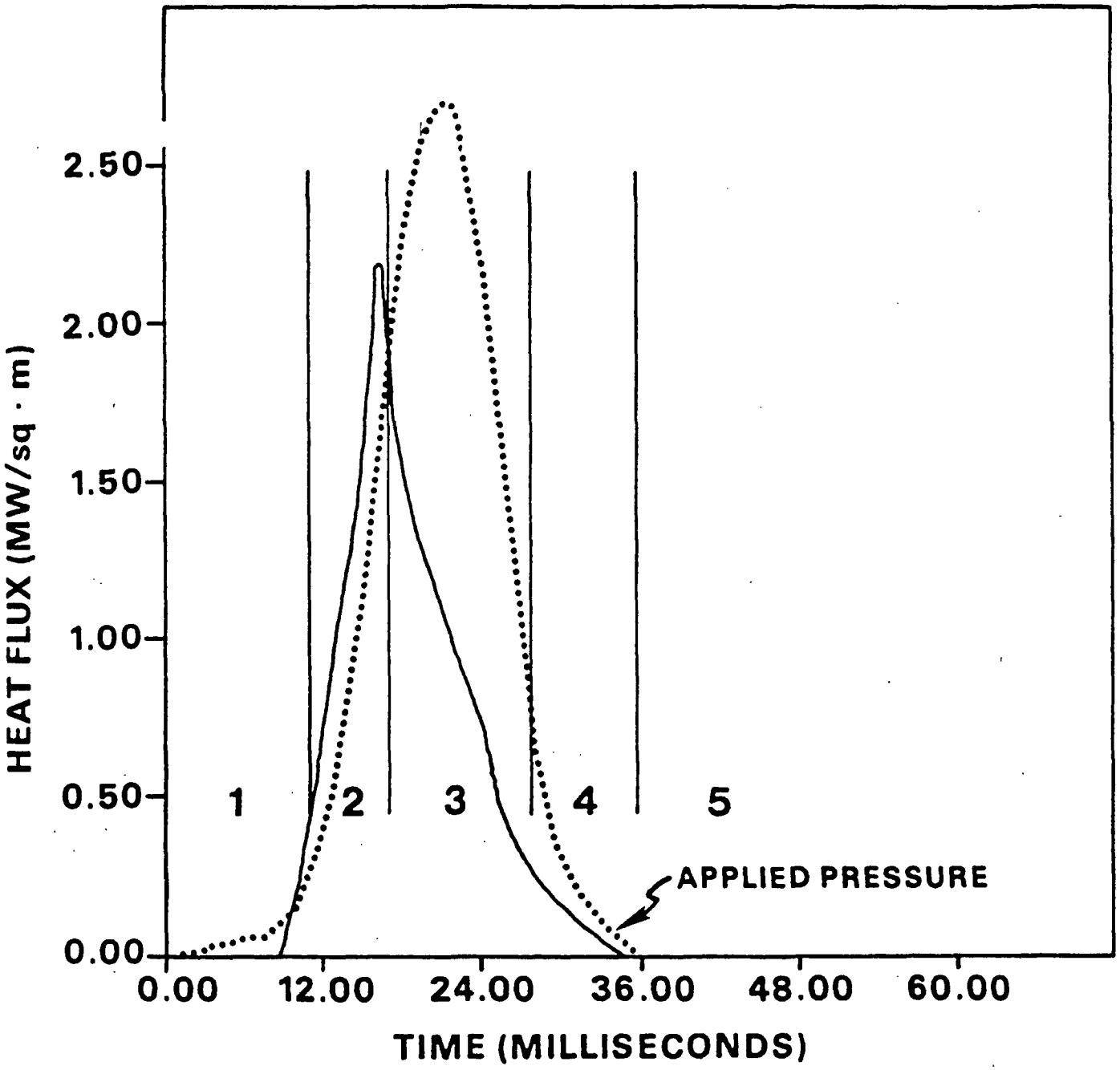

Figure 48. The instantaneous applied pressure and heat flux for impulse drying of a 100 g/m^2, 735 CSF sheet at an initial moisture ratio of 1.3. Hot surface temperature = 260°C, Peak pressure = 3.8 MPa.

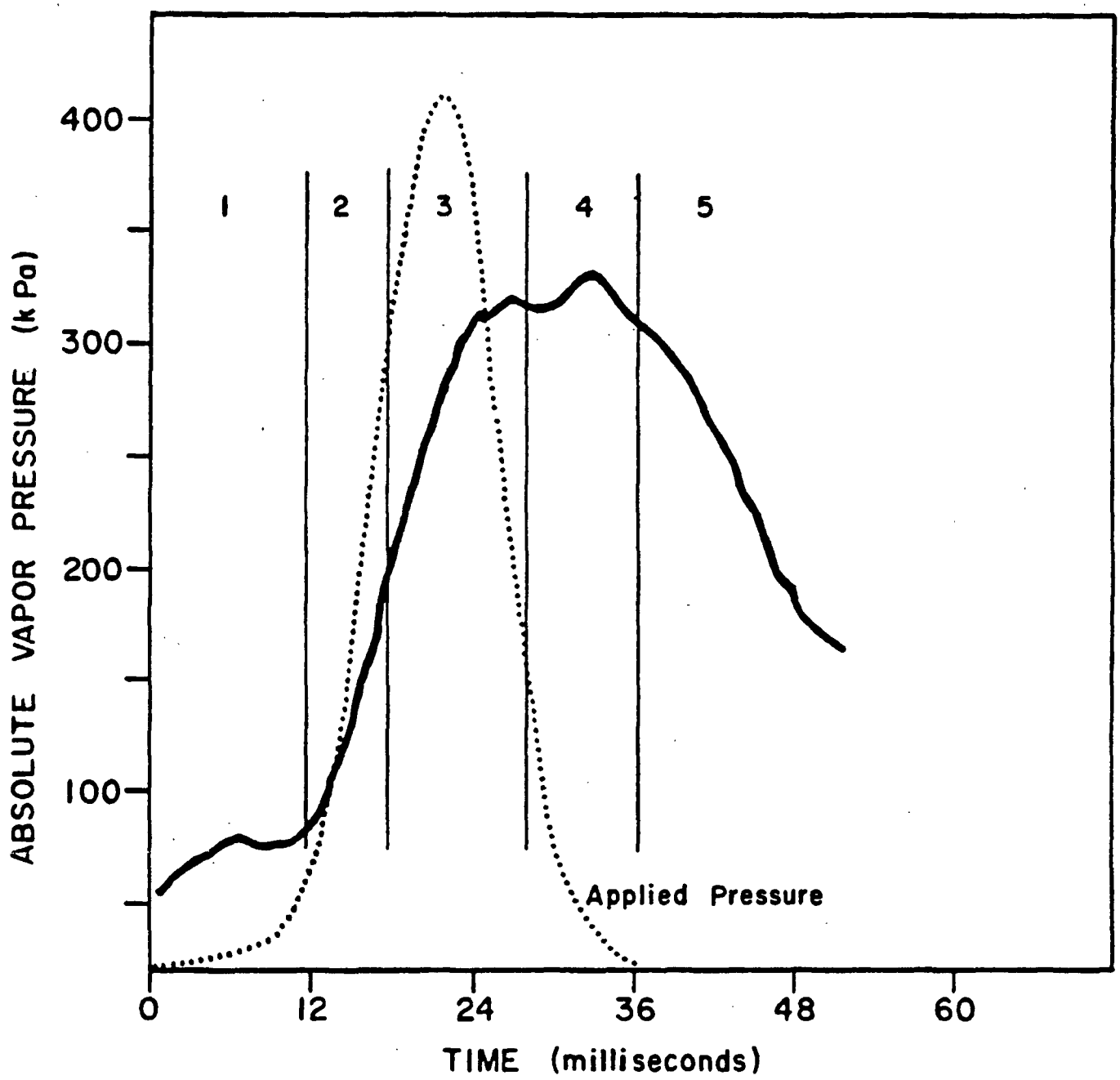

Figure 49. Instantaneous applied pressure and hot surface-sheet interfacial vapor pressure of a 100 g/m^2, 735 CSF sheet at an initial moisture ratio of 1.3. Hot surface temperature = 260°C, Peak pressure = 3.8 MPa.

Interval 2 in Fig. 47) much faster than could be supported by a conduction heat transfer mechanism alone. The evaporation/condensation process, combined with the mechanical compression of the web, results in a liquid redistribution in which the lower regions become saturated with liquid water while the hot surface region remains predominantly filled with vapor. Internal temperature data show that this situation persists for the duration of the impulse. For faster pressure applications, liquid dewatering due to hydraulic pressure generation in the lower regions may occur.

Shortly after the start of Interval 2, a new dewatering mechanism develops which is unique to impulse drying. Continued vapor generation combined with an increasing network flow resistance generates a substantial internal vapor pressure in the hot surface region. This vapor pressurization, acting on the liquid saturated lower region, induces liquid dewatering by liquid displacement. The onset of pressurization is detected experimentally by the hot surface vapor pressure measurement (Fig. 49) and by the appearance of hot surface region temperatures above 100°C.

The intense densification of the hot surface region during Interval 2 results from the combined effect of increased mechanical compression, moisture redistribution, and thermal softening of fiber components. Although the middle and flow exiting regions continue to densify under the action of mechanical compression and vapor induced dewatering, the hot surface region density reaches a temporary maximum due to internal pressurization. This signals an end to Interval 2.

The vapor pressure in the hot surface region continues to build during Interval 2. The heat flux curve peaks at the end of Interval 2, then rapidly

declines (Fig. 48). The decrease in heat flux is probably due to a combined effect of drying out of the region immediately adjacent to the hot surface and to an insulating effect of the vapor.

Although the moisture redistribution started in Interval 2 tends to remove liquid from the upper region of the sheet, heat flux measurements for Interval 3 indicate that sufficient liquid remains for evaporation to sustain the heat transfer required by the progressive heatup of the sheet. According to the temperatures measured in the web and assuming open surface saturation at these temperatures, vapor pressures as high as 1.25 MPa may be generated in the hot surface region by the end of this interval. Vapor pressure measurements in Fig. 48, however, show much lower values. It is believed that drying out of the fibers immediately adjacent to the hot surface restricts the flow of vapor to the measurement cavity, resulting in erroneously low vapor pressure measurements. In any case, it is believed that sufficient pressurization may exist to inhibit further consolidation of the hot surface region during Interval 3.

Although the hot surface region density in Fig. 46 remains relatively constant during Interval 3, other experiments show that this region may experience a gradual increase or decrease in density. Even with the region predominantly filled with vapor, it is believed that a significant amount of water is still present in the cell wall. This water, at or slightly below the bulk temperature of the region, is difficult to remove due to the hygroscopic nature of the cellulosic fibers. A gradual increase in hot surface region density over this period suggests a progressive drying out of the region, particularly near the hot surface. A rapidly decreasing heat flux supports this interpretation. In some cases, the internal pressurization of the hot surface region may be great enough to decrease the density of the region during Interval 3. This is

indicated by the measured decrease in Region 1 density for a number of experimental tests, similar to that plotted in Fig. 46.

The flow exiting region in Fig. 46, which is liquid saturated at a temperature less than 100°C during Interval 3, reaches a maximum density under the action of mechanical compression and vapor induced dewatering.

As the applied pressure decreases, it reaches a point where it can no longer sustain the vapor pressure, allowing vapor to escape from the sheet. The decrease in internal vapor pressure creates a condition in which pore water existing in the cell wall becomes superheated and flashes, allowing the fiber structure to collapse under the applied load. Hence, the fast rise in density of the hot surface region at the onset of Interval 4 is thought to result primarily from cell wall collapse associated with reduced vapor pressure and pore water flashing. This interpretation is supported by a rapidly decreasing bulk temperature of the hot surface region which suggests an evaporative cooling of the region as well as a decline in the internal vapor pressure. The same process is seen to occur to a lesser extent in the middle region, although lagging in time. Further heating of the lower regions probably results from continued condensation of low pressure vapor and conduction from the upper hotter regions.

After the applied pressure is removed, the onset of Interval 5, flash evaporation and vapor release from the sheet are believed to continue for some time. This is indicated by the sheet temperatures at or above 100°C after the pressure has been removed. For very intense drying conditions, this has been seen to result in delamination of the fiber network. However, under controlled conditions, this postnip vapor release process is believed to contribute to the bulkiness of the middle region. The bonding which develops during the closed

nip portion of impulse drying is sufficient in most cases to maintain sheet integrity during vapor release.

Relationships Between Heat Transfer, Vapor Pressure Development, and Hot Surface Region Densification During Impulse Drying

The density development discussed in the preceding section is intricately related to heat transfer and vapor pressure development. Figure 50 shows the instantaneous vapor pressure and hot surface region density measurements for a typical impulse drying event. As the vapor pressure rapidly increases, the hot surface region density starts leveling out, suggesting that internal pressurization of the fibers or fiber network is resisting compression. During the last part of the nip, the density increases despite the fact that the measured vapor pressure, although slightly decreasing, remains at a high value. Once the region has reached its maximum density value the vapor pressure decreases at a high rate. As mentioned earlier, the validity of the vapor pressure measurement has not been satisfactorily established. Although measured vapor pressures remain high at the "beginning" of the period of final density increase, temperature measurements show a rapid drop in internal sheet temperature, suggesting a drop in internal vapor pressure. It is plausible that escaping vapor through the hot surface-sheet interface could maintain the "measured" vapor pressure at a high value through this final densification phase. This explanation is supported by the lift off phenomenon discussed later in this section (see Fig. 54).

The shape of the hot surface region density curve described above is characteristic of impulse drying. The magnitude of density may vary with condition but the general shape remains the same. Figure 51 is a plot of a number of hot surface density curves for various impulse drying conditions.

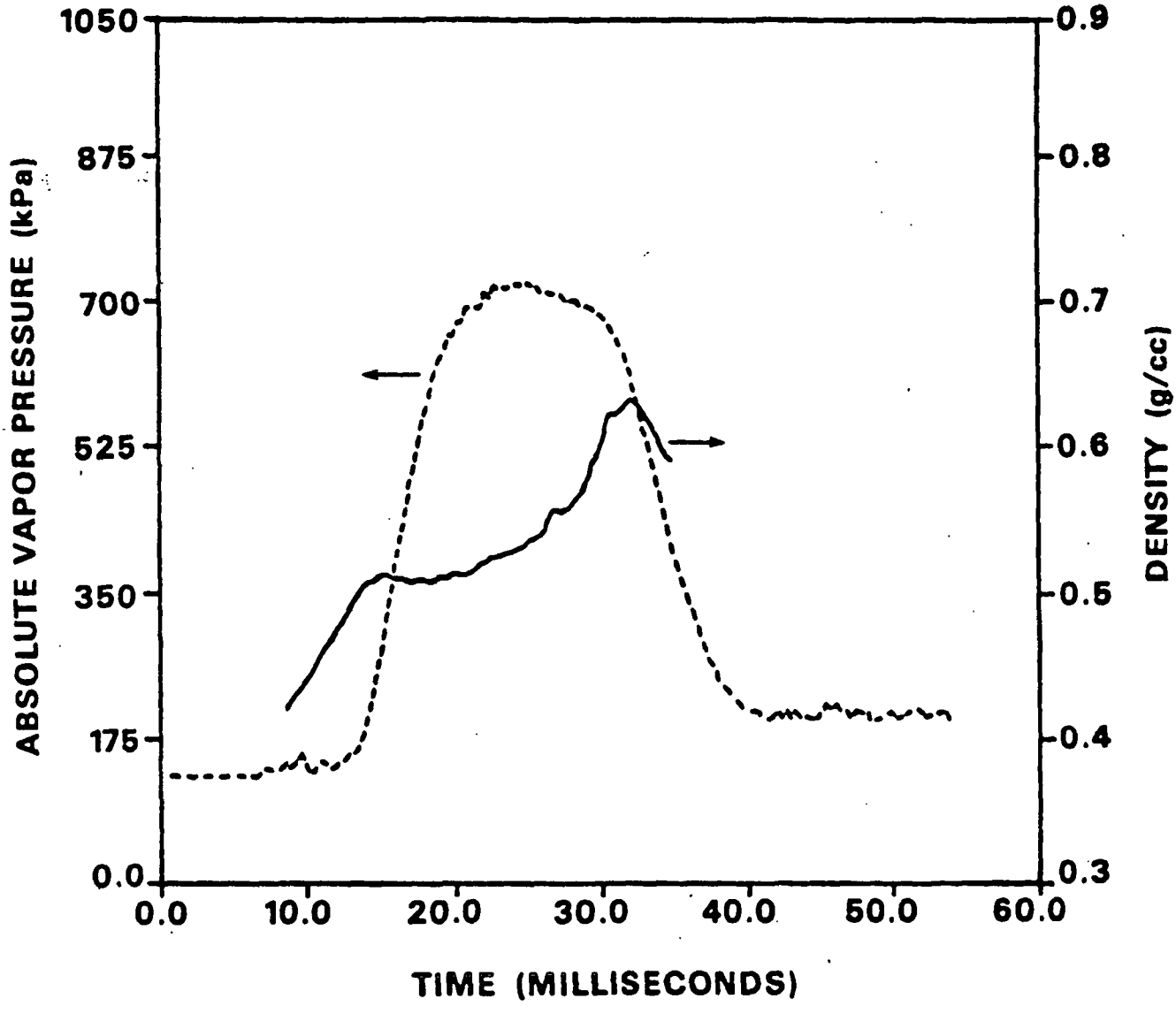

Figure 50. Instantaneous vapor pressure and hot surface region density for impulse drying a 173 g/m^2, 735 CSF sheet with an initial moisture ratio of 1.4. Hot surface temperature = 315°C, Peak pressure = 4.0 MPa.

In general, the higher the temperature, the more pronounced the characteristic shape. Note that the internal pressurization, as discussed earlier can result in a levelling, increase, or decrease in the density curve during the central part of the nip.

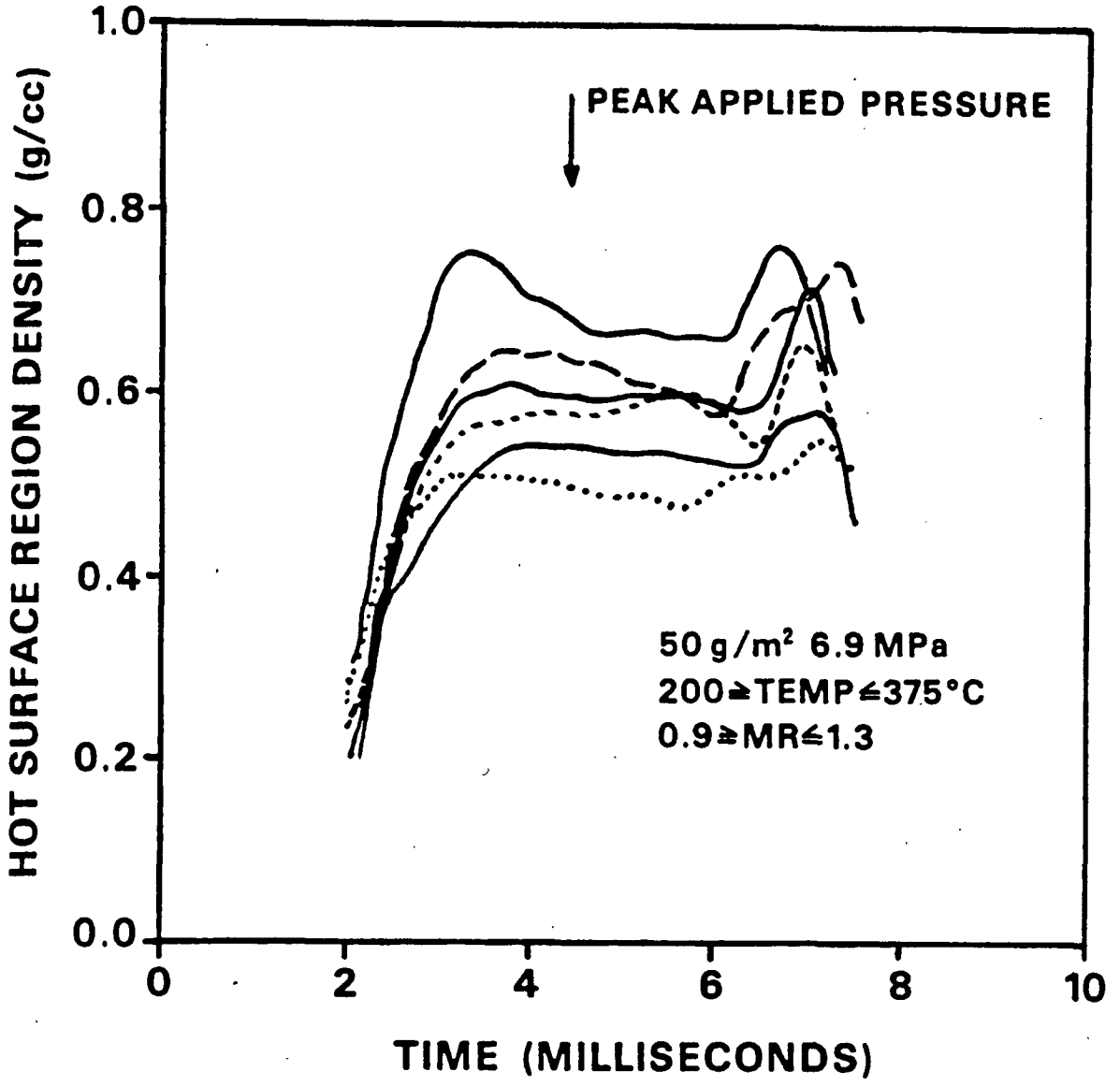

Figure 51. Hot surface density response with time for various impulse drying conditions.

The instantaneous heat flux is compared with the vapor pressure and hot surface region density measurements in Fig. 52 and 53, respectively. The peak heat flux occurs early in the nip before the rapid increase in vapor pressure. These high values of heat flux result from the evaporative boiling of water most accessible to the hot surface. The vapor that is generated during this initial boiling moves to cooler sites in the sheet where it condenses. As a result, a

significant vapor pressure does not yet develop. About the time the hot surface region density levels out and the vapor pressure rapidly increases, the heat flux reaches a period of decline. This condition continues until the time at which the density starts increasing and the sheet temperature and vapor pressure starts decreasing. At this time, a more rapid decline in the heat flux follows, which results from an insulating effect of the vapor, from drying out of the hot surface region, and from a decrease in thermal contact between the sheet and hot surface.

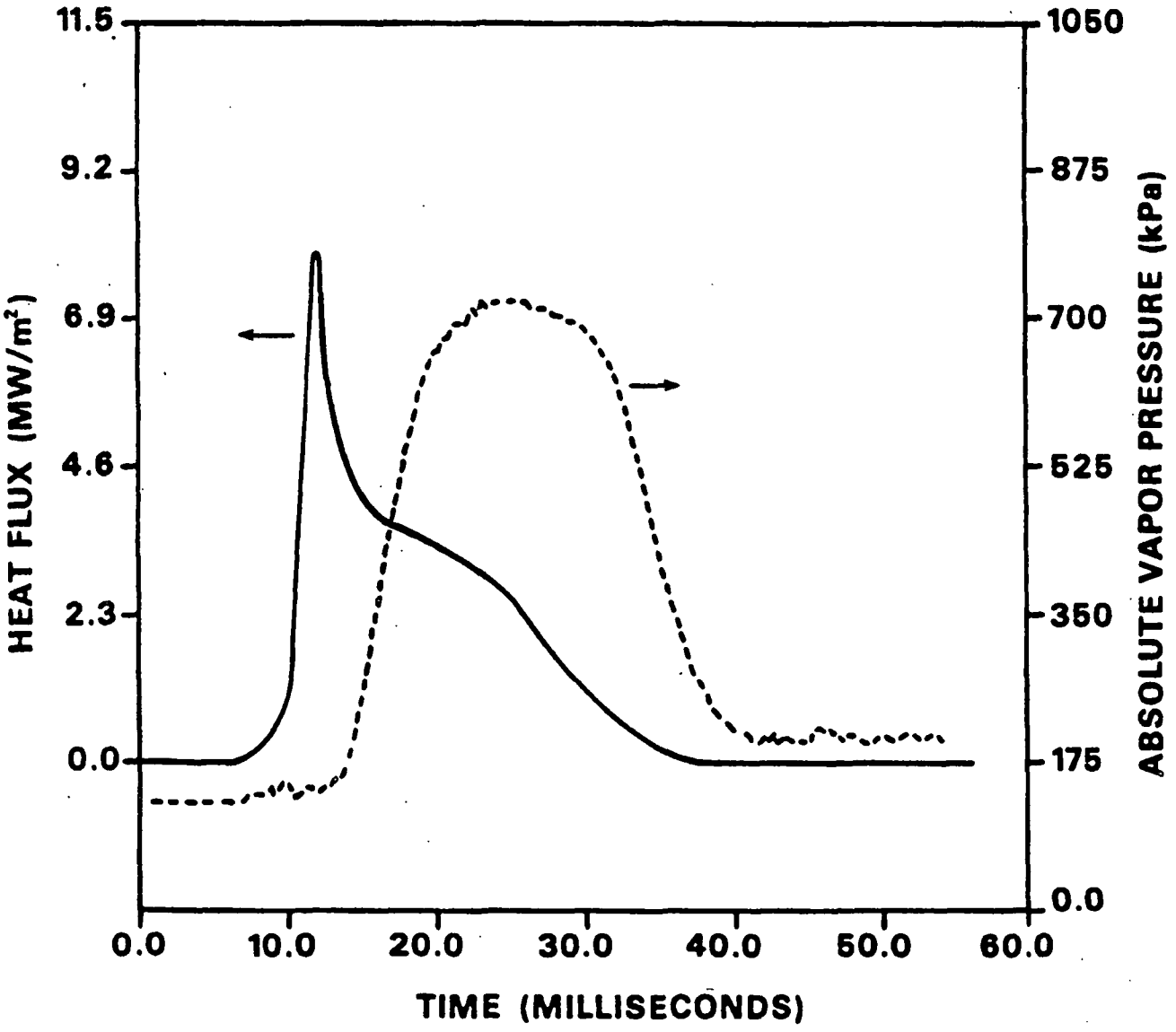

Figure 52. The instantaneous heat flux and vapor pressure for impulse drying a 173 g/m^2, 735 CSF sheet at an initial moisture ratio of 1.4, 315°C, 4.0 MPa.

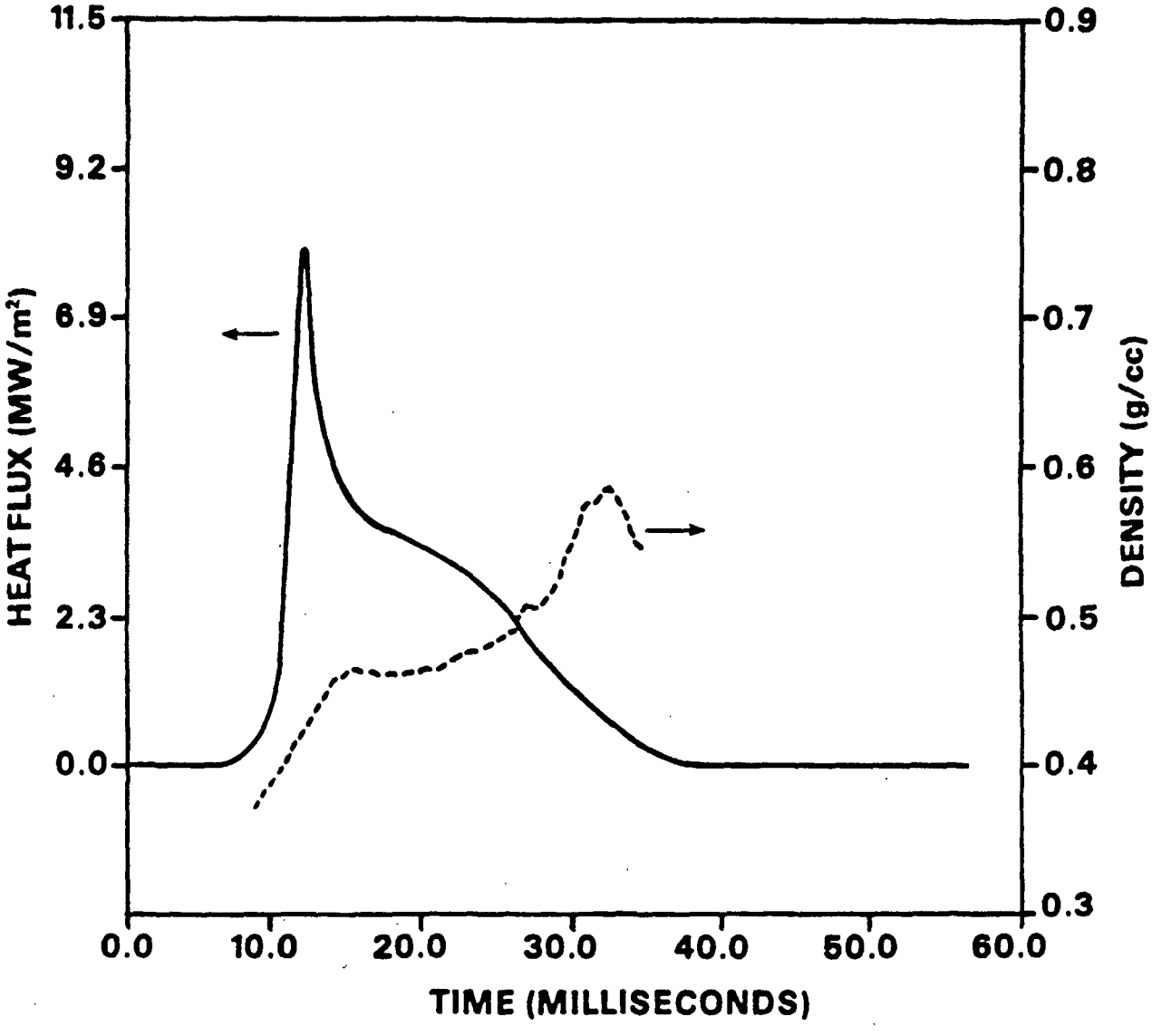

Figure 53. Instantaneous heat flux and hot surface region density for impulse drying a 173 g/m^2 sheet at an initial moisture ratio of 1.4, 315°C, 4.0 MPa.

During the final period of densification, a decrease in thermal contact between the hot surface and sheet may occur. At some point in time toward the end of the nip, the vapor pressure is comparable in magnitude, but opposed to, the applied mechanical pressure. This may result in a lift-off phenomenon similar to that described by Ahrens and Åström[59] during high intensity drying at low

mechanical pressures. The rapid drop in heat flux during the final densification period suggests a corresponding loss of thermal contact.

The lift-off phenomenon is demonstrated in Fig. 54 in which the displacement measurements of the hot surface and sheet surface are compared. The hot surface region density response is included for reference. At contact, the two surfaces are in intimate contact. As time progresses, however, separation of the surfaces develops. This separation corresponds to the leveling out of the hot surface region density. As the separation decreases, the density gradually increases until lift-off occurs and the region density rapidly increases.

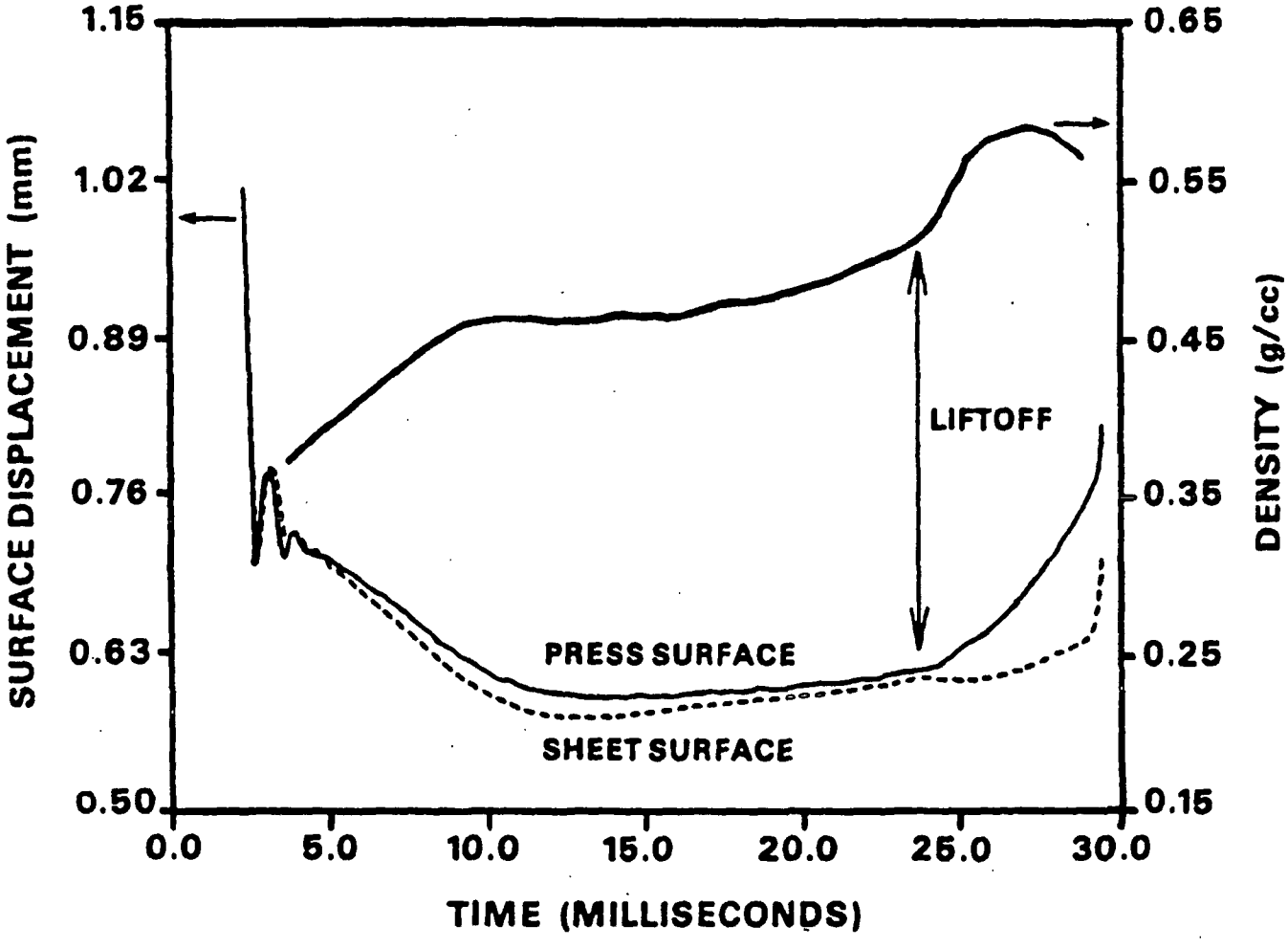

Figure 54. Instantaneous hot platen and sheet surface displacement during impulse drying at 315°C plotted with hot surface region density to demonstrate lift-off.

The shapes of the heat flux curves presented in Fig. 48 and 52 have been characteristic of the experiments performed in this thesis. This includes a peaking of the heat flux early in the nip, followed by a period of a constant or slowly declining heat flux, and finally a more rapid decline in heat flux to zero at the end of the nip. As the moisture of the sheet is increased, the heat flux increases, but the shape remains relatively the same.

Density Retention and Structural Analysis

The z-direction density distribution observed in the sheet after impulse drying usually closely resembles that observed dynamically during impulse drying. Hence, the bonding that develops under the considerable restraint of impulse drying, especially in the hot surface region, is not lost in the postnip drying and conditioning processes. The density profile is typically J shaped with the hot surface region having the highest average density followed in magnitude by the flow exiting region. The middle region, viewed under the scanning electron microscope (SEM), has a greater occurrence of interfiber voids and a lower degree of fiber collapse, which are believed to result from the postnip vapor release process. In contrast, the hot surface region appears to be highly bonded with a high degree of fiber collapse. This unique distribution has been verified qualitatively by visual inspection under the SEM and by a SEM mapping technique, and quantitatively by a sheet grinding technique. In addition, density profiles have been determined immediately after the nip using the dynamic density profile measurement system.

Figure 55 shows the postnip density ratio as a function of hot surface temperature and freeness. Postnip density ratio is defined as the bottom region density divided by the top region density where the top region is next to the hot surface. This ratio is determined immediately after the impulse drying nip.

As the platen temperature is increased up to 150°C, the ratio increases, with the 420 CSF pulp showing the greatest increase. This increase results from an enhanced wet pressing effect. Considering the higher flow rates that may develop as a consequence of increased water temperature, it is reasonable to expect the high flow resistance furnish (420 CSF) to exhibit a greater nonuniform density development.

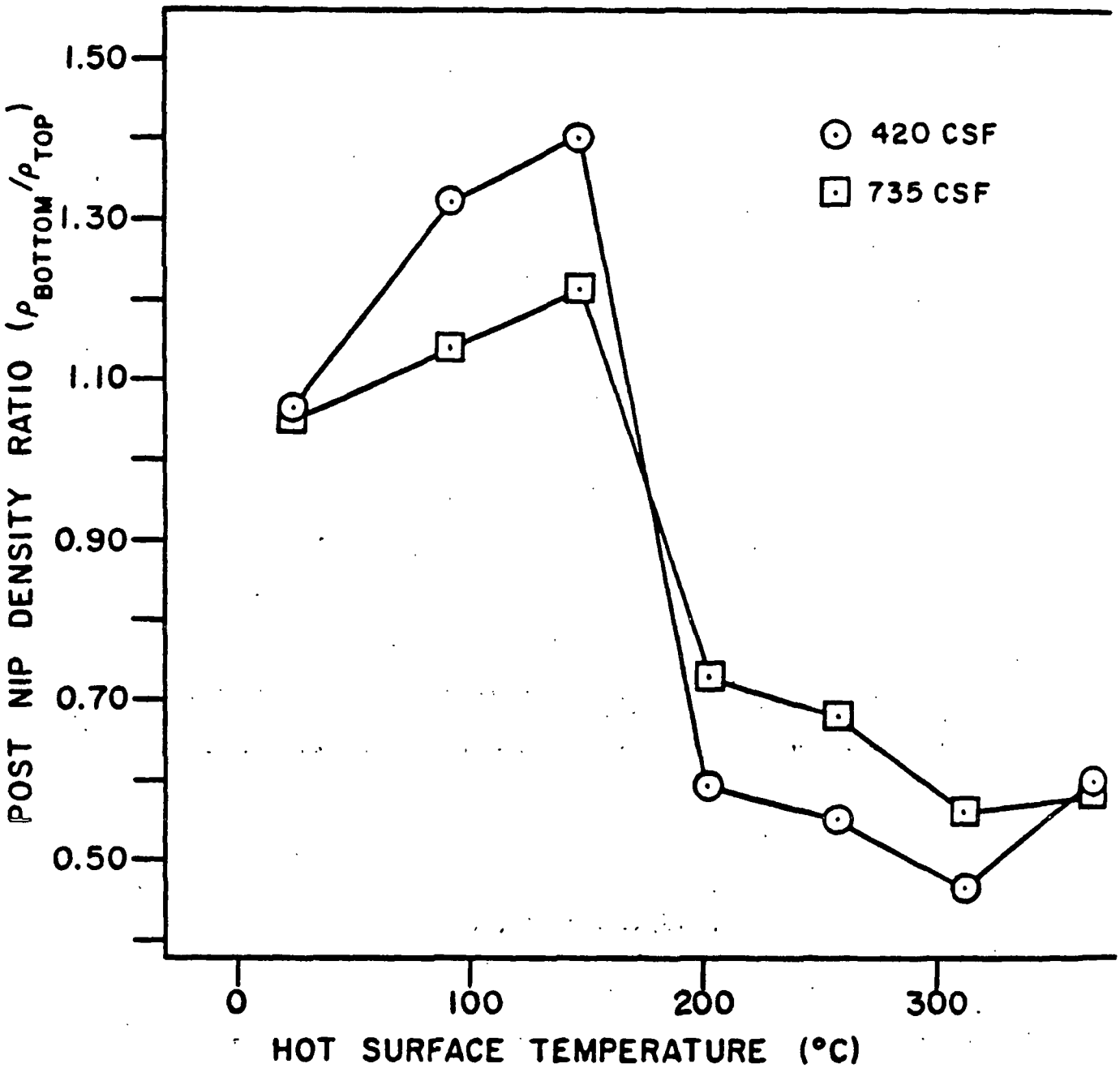

Figure 55. Postnip density ratio as a function of hot surface temperature and freeness. Basis weight = 50 g/m^2, Peak pressure = 5.3 MPa, NRT = 4.5 msec, Moisture ratio = 1.3.

As 200°C is reached, an abrupt shift in the ratio is seen to occur which suggests the development of new densifying mechanisms. These mechanisms, discussed in the previous sections, result in a sheet more dense in the top fiber regions exposed to the hot surface. The effect is, once again, greater for the high flow resistance furnish. The shift in postnip density ratio signals the emergence of the impulse drying regime.

Figure 56 shows two SEM photographs of the cross sections of a wet pressed sheet and an impulse dried sheet. The density profile of each sample, as determined by the SEM mapping technique, is superimposed on the photographs. The density profile of the wet pressed sheet appears fairly uniform while a J shaped profile is evident for the impulse dried sheet.

Close examination of the SEM photographs in Fig. 56 (and others) shows that the fibers of the wet pressed sheet tend to be more uniformly collapsed. In contrast, the fibers of the impulse dried sheet are highly collapsed in the region adjacent to the hot surface region and collapsed to a lesser degree in the middle region. The fibers in the region adjacent to the ceramic surface appear similar to those in the wet pressed sheet. The highly collapsed fibers are believed to result from the combined effect of thermal softening and drying out while under mechanical restraint. The uncollapsed fibers, as well as the greater occurrence of interfiber voids are believed to result from postnip evaporation and vapor release. The continued flashing of intrafiber water after the applied pressure is released may cause some of the fibers to increase in volume. The interfiber voids may be created in a similar manner except it is the vapor pressure arising from the resistance to vapor flow out of the fiber network that causes an increase in sheet volume. Since the sheet is fairly moist in this region, local separation of the fiber network results. Total

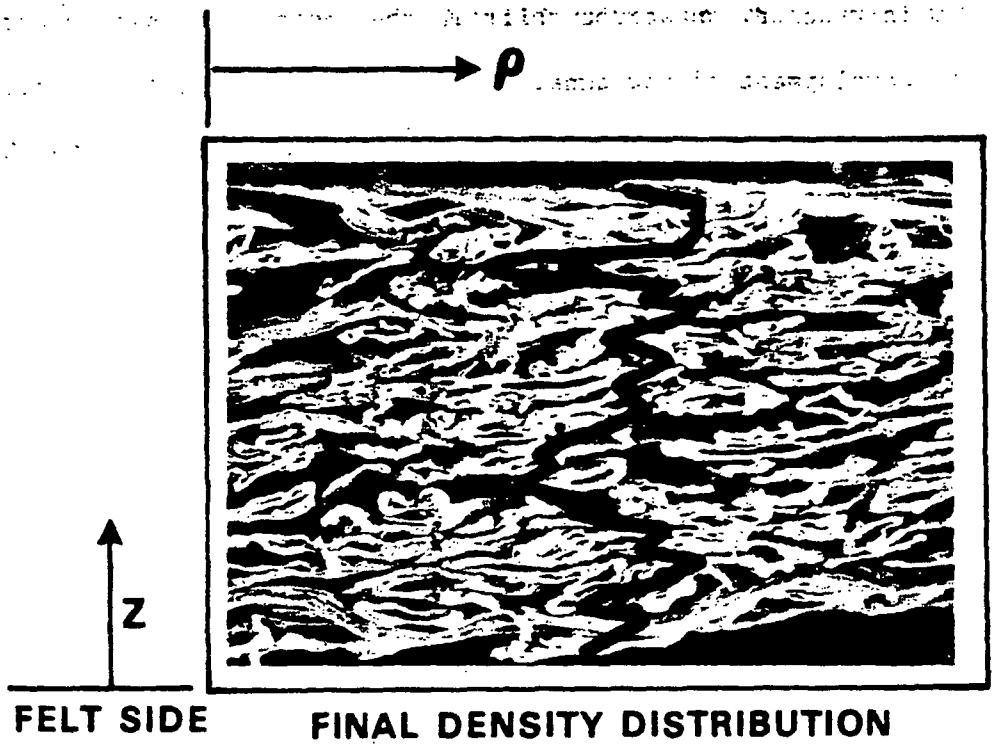

Cross Section of Wet Pressed Sheet

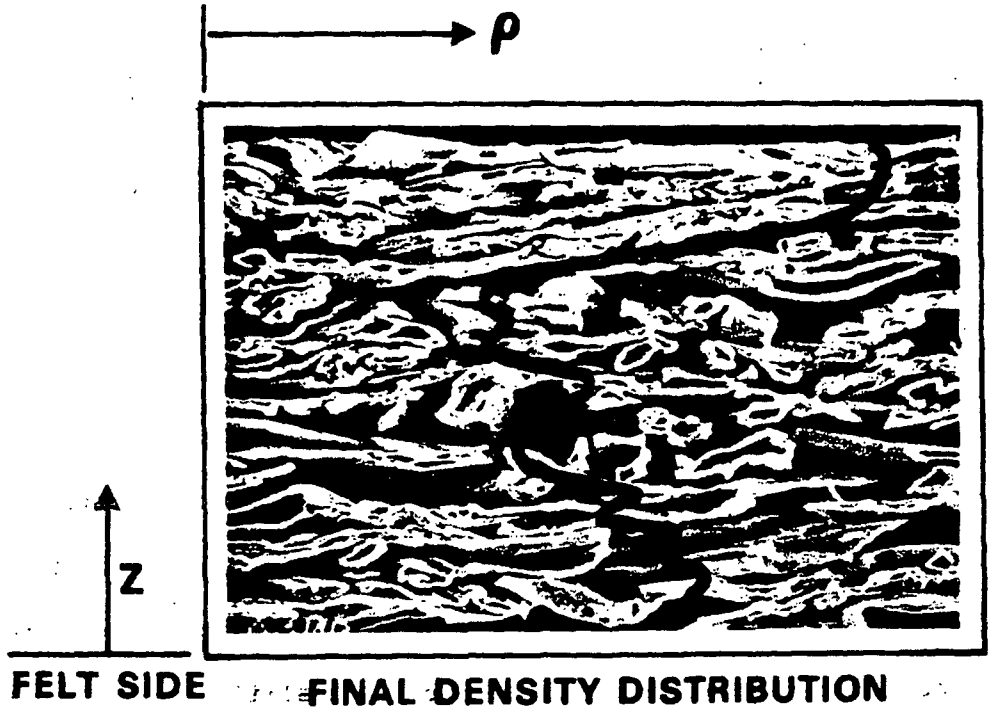

Cross Section of Impulse Dried Sheet

Figure 56. SEM cross sections with density profile mappings of a wet pressed sheet (20°C) and an impulse dried sheet (315°C). Basis weight = 100 g/m^2, Freeness = 735 CSF, Peak pressure = 5.4 MPa, NRT = 4.5 msec, Moisture ratio = 1.3.

separation, or delamination, can occur in some severe cases, as shown in the cross section in Fig. 57. Under controlled conditions, however, the process contributes to the development of bulk in the sheet structure.

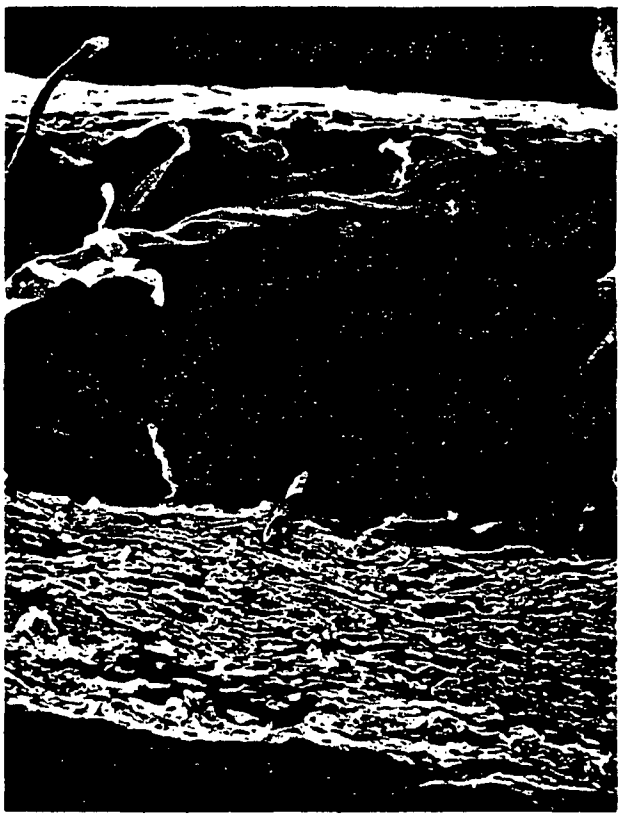

Figure 57. SEM cross section of impulse dried sheet exhibiting delamination. Basis weight = 200 g/m^2, Moisture ratio = 2.1, Freeness = 550 CSF, Peak pressure = 5.0 MPa, NRT = 4.5 msec, Temperature = 400°C.

Results of sheet grinding tests on wet pressed and impulse dried sheets also support the retention of a J shape density profile. Table 2 shows the tabulated data for the density profiles of wet pressing and an impulse drying condition. The grinding technique required three sheets for each profile, and the data in Table 2 are the averages of five profiles.

Table 2. Three region density profiles for wet pressing and impulse drying conditions. Wet pressing: 170 g/m^2, 65°F, 600 psi, 25 msec. Impulse drying: 170 g/m^2, 600°F, 600 psi, 25 msec.

Condition	Density,[a] g/cc			
	Hot Surface Region	Middle Region	Bottom Region	Sheet
Wet pressing	0.528	0.491	0.495	0.500
Impulse drying	0.832	0.453	0.470	0.602

[a]Determined by IPC rubber platen method.

Although the average density of the impulse dried sheets is greater than for the wet pressed sheets in Table 2, the middle and bottom regions are slightly lower in density. Thus, it is the density of the hot surface region that contributes the most to the average density increase. The final density profile is in the shape of a J, as seen earlier in the SEM mappings in Fig. 56. A U shape density profile may be obtained if the sheet is impulse dried a second time, with the opposite side in contact with the hot surface.

If the surface fibers next to the hot surface are examined, the effects of high temperature on the fibers are readily apparent. Figure 58 consists of two high magnification photographs of the surface fibers from the sheets shown earlier in Fig. 56. The wet pressed fibers, although apparently well bonded, have a great deal more contour, wrinkles, and depth in comparison to the impulse dried fibers. The plasticization that has taken place during impulse drying is so extreme that the definition between fibers is difficult to discern. There is very little depth and the wrinkles have been smoothed out. The surface of the impulse dried sheet is characteristically smooth and glossy. An unusual feature of the impulse dried sheet in Fig. 58 is the almost circular "hole," which appears to extend several fiber layers into the sheet. This is believed to

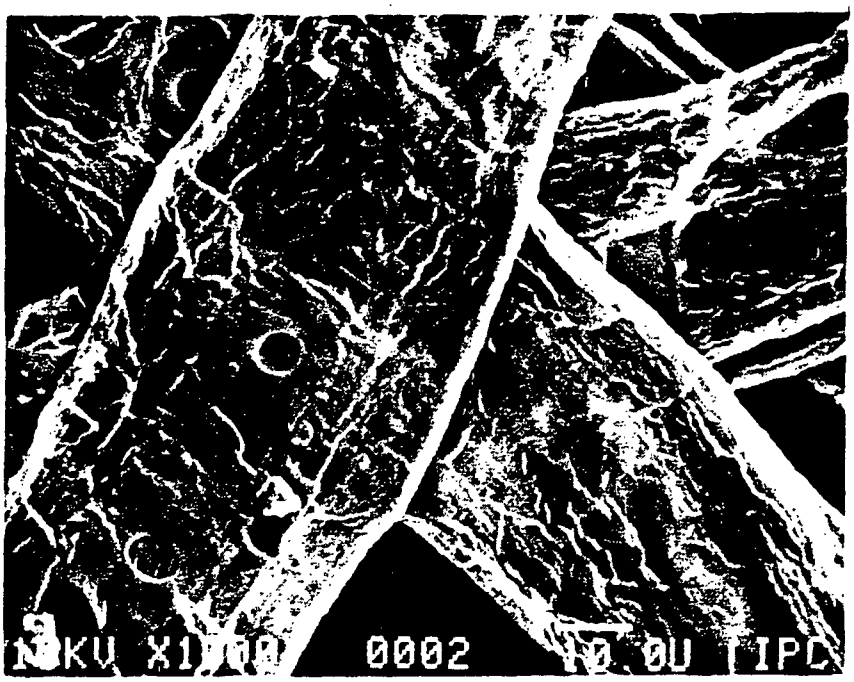

Surface of Wet Pressed Sheet

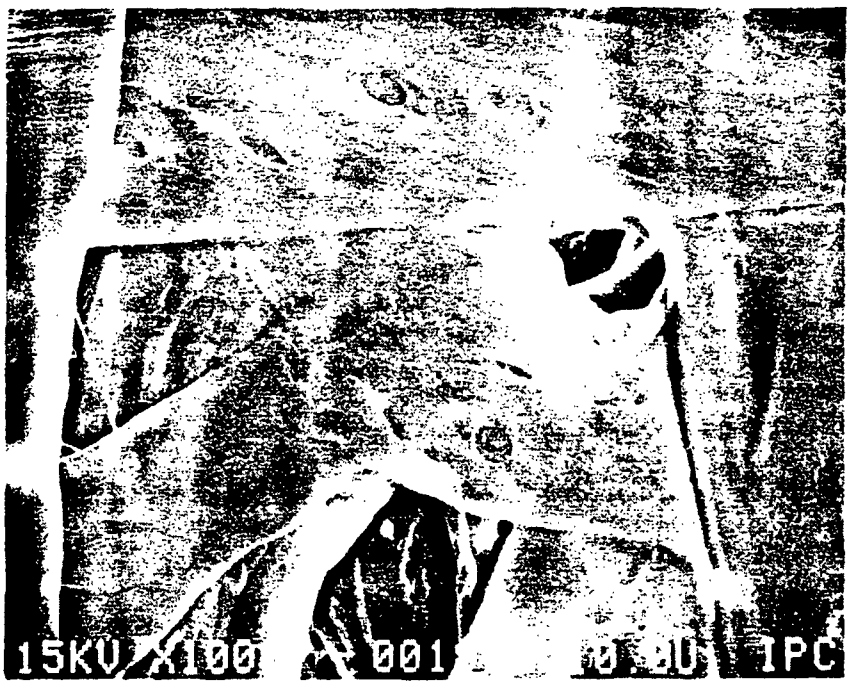

Surface of Impulse Dried Sheet

Figure 58. SEM surface photographs of a wet pressed sheet (20°C) and an impulse dried sheet (315°C). Moisture ratio = 1.3, Basis weight = 100 g/m^2, Freeness = 735 CSF, Peak pressure = 5.4 MPa, NRT = 4.5 msec.

serve as a pathway for vapor release during the exit of the sheet from the impulse drying nip.

The specific density distribution created by impulse drying depends on the operating conditions in the nip, such as hot surface temperature, applied pressure and nip residence time, and also on sheet characteristics, such as initial moisture ratio, basis weight, and freeness. The average sheet density, as shown by Sprague,[1] increases with pressure and thermal impulse, with thermal impulse being the most important variable. Thermal impulse is defined as the product of hot surface temperature and nip residence time. This increase in average density is usually associated with an increasing uniformity of the density profile. As the intensity of drying conditions is increased (increased time, temperature, pressure), the high degree of densification created in the hot surface region extends further into the sheet.

Sheet conditions have a considerable influence on density development. Increasing basis weight or lowering freeness tends to increase the flow resistance. This results in the development of higher internal fluid pressure gradients which, in turn, result in a more nonuniform density profile. For a higher basis weight and a given set of impulse drying conditions, the hot surface region comprises a smaller percentage of the total sheet thickness. Thus, the overall density is more dependent on the bulkier regions of the web. Longer nip residence times are required to achieve high average densities in the heavier sheets.

In most cases, impulse drying is performed on sheets with moisture ratios of 1.5 or less. Increasing the sheet moisture content generally reduces the degree of densification during impulse drying. As the moisture ratio is increased,

vapor movement is restricted, since liquid water is present in the voids. This results in compression behavior more typical of wet pressing. Decreased water viscosity and surface tension and increased thermal softening enhance the wet pressing process in a manner similar to the hot pressing results obtained by Back.[31]

SUMMARY AND CONCLUSIONS

Impulse drying results in high average sheet densities and nonuniform z-direction density profiles. This density profile results from the combined action of mechanical compression, intense heat transfer, moisture redistribution, vapor induced dewatering, thermal softening of fiber components, and flashing of superheated water. The profiles are typically J or U shaped, depending on applied pressure, thermal impulse, sheet moisture, basis weight, or freeness, and whether the sheet is impulse dried on one side or two.

A special measurement technique for dynamically determining the z-direction density profile during impulse drying has been developed. While this technique has increased our understanding of the intense physical processes that operate during impulse drying, it has also been quite useful in wet pressing studies. Detailed information on the effects of flow resistance and press surface temperature on density development as well as information on rewetting, stratification, and crushing have been obtained.

In this thesis, the density development during impulse drying has been discussed by dividing the impulse drying event into five consecutive time intervals. In the first interval the sheet densifies uniformly under mechanical compression as rapid sensible heating of the hot surface region brings its temperature to the ambient boiling point. Liquid dewatering by mechanical compression may occur, depending on pressing conditions. In Interval 2, boiling at the hot surface, followed by condensation further into the sheet raises the local temperature and results in significant moisture redistribution. Temperature measurements indicate that this evaporation/condensation mechanism progresses into the sheet with time. A new, intense mechanism is initiated during Interval 2 as mechanical compression and continued vapor generation cause

an internal pressurization leading to "vapor induced dewatering." In Interval 3, the pressurization of the fibers and fiber network resists further densification of the hot surface region while the middle and flow exiting regions densify under mechanical compression and vapor induced dewatering. As the compressive pressure is reduced on the exit side of the nip, it reaches a point where it can no longer sustain the vapor pressure. This marks the beginning of Interval 4. A rapid density increase in the hot surface region at this point is believed to involve reduced internal vapor pressures and appreciable flashing of superheated fiber pore water. As the vapor pressure is reduced and superheated fiber pore water flashes, the cell walls collapse under mechanical compression. Surface tension forces may play an important role. In Interval 5, evaporation and vapor release from the web continue as the applied pressure is removed from the sheet. This postnip vapor release process leads, under proper nip conditions, to a bulkier sheet interior.

The mechanisms of impulse drying inferred from the measurement techniques described in this thesis include:

1) An enhanced wet pressing mechanism arising from thermal softening and decreased liquid water viscosity and surface tension at elevated temperatures;
2) Moisture redistribution by an evaporation/condensation mechanism;
3) A vapor induced dewatering mechanism;
4) An internal pressurization mechanism which resists compression;
5) A mechanism which involves the release of vapor pressure, causing flashing of superheated pore water which then allows the cell walls to collapse under the mechanically applied load;
6) And, a postnip vapor release mechanism leading to expansion of the interior of the impulse dried sheet.

SIGNIFICANCE OF WORK AND THOUGHTS FOR FUTURE WORK

This investigation represents the first study which gives quantitative measurements of the development of a z-direction density profile in a dynamic press nip. The results give credence to certain aspects of existing wet pressing theory and clarify key densifying and dewatering mechanisms that are active during impulse drying.

The development of the density profile measurement technique is the most important instrumental contribution of this thesis. These measurements show promise for a number of other applications, such as characterization of consolidation processes, evaluation of improvements to these processes, characterization of fiber furnishes, and collection of quantitative data for process modeling.

Since impulse drying is in its infancy, it would be difficult to enumerate all the work which needs to be done. However, specific research work to further clarify heat transfer, liquid and vapor flow, and sheet compression characteristics at elevated temperatures is needed. A mathematical model of impulse drying could serve as a means for defining research needs. Thus, development of such a model should be the priority of any research effort into impulse drying.

The need for fundamental information concerning permeability, porosity, and compressibility of fiber networks, especially under dynamic conditions, is a problem in developing a mathematical model of impulse drying. Despite years of research directed at characterization of these fiber network parameters, much more work is needed.

The densifying mechanisms that are hypothesized in this thesis need to be further evaluated. For example, during impulse drying it appears that an internal pressurization mechanism develops which resists compression of the hot surface region. Unfortunately, the reliability of the vapor pressure measurement was never resolved in this thesis. Development and application of accurate vapor pressure measurement techniques would be an important step toward understanding this mechanism as well as the vapor-induced dewatering mechanism.

Investigation of the moisture redistribution mechanism presents a difficult problem. Electrical conductivity measurements in the sheet during impulse drying may serve as an investigative tool for studying this phenomenon.

Another mechanism which deserves further attention is the fiber collapse mechanism. According to the theory, the density increase at the end of the impulse drying nip results from fiber cell wall collapse under the action of mechanical compression as the vapor pressure is reduced and superheated pore water flashes. The thermodynamics of such a mechanism need to be addressed in a mathematical model of the process. Suggested experiments for obtaining fundamental information dealing with this phenomenon include a set of experiments which concentrate on boiling and flashing of superheated pore water in porous media. Perhaps a well defined, rigid, porous material could be the first structure investigated, followed by more complex systems. The porous systems could be pressurized at a high temperature and the pressure quickly released. Temperature and pressure profiles, porous media thickness, electrical conductivity measurements, and high speed photography could all be employed as a means of investigation.

Finally, a more systematic study of the effect of process variables on density development should be performed. Variables, including nip residence time, applied pressure, shape of the pressure-time pulse, sheet temperature, and type of flow receiver, should be evaluated.

ACKNOWLEDGMENTS

I would like to express my sincere appreciation to the members of my advisory committee, Fred Ahrens, Nai Chang, Harry Cullinan, Hugh Lavery, Clyde Sprague, and Douglas Wahren, for their invaluable advice and encouragement given throughout this investigation. To Clyde Sprague, who succeeded Fred Ahrens as my primary advisor, I am especially grateful for his direction, support, and numerous hours he devoted to advancing my work.

A number of other staff at The Institute of Paper Chemistry have contributed in many different ways to the successful completion of this thesis. In particular, I would like to gratefully acknowledge Mike Gabrielski, Jim Loughran, Dale Young, Bruce Andrews, Russ Tyler, Marvin Filz, Glenn Winkler, Paul Van Rossum, Doug Wheeler, Lester Nett, and Leon Straub for their contributions in the design, construction, and maintenance of the experimental equipment.

Finally, I would like to express my appreciation to my wife, Elizabeth, for her continuous encouragement, love, and understanding throughout this academic endeavor.

LITERATURE CITED

1. Sprague, C. H. Impulse drying: a performance overview. Proceedings of International Conference - New Technologies in Web Consolidation and Drying, May 19-23, 1986.

2. Sittig, M. Pulp and paper manufacture: energy conservation and pollution prevention. Noyes Data Corporation, Park Ridge, NJ, 1977.

3. Osswald, M. Energieverbrauch der Papiermaschine in Abhangigkeit ihrer Breite und Geschwindigkeit. Wochbl. Papierfabr. 105(11/12):411(1977).

4. Sprague, C. H.; Burton, S. W. New mechanisms in web consolidation. Proceedings of International Conference - New Technologies in Web Consolidation and Drying, May 19-23, 1986.

5. Ahrens, F. W. Proceedings of the 45th Executives' Conference, May 1-7, 1981, The Institute of Paper Chemistry, Appleton, WI. p. 21.

6. Burton, S. W. A-291 Project, The Institute of Paper Chemistry, Appleton, WI, 1983.

7. Arenander, S.; Wahren, D., Tappi 66(9):123(1983).

8. Heller, H. H., et al., Tappi 55(6):893-6(1972).

9. Wahlstrom, P. B., Pulp Paper Mag. Can. 61:T379, T418(1960).

10. Wahlstrom, P. B., Pulp Paper Mag. Can. 70:T349(1969).

11. Nilsson, P.; Larsson, K. O., Pulp Paper Mag. Can. 69:T438(1968).

12. Chang, N. L., Proc. TAPPI Eng. Conf., 1978. p. 93.

13. Ceckler, W. H.; Thompson, E. V. Final Report of the University of Maine at Orono Wet Pressing Project, DE AC02-78-CS40064.M007, Aug. 24, 1982.

14. Carlsson, G. Some fundamental aspects of the wet pressing of paper. Doctoral Dissertation. Stockholm, Sweden, Royal Institute of Technology, 1983.

15. Chang, N. L.; Han, S. T., The Institute of Paper Chemistry, Project 3258, Progress Report Two, July 1, 1976.

16. Ward, I. M. Mechanical properties of solid polymers. John Wiley & Sons Ltd., 1979.

17. Wegner, T. H.; Young, T. L.; Caulfield, D. F., Tappi 66(4):85-8(1983).

18. MacLaurin, D. J.; Whalen, J. F., Tappi 37(12):608(1954).

19. Clark, J. d'A., Pulp Paper Mag. Can. 44(1):92-102(Convention Issue, 1943).

20. MacGregor, M. A., Tappi 66(6):53-7(1983).

21. MacGregor, M. A., Tappi 66(7):65-9(1983).

22. Wicks, L., Tappi 65(9):73-7(1982).

23. Han, S. T. 2nd International Symposium on Water Removal at the Presses and Dryers, Quebec, Oct. 8-11, 1968. p. 65-77.

24. Elias, T. C., Tappi 50(3):125-32(1967).

25. Qviller, O., Papier-Journalen 26(23):312(Dec. 15, 1938).

26. Campbell, W. B., Pulp Paper Mag. Can., Convention Issue, 1947. p. 103.

27. Ingmanson, W. L.; Andrews, B. D.; Johnson, R. D., Tappi 42(10):840(1959).

28. Wilder, H. D., Doctoral Dissertation, Appleton, WI, The Institute of Paper Chemistry, Appleton, WI, 1960.

29. Busker, L. H.; Cronin, D. C. CPPA International Water Removal Symposium, Vancouver, Preprints, 1982.

30. Francik, C. J.; Busker, L. H. 70th Annual Meeting Canadian Pulp & Paper Association, Montreal, Preprints B83-9, 1984.

31. Anderson, L.; Back, E., Proc. TAPPI Eng. Conf., 1981. p. 311-23.

32. Back, E.; Norberg, K. G., Svensk Papperstid. 70:668(1967).

33. Back, E. L.; Salmen, N. L., Tappi 65(7):107-10(1982).

34. Back, E. L., EUCEPA, Web Formation and Consolidation, London, 1979.

35. Beatty, A. J.; Larson, K. H.; Ellick, B. S., CPPA Tech. Sect. Annual Meeting, Montreal, 1982.

36. Cutshall, K. A. 70th Annual Meeting Canadian Pulp & Paper Association, Montreal, Preprints B243-8, 1984.

37. Dreshfield, A. C.; Han, S. T., Tappi 39(7):449(1956).

38. McConnell, R. R., The Institute of Paper Chemistry, Project 3394, Report One, Feb., 1980.

39. Han, S. T., Tappi 53(6):1034(1970).

40. Han, S. T.; Ulmanen, T., Tappi 41(4):185(1958).

41. Cowan, W. F., Tappi 47(12):808(1964).

42. Holm, R. A., The Institute of Paper Chemistry, Project 2693, Report Two, 1969.

43. Riddiford, A. W., Tappi 52(5):939(1969).

44. Redfern, A. P., Papermaker 145(6):57(1963).

45. Holm, R. A.; Perry, J. F.; Holderby, J. M., The Institute of Paper Chemistry, Project 2693, Report Three, June, 1970.

46. Ahrens, F. W.; Kartsounes, G. T.; Ruff, D. L. Proceedings of the CPPA Technical Section Annual Meeting, Vol. B., Montreal, 1982. p. 93-7.

47. Ahrens, F. W. Fundamentals of drying status report to the Engineering Project Advisory Committee. Project 3470, Appleton, WI, The Institute of Paper Chemistry, 1984. p. 31.

48. Burton, S. W., unpublished work, 1985.

49. Wahren, D., U.S. pat. 4,324,613(April 13, 1982).

50. Ahrens, F. W. Status report to the Engineering Project Advisory Committee, Sept. 14, 1984, p. 66.

51. Davis, E. J.; Stratton, R. A.; Chang, N. L. CPPA International Water Removal Symposium, Vancouver, Preprints, 1982.

52. Wahren, D.; Zotterman, C., Paper Trade J. 162(16):37(1978).

53. Chang, N. L.; Nett, M. R.; Beck, D. A., J. Pulp Paper Science 12(2):J39-43 (March, 1986).

54. Beckman, N. J.; Plucker, E. I., Proc. TAPPI Eng. Conf., 1981. p. 311-23.

55. Litvay, J., personal communication, 1985-1986.

56. Cowan, W. F., Doctoral Dissertation, Appleton, WI, The Institute of Paper Chemistry, June, 1961.

57. Fang, Y. P., Doctoral Dissertation, Appleton, WI, The Institute of Paper Chemistry, June, 1986.

58. Ibrahim, A., Tappi 82(2):T46-8(Feb., 1981).

59. Ahrens, F. W.; Astrom, A. High-intensity drying of paper drying technology: an International Journal, Dec. 31, 1984.

60. McCabe, Smith. Unit Operations of Chemical Engineering, 3rd ed., McGraw Hill, 1976.

61. Ahrens, F. W., personal communication, Dec., 1983.

APPENDIX I

DETERMINATION OF THE TIME CONSTANT OF THE VAPOR PRESSURE MEASUREMENT CAVITY

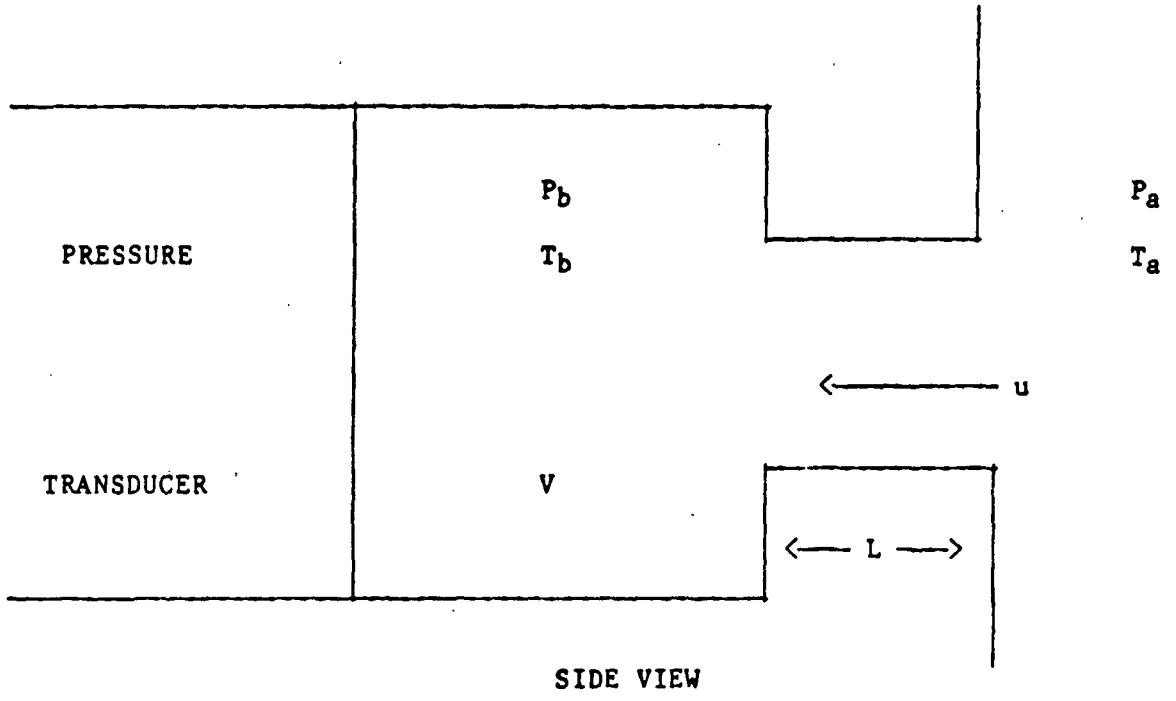

Figure 59. Illustration of the pressure measuring system used for measuring the vapor pressure at the hot surface.

Consider isothermal, compressible, and frictional flow of a gas into the system depicted in Fig. 59 which results from a step change in pressure, P_a. Thus:

$$T_a = T_b \text{ and } P_a > P_b \tag{1}$$

Mass Balance:

$$\frac{dM_v}{dt} = \dot{m}_v$$

According to the ideal gas law:

$$\rho = \frac{P\ MW}{R\ T} \tag{2}$$

Differentiating Eq. (2) with time:

$$\frac{d\rho}{dt} = \frac{MW}{RT}\frac{dP}{dt} \tag{3}$$

$$\dot{m}_v = \frac{d(\rho V)}{dt} \tag{4}$$

Since V = constant:

$$\dot{m}_v = \frac{V d\rho}{dt} \tag{5}$$

Combining Eq. (3) and (5):

$$\dot{m}_v = \frac{VMw}{RT}\frac{dP}{dt} \tag{6}$$

Where:

M_v = mass of vapor (lb)

t = time (sec)

$\dot{m}_v$ = mass flow rate (lb/sec)

ρ = density (lb/ft^3)

P = pressure (lb/ft^2)

T = temperature (°R)

MW = molecular weight (lb/lb-mole)

R = universal gas constant (ft-lb/lb-mole °R)

V = cavity volume (ft^3)

Momentum Balance:

Using Bernoulli's equation, including fluid friction, but neglecting potential energy:[60]

$$\frac{dP}{\rho} + \frac{d(u^2)}{(2g_c)} + d(h_{fs}) = 0 \tag{7}$$

The friction loss, h_{fs}, is related to the friction factor by:

$$h_{fs} = \frac{u^2 f}{2g_c} \frac{dL}{r_h} \tag{8}$$

For a circular pipe:

$$r_h = D/A \tag{9}$$

Combining Eq. (7), (8), and (9):

$$\frac{dP}{\rho} + \frac{d(u^2)}{(2g)} + \frac{2u^2 fDL}{g_c D} = 0 \tag{10}$$

Multiplying through by ρ^2, and letting:

$$\rho u = \frac{\dot{m}_v}{A} \quad , \quad udu = \frac{\dot{m}_v{}^2 \rho^{-3} d\rho}{A^2} \quad , \quad \rho = \frac{PM}{RT}$$

Where A is the area of flow, Eq. (10) becomes:

$$\frac{MP\ dP}{RT} = \frac{\dot{m}_v{}^2\ d\rho}{A^2 g_c \rho} + \frac{2\dot{m}_v{}^2 f\ dL}{A^2 g_c D} = 0 \tag{11}$$

Integrating Eq. (11) between a and b gives:

$$\frac{M}{2RT}\ (P_a{}^2 - P_b{}^2) - \frac{\dot{m}_v{}^2}{A^2 g_c} \frac{\ln(\rho_a)}{\ln(\rho_b)} = \frac{2\dot{m}_v{}^2 fL}{A^2 g_c D} \tag{12}$$

Inserting Eq. (6) into (12) and dividing through by M/2RT:

$$(P_a{}^2 - P_b{}^2) - \frac{2V^2 MW}{A^2 RT g_c} \frac{(dP)^2}{(dt)} \frac{\ln(\rho_a)}{\ln(\rho_b)} = \frac{4V^2 MEfL}{A^2 RT g_c D} \frac{(dP)^2}{(dt)} \tag{13}$$

When a step change occurs in P_a, the time constant of the system may be defined by:

$$t_c = \sqrt{\frac{4V^2\ MW\ f\ L}{A^2\ R\ T\ g_c\ D}} \tag{14}$$

Where:

h_{fs} = friction loss due to wall shear

u = fluid velocity (ft/sec)

g_c = 32.174 ft-lbm/lbf-sec

f = friction factor

r_h = hydraulic radius (ft)

L = pipe length (ft)

t_c = time constant (sec)

A = area of flow (ft^2)

A disadvantage to these calculations is that the friction factor must be estimated. This may be done by trial and error. First, a reasonable value for the friction factor is assumed, such as 0.008. Then, values for the appropriate conditions that apply to the particular system at hand are used to calculate a Reynolds number. The friction factor corresponding to the calculated Reynolds number is obtained from a standard table and compared to the assumed factor. This process is repeated until a consistent factor is obtained.

In estimating the friction factor, it was apparent that the friction factor was less than 0.01 in all cases considered. Therefore, 0.01 was selected as a conservative estimate of the friction factor.

Figure 60 is a plot of the system time constant correlated with hole diameter for several sets of hole arrays. As the number of holes decreases, the time constant of the system increases. This frictional effect increases in importance as the hole diameter is reduced below 0.20 inch.

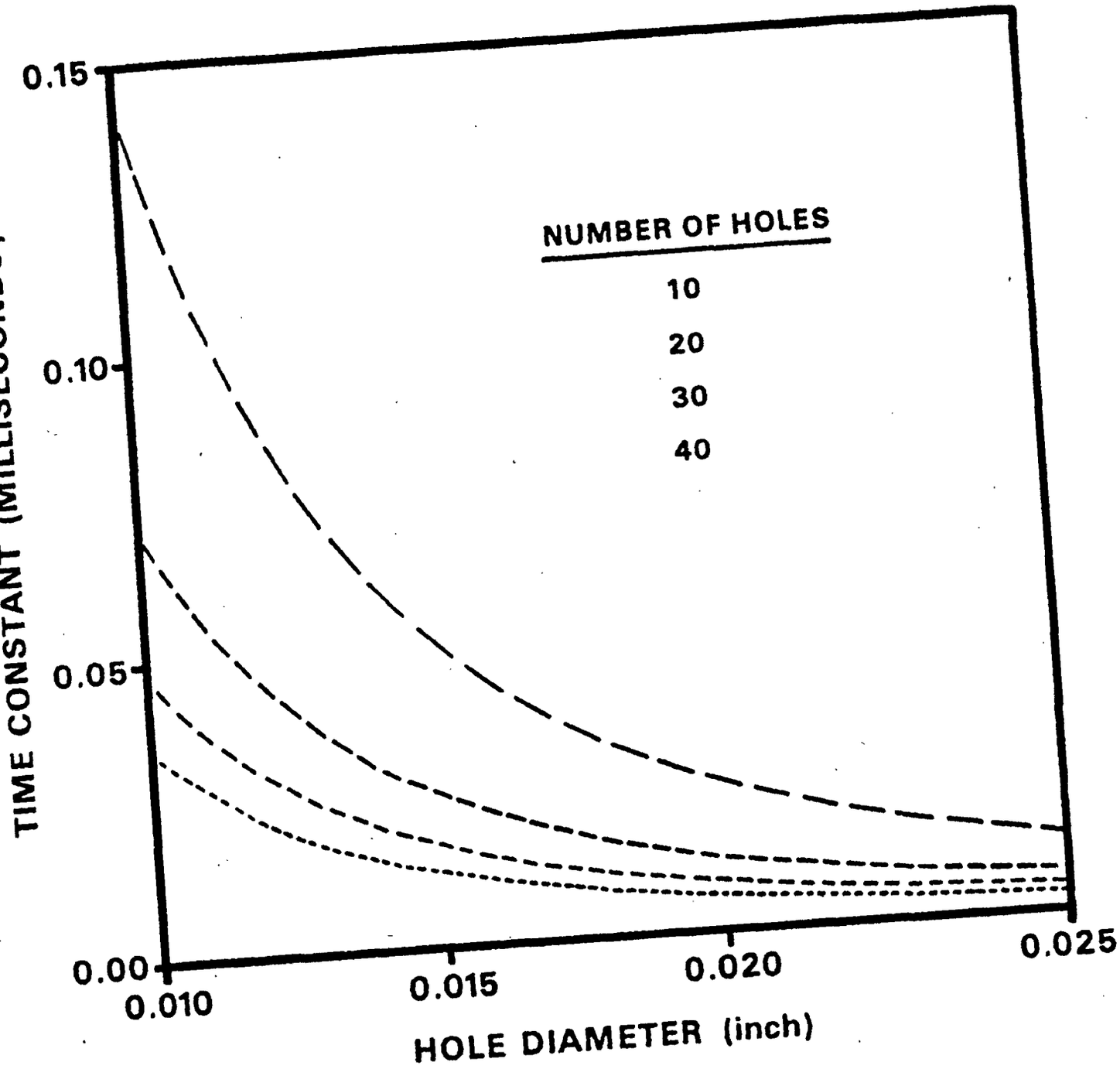

Figure 60. System time constant correlated with hole diameter for 10, 20, 30, and 40 hole arrays calculated using frictional flow model.

Figure 61 is a comparison of the frictional model with the frictionless model of Ahrens.[61] It appears that the frictional effects become dominant for hole diameters less than 0.02 inch while inertial effects become dominant for larger hole diameters. The magnitude of the time constants are in good agreement for the two models.

The following is a list of values used in the calculations.

$V = 1.775 \times 10^{-6}$ ft^3

$R = 1545.3$ ft-lb/lb-mole °R

$MW = 18$ lb/lb-mole

$g = 32.174$ ft-lb/lb-sec

$f = 0.01$

$T = 960$°R

$L = 0.01042$ ft

$c = 1500$ ft/sec

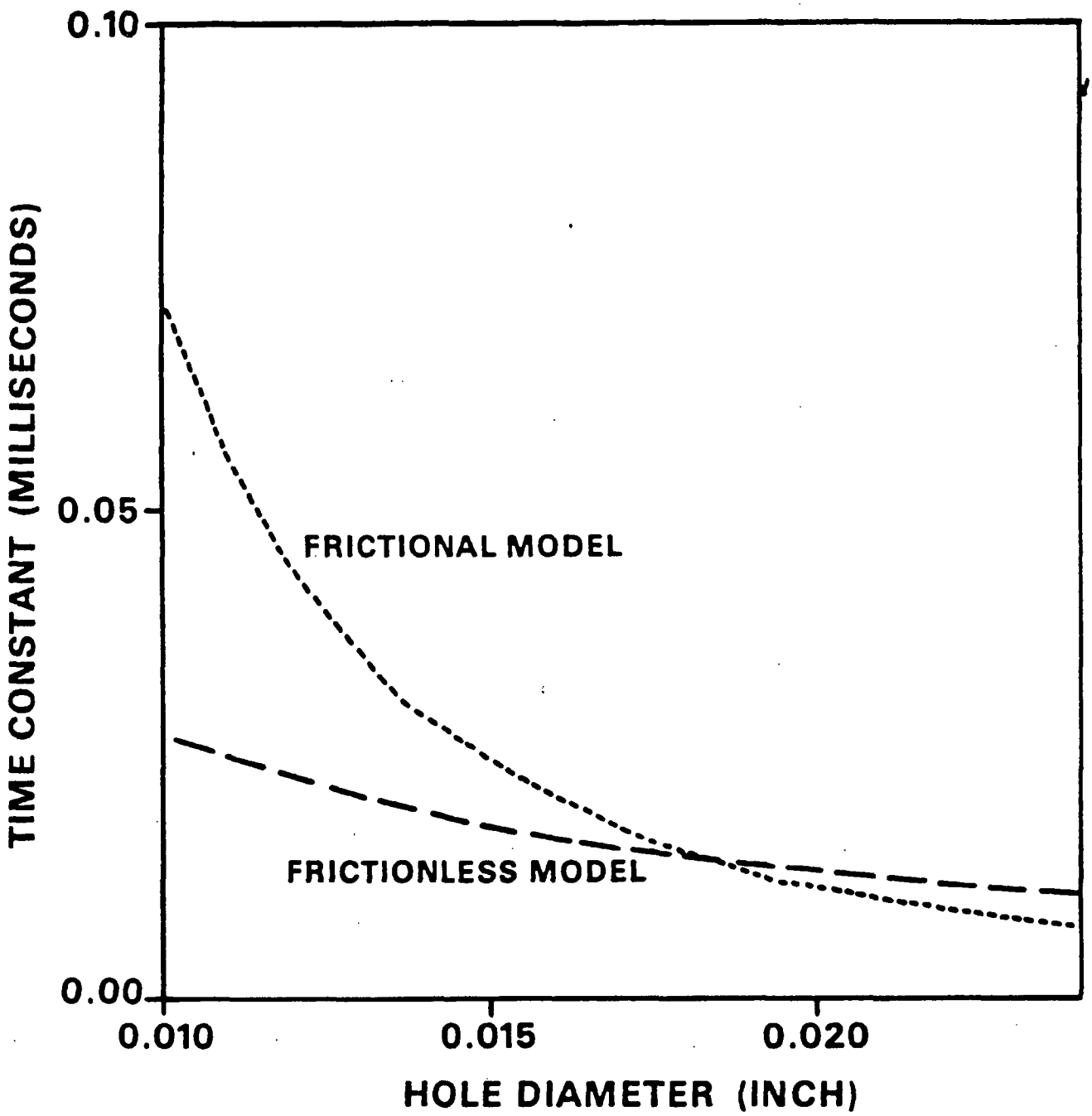

Figure 61. Comparison of time constants for a 20 hole array calculated using a frictional model and a frictionless model derived by Ahrens.[61]

APPENDIX II

COMPILATION OF EXPERIMENTAL CONDITIONS EXAMINED

DYNAMIC DENSITY DEVELOPMENT STUDY

Run	Basis Weight (g/m^2)	Moisture Ratio	Freeness (CSF)	Temperature (°C)	Peak Pressure (MPa)	Nip Residence Time (msec)
R1C	172.6	1.38	735	315	4.14	25
R2C	171.5	1.28	735	315	4.14	25
R3C	166.3	1.52	735	18	4.14	25
R4C	168.4	2.30	735	18	4.14	25
R5C	165.5	1.23	735	18	4.14	25
R6C	165.6	2.17	735	315	4.14	25
R7C	166.7	1.23	735	315	4.14	25
R8C	164.2	1.99	735	315	4.14	25
R9C	168.4	1.42	735	315	4.14	25
R10C	169.8	1.16	735	315	4.14	25
R1D	171.2	6.33	735	22	5.48	4.5
R2D	168.7	2.60	735	22	6.65	4.5
R3D	168.3	1.58	735	22	6.70	4.5
R4D	173.3	0.92	735	22	6.70	4.5
R5D	172.6	5.88	735	315	6.70	4.5
R6D	174.0	1.87	735	315	6.70	4.5
R7D	169.8	1.43	735	315	6.70	4.5
R8D	178.2	1.02	735	315	6.70	4.5
R1E	102.6	2.00	735	20	4.48	4.5
R2E	98.8	1.97	735	20	4.48	4.5
R3E	50.9	1.72	735	20	4.48	4.5
R4E	51.8	1.67	735	20	4.5	4.5
R5E	100.5	1.90	735	315	4.5	4.5
R6E	102.7	1.91	735	315	4.5	4.5
R7E	50.1	1.69	735	315	4.5	4.5
R8E	50.7	1.58	735	315	4.5	4.5
R9E	105.8	0.81	735	20	4.5	4.5
R10E	104.3	0.82	735	20	4.5	4.5
R11E	54.3	0.60	735	20	4.5	4.5
R12E	52.3	0.65	735	20	4.5	4.5
R13E	104.7	0.99	735	315	4.5	4.5
R14E	106.9	0.84	735	315	4.5	4.5
R15E	53.5	0.62	735	315	4.5	4.5
R16E	53.5	0.62	735	315	4.5	4.5

Run	Basis Weight (g/m^2)	Moisture Ratio	Freeness (CSF)	Temperature (°C)	Peak Pressure (MPa)	Nip Residence Time (msec)
R1F	104.6	1.84	735	20	7.6	4.0
R2F	104.6	1.82	735	150	7.6	4.0
R3F	106.6	1.78	735	230	7.6	4.0
R4F	106.6	1.76	735	315	7.6	4.0
R5F	106.6	1.33	735	20	7.6	4.0
R6F	105.2	1.36	735	150	7.6	4.0
R7F	106.6	1.34	735	230	7.6	4.0
R8F	105.2	1.27	735	315	7.6	4.0
R1H	102.2	4.1	420	21	5.5	4.5
R1HB	102.2	3.6	420	21	5.5	4.5
R2H	105.2	4.3	735	21	5.5	4.5
R3H	103.4	1.5	420	21	5.5	4.5
R4H	102.6	1.6	735	21	5.5	4.5
R5H	100.3	1.3	420	315	5.5	4.5
R6H	103.6	1.6	735	315	5.5	4.5
R7H	102.2	3.7	420	315	5.5	4.5
R1L	55.6	4.8	420	20	6.9	4.5
R2L	52.8	4.7	735	20	6.9	4.5
R3L	56.3	1.3	420	20	6.9	4.5
R4L	53.5	1.1	735	20	6.9	4.5
R5L	53.0	1.4	420	93	6.9	4.5
R6L	50.4	1.0	735	93	6.9	4.5
R7L	53.6	1.3	420	150	6.9	4.5
R8L	53.8	1.1	735	150	6.9	4.5
R9L	52.5	1.3	420	204	6.9	4.5
R10L	55.2	1.1	735	204	6.9	4.5
R11L	52.8	1.2	420	260	6.9	4.5
R12L	52.5	1.0	735	260	6.9	4.5
R13L	50.9	1.2	420	315	6.9	4.5
R14L	53.9	0.9	735	315	6.9	4.5
R15L	50.8	1.2	420	370	6.9	4.5
R16L	51.6	1.1	735	370	6.9	4.5

SHEET STRUCTURAL EVALUATION

Run	Basis Weight (g/m^2)	Moisture Ratio	Freeness (CSF)	Temperature (°C)	Peak Pressure (MPa)	Nip Residence Time (msec)
Control	107.5	1.64	735	—	--	--
R1G	98.9	1.61	735	24	5.4	4.5
R2G	106.6	1.72	735	150	5.4	4.5
R3G	95.9	1.38	735	232	5.4	4.5
R4G	109.9	1.52	735	315	5.4	4.5
R5G	170.1	1.28	735	371	5.4	4.5
Control	109.2	1.75	735	—	--	--
R7G	108.2	1.71	735	24	5.4	4.5
R8G	107.5	1.68	735	150	5.4	4.5
R9G	107.9	1.71	735	232	5.4	4.5
R10G	105.1	1.49	735	315	5.4	4.5
R11G	106.3	1.52	735	315	5.4	4.5
R12G	107.4	1.62	735	371	5.4	4.5
R1T	100.2	1.57	420	28	3.7	30
R2T	96.3	1.59	420	150	3.7	30
R3T	96	1.60	420	205	3.7	30
R4T	97.9	1.52	420	260	3.7	30
R5T	93.2	1.5	420	315	3.7	30

(5 runs each)